# Methanol and Formic Acid Activation Over Dispersed Metals (Pd, Pt, Au, Cu) on Ceria

A dissertation

Submitted by

Nan Yi

In partial fulfillment of the requirements

for the degree of

Doctor of Philosophy

in

*Chemical Engineering*

**TUFTS UNIVERSITY**

February, 2012

**Advisors: Professor Maria Flytzani-Stephanopoulos**

**Professor Howard Saltsburg**

# Abstract

## Title: "Methanol and Formic Acid Activation Over Dispersed Metals (Pd, Pt, Au, Cu) on Ceria"

Clean and efficient hydrogen production is of interest because of the potential of hydrogen to be the energy carrier of the future. Production of hydrogen from water-splitting is the long-term goal as it would be a clean and sustainable technology, once enough progress has been made to reduce the associated cost. For the short-term, hydrogen can be derived from renewable biomass or biomass plus fossil (or waste) fuel mixtures, in ways that minimize the carbon footprint of the process. In order to harness chemical energy into a practical and usable form, catalytic processes that efficiently extract the hydrogen are required. For these applications, new type catalysts containing only trace amounts of expensive noble metals are under intense investigation. In this thesis, highly dispersed metals as sub-nm clusters and cations on cerium oxide support have been prepared, characterized, and evaluated for the production of hydrogen by methanol steam reforming. An earth-abundant oxide, silica, has also been considered as support for alkali-promoted Pt, a new catalyst for the decomposition of formic acid to hydrogen and carbon dioxide.

The first part of my thesis demonstrates how a small amount (<1 wt%) gold on nanoscale ceria, is a novel, highly active catalyst for the steam reforming of methanol and the decomposition of formic acid. For these studies, a mixture of vapor-phase methanol and water, at a molar ratio of 1:1.3 was used, with the amount of water vapor typically not exceeding 3 %, the saturation vapor pressure of water at ambient conditions. Dispersion of the gold in ceria is crucial for activity. A shape effect of ceria on the catalytic activity of gold was identified by using single crystals of ceria prepared at the nanoscale as nanorods, nanocubes, and nanopolyhedra. Gold was found to

disperse atomically on the {110} surfaces of the nanorods, but not at all well on the {100} surfaces of the ceria nanocubes, where it formed nanoparticles, ~ 3 nm in size. Consequently, the activity of the latter was negligible while the gold dispersed on the {110} surfaces of ceria was a high-activity catalyst, converting methanol to $H_2$ and $CO_2$ at temperatures below 250 $^oC$. The $Au_n$-O-Ce catalyst sites are active also for the water-gas shift reaction. However, in the presence of methanol they preferentially adsorb methanol over carbon monoxide; hence they catalyze the reactions of the former selectively. The apparent activation energies and the turnover rates on the gold-ceria catalysts were the same irrespective of the shape of ceria; i.e. the shape effect is indirect, controlling simply the number of active Au-$O_x$ active sites on each surface of ceria.

Cerium oxide is an excellent dispersant for all metals, which it stabilizes in cationic surface oxygen species over its oxygen defects. It thus allows to compare the different M-$O_x$ catalytic properties for various reactions, especially for oxidation reactions of interest in the production of hydrogen. By using ceria nanorods, which have a large number of oxygen vacancies on their {110} surfaces, it was possible to disperse and evaluate different metals as M-$O_x$ catalytic sites for the steam reforming of methanol. Different reaction pathways over the Group VIII (Pd, Pt) and Group IB (Cu, Au) metal sites on ceria were identified. As a screening tool, temperature - programmed reactions under dynamic heating, as well as isothermal kinetics testing in microreactor were used. Group IB metals (Cu, Au) catalyzed the methanol coupling reactions to produce methyl formate. In the presence of water, methyl formate is hydrolyzed into formic acid, and finally $H_2$ and $CO_2$ are produced by the decomposition of formic acid on the gold species. This pathway explains gold-ceria displayed excellent $CO_2$ selectivity in steam reforming of methanol. The water-gas shift reaction equilibrium does not limit this pathway; hence the selectivity to $H_2$ is maximal. On the other hand, decomposition of methanol followed by the water gas shift reaction is the sole pathway for Group VIII metals (Pd and Pt) on ceria.

In separate studies of the formic acid decomposition, the dehydrogenation pathway was established to derive from the presence of the gold species. On gold-free ceria, the dehydration pathway is followed. Stability tests under shut-down/start-up cyclic operation showed the Au-

$CeO_x$ to be stable. Their resistance to water and carbon monoxide poisoning opens the way for application of gold-ceria as electrocatalyst component to direct formic acid fuel cells.

The second part of my thesis focused on understanding the mechanisms of sodium- modified platinum species for methanol and formic acid reactions. The formation of Na-Pt-$O_x$(OH) ensembles active for the low-temperature water-gas shift reaction was shown in recent work from our lab. Activity of these species was found even on silica supports, on which Na-free Pt is inactive. In this thesis the same materials were investigated as catalysts for methanol and formic acid reactions. Activity for these reactions was indeed promoted and hydrogen was produced at ambient temperatures. The reaction pathway over the Na-promoted Pt on silica was the same as that of Pt-$CeO_x$. However, the atomic dispersion of Pt-O species by the Na addition, allows the use of an earth-abundant support, i.e. silica, and the use of much less platinum for the same activity. These catalysts are then to be preferred as they make better use of valuable resources and are good candidates for sustainable hydrogen and energy production applications.

In summary, the findings of this thesis demonstrate that through the choice of suitable supports and promoters as ligands, noble metal catalysts can be prepared in atomic dispersions with high activity and stability for the reactions of interest to fuel processing to produce hydrogen, which also minimize their associated cost. As a concluding remark, potentially these findings are general, and it is recommended that they be explored also for base metal oxide catalysts in future work.

**Keywords: fuel cell, methanol, formic acid, platinum, palladium, gold, copper, ceria, silica**

# Acknowledgements

A Ph.D. thesis is both a challenging and rewarding endeavor, which could not have been completed without the help and support of a large number of people, some of whom I would like to acknowledge. Should I fail to explicitly mention someone, I hope they will attribute this not to my lack of appreciation but rather to my forgetfulness that is the result of the lack of sleep during this busy time.

I am most indebted to my mentors Prof. Maria Flytzani-Stephanopoulos and Prof. Howard Saltsburg. I chose Tufts years ago, simply looking forward to working with Prof. Maria Flytzani-Stephanopoulos to fulfill my scientific dreams in environmental catalysis. Later, I had the fortune to have Prof. Maria Flytzani-Stephanopoulos and Prof. Howard Saltsburg as my supervisors, both of whom are excellent scientists in the catalysis field. They provided me with continuous, sincere, and kind help during my study at Tufts. Their patience, encouragement, and support made my time memorable and my efforts accomplished. Most importantly, they provided me with a unique training, which is attributable to their different expertise and experience. They always had time for me when I had difficulties in my projects and needed their suggestions to overcome those challenges. Also they helped to improve my English and supported me during every public presentation.

Prof. Maria Flytzani-Stephanopoulos, with her excellent vision in sustainable energy and environmental catalysis, provided me with great opportunity to investigate hydrogen production through methanol and formic acid activation processes, which are some of the most promising and interesting research fields in the fuel cell process. Her passions for research, bravery for trying new ideas, hard-working spirit, and disciplined research inspired me through the years. My discussions with her always sparkled my mind. She encouraged me and supported my pursuit of *aien aristeuein* (Ever to Excel) in my own scientific journey. Her patient guidance and day-to-day support, along with the freedom she allowed in research, benefited me in the progress of my thesis projects.

I would also like to express my deepest gratitude to my co-supervisor Prof. Howard Saltsburg for his invaluable advice and encouragement over the years. First, I regard him as one of the few

science legends to whom I always looked up. I always admired his profound experience in industry and academia, his attitude and unique approach to solve problems, and his refreshing frankness in training students. Second, Prof. Saltsburg has encouraged me to think through ideas thoroughly and to propose outside-of-the-box solutions. I always appreciated, and over time enjoyed, his candor, as this helped me to mature as a scientist. Third, I especially thank him for his suggestions about how to make concise and memorable presentations and the time he took to prepare me before each presentation. In short, without the wonderful opportunity to work with Prof. Maria Flytzani-Stephanopoulos and Prof. Howard Saltsburg, my thesis would lose its novelty and profound impact for the following studies.

A special thanks is given to Dr. Robert Weber, for his valuable guidance, active participation, and continuous discussion throughout my research projects. At my proposal meeting, his first suggestion was to *be brave*, and his advice encouraged me to think freely and to attempt every idea to prove or disapprove the assumptions in my projects. Many thanks are his for his kind support to write recommendation letters during my search for jobs after Tufts. I also would like to thank Prof. Hyunmin Yi and Prof. Terry Haas for serving as my thesis committee members. I enjoyed collaborating with Prof. Yi's group, as well as, my many discussions with him. Prof. Haas deserves my appreciation for sparing his time to give me suggestions.

Experiments could not go smoothly without tremendous help over the years from Ms. Erin Quigley, Beth Frasso, Ann Tropeano, Julia Poirier, and Joanna Huckins. They helped me a lot to make orders for my experiments, plan trips to the national lab and meetings, and figure out the logistics of my lab. Special acknowledgement goes to Ann who retired in 2009 after serving the department for 28 years.

Time would have been different without good friends at Tufts. Yangping Zhai and Ioannis Valsamakis came to Tufts and joined the Nano Catalysis and Energy Lab with me during the same year. Their company made my experiments more enjoyable and less stressful. Special thanks go to Dr. Rui Si, who collaborated with me over many projects during his stay at Tufts and who helped me during my experiments at Brookhaven National Lab. I would like to extend my gratitude to Dr. Zheng Zhou, Ms. Alketa Gioka, Mr. Peter Kracker and Mr. Chris Hunt for their sincere and nice help at the beginning of my project. Dr. Weiling Deng, Dr. Zheng Wang, and Dr. Xiaoyan She deserve my thanks for their training and help when I started at Tufts. Dr.

Simone Goergen, Dr. Liuye Mo, Danny Perry, Emily Coombs, Ming Pan, Branko Zugic, Matthew Boucher, Yuan Wang, Chongyang Wang, Joe Lessard and Peng Wu, provided me with the happiest environment in which to work.

I also want to thank Dr. Joan Raitano and Prof. Siu-Wai Chan from Columbia University for providing me with ceria mixed oxide samples for my projects and having thoughtful discussions. The technical support from Emily Edwards (Tufts), Dr. Qi Wang and Dr. Nebojsa Marinkovic (Brookhaven Nation Lab) which facilitated my experiments without the worry of equipment problems, is gratefully acknowledged.

Skyler Brader deserves my thousands of thanks. Drinks change with the seasons: green tea in the spring, green tea frappuccino in the summer, pumpkin spice latte in the fall, and hot chocolate in the winter, but they all came during the right time. I am very grateful to have met you here and to have the opportunity to share my sadness and happiness with you. You stood by me with my moments of laughing, crying, and complaining, and have supported me to the end of my student life. I especially appreciate that you were beside me during my hard times. Also you helped to improve my English and explore the wonderful places around Boston together.

Last but not least, my sincere thanks and appreciation are given to my parents. They may not understand everything about my research, but they've been there for me 1000 percent. They made me believe that there is nothing in the world that I cannot do if I try my best. They always stood beside me and generously supported every dream. Finally, they accepted who I am and respected the decisions I made through years. They are the best father and mother in the world. My father taught me that every effort would be counted, and he also encouraged me to work hard and to pursue my dreams without regret. My mother always told me to smile to the world and to think of things positively, which is why I keep smiling in my deep heart no matter how hard the challenges may be. I also felt very sorry I did not spend too much time with them since I went to college at the age of 18. However, they did not complain about the loneliness that they endured since I went to school. I appreciate their sacrifice to support me.

Funding and fellowships for my research projects provided through the Department of Energy, The International Precious Metals Institute (Johnson Matthey Student Award), AIChE (Catalysis Reaction and Engineering Division Student Travel Awards), The North American Catalysis

Society (Kokes Awards), and Tufts University (Graduate Student Awards and Travel Funds) are greatly appreciated. They not only recognized my work as a student researcher but also provided generous supports for me to travel around country to present my works in national meetings.

Without the wonderful and incredible persons I met during these years, I could not have finished the pursuit of my Ph.D. degree. I would simply like to extend my great appreciation at all.

Thank you all,

November 2011, Medford, Massachusetts

.

# Table of Contents

# List of Tables

# List of Schemes

# List of Figures

# Chapter 1: Introduction

Fossil fuels have played a key role in improving our standard of living since industrialization. Yet this progress has released carbon dioxide and other greenhouse gases to march relentlessly across the world, leaving its insidious footprints for future generations [1]. With the world's consumption of fossil fuels, progressive emissions of greenhouse gases have caused an increase in the Earth's temperature [2]. As fossil fuels become much scarcer and their harmful effects become less convenient to ignore, sustainability has attracted much attention among the public, media, politicians, and scientists. Renewable energy sources, like solar, wind, have been researched with the hope of replacing traditional methods of energy production [3].

## 1.1 Fuel options for hydrogen generation

Hydrogen is regarded as the cleanest fuel since water is the only product of its combustion. Industrially, hydrogen is largely manufactured through natural gas steam reforming [4]. Ideally, splitting water would be the best way to produce hydrogen and researchers working on photo-catalysis and photo-electrochemistry have worked for decades to split water efficiently with sunlight or electricity, but sustainable and cost efficient methods that allow the process to operate in larger scale are still a challenge [5].

Absent a process that is entirely sustainable and efficient, industry currently uses other processes to produce hydrogen. For example, natural gas has a high hydrogen to carbon ratio, however, the biggest disadvantages are that it is gaseous at ambient temperature and is difficult to transport. Steam reforming of hydrocarbon is a well-established process in industry. Generally, this process involves two separate reactions: the splitting of hydrocarbons with steam and the water gas shift reaction. Methane, the simplest hydrocarbon, for example, was investigated using both steam reforming (with $H_2O$) and dry reforming (with $CO_2$) over groups 8, 9, and 10 metals. Methane is a very stable molecule, and, in order to break the C-H bond, 439 kJ/mol of energy is

required. High energy input makes this process unfavorable at low temperatures. Also carbon formation may lead to catalyst degradation, which is inevitable at higher temperatures [6].

Liquid sources, like alcohol, overcome gas transportation problems. Liquefied petroleum gas (LPG) requires high temperature reforming (1073 K - 1173 K), which makes its use susceptible to deactivation by coking [7]. Ethanol has been widely investigated during the past decades as an interesting candidate for hydrogen production, since it can be produced from renewable sources; however, it has to perform at above 550 $^{o}$C temperatures to break carbon-carbon bonds and several undesired by-products are formed at the same time [8].

Methanol and formic acid, which are sulfur-free liquid fuels with high ratios of hydrogen to carbon are promising choices for hydrogen production from liquid resources, especially for the application to portable fuel cells [9, 10]. Also the attractiveness of those two simple organic molecules comes from the fact that they can be synthesized from energy-neutral carbon dioxide and hydrogen, which reduces their carbon footprint [11, 12].

### 1.2 Catalytic hydrogen generation from methanol

Methanol is one of the largest bulk chemicals in the world and a suitable hydrogen carrier which is readily convertible into hydrogen at low temperatures through catalytic processes. Methanol has the highest ratio of hydrogen to carbon among all alcohols, and it is also a sulfur-free fuel. Methanol can be produced from synthesis gas, which is primarily manufactured from steam reforming of natural gas. Well established industrial catalysts such as copper-based mixed oxides have been developed for methanol synthesis. Methanol formation through CO was shown to be negligible, because the oxidation of CO to $CO_2$ by surface-bound oxygen is a very fast reaction. Typically, reaction takes place over $Cu/ZnO/Al_2O_3$ catalyst at 250 $^{o}$C and 5-10 MPa [9, 13]. However, new processes that decrease the required temperature and pressure are under development. For example, production of methanol could be achieved through a liquid phase reaction system and even from renewable sources such as biomass. As cost and reaction efficiency for carbon dioxide reduction through photo-catalysis are improved, methanol will find more applications as a hydrogen carrier.

In this chapter, the following three sections are presented: (1) hydrogen production through methanol reactions, (2) catalysts for methanol reactions, and (3) mechanistic investigation. There are plenty of related reports in this field, however, the focus here is on copper and precious metals related catalysts based on the rationale and objectives of my thesis.

### *1.2.1 Processes for methanol reactions*

In principle, there are four routes available to produce hydrogen through methanol reactions: (i) decomposition of methanol, (ii) steam reforming of methanol, (iii) partial oxidation of methanol, and (iv) combined methanol oxidative reforming. Those four reactions can be carried out at moderate temperatures with the help of metal oxide catalysts.

*Decomposition of methanol*: Methanol decomposition has been studied for decades. This reaction is the reverse of the methanol synthesis process.

$$CH_3OH \rightarrow CO + 2H_2$$

The drawback of this reaction is obvious: it is an endothermic process, and large amounts of carbon monoxide are produced. The chemistry behind methanol decomposition is significant, because decomposition of methanol can be used as a probe reaction to discriminate the different surface properties and also improve our understanding of the interaction between methanol and catalysts [14]. Although it is not a suitable reaction for supplying hydrogen for fuel cell applications, decomposition of methanol is applied in industrial processes to recover waste heat around 200 $^{o}$C, thereby increasing the heating value of the fuel [15].

*Steam reforming of methanol*: This is one of key processes to produce hydrogen from methanol for fuel cell applications. The yield of this approach is high, ideally 75% hydrogen produced:

$$CH_3OH + H_2O \rightarrow CO_2 + 3H_2$$

Although this process is also an endothermic reaction, it is well suited for operation under stationary conditions where high hydrogen production capacities are needed.

*Partial oxidation of methanol*: This process typically uses air or oxygen as the oxidant.

$$CH_3OH + \tfrac{1}{2}O_2 \rightarrow CO_2 + 2H_2$$

The theoretical maximum hydrogen concentration in the products is 67% when using oxygen and 41% when using air as the oxygen source. This process is an exothermic process, thus extra heat is not needed to start the reaction.

*Combined Reforming*: This process combines the advantages of steam reforming of methanol and partial oxidation of methanol. The general equation is below:

$$(x+y)CH_3OH + xH_2O + 0.5yO_2 \rightarrow (x+y)CO_2 + (3x+2y)H_2$$

By changing the reactant feed ratio, the process can be carried out over a large range of operating conditions, from endothermic to exothermic conditions. Therefore, this process can easily adapt to the requirement of the system at various given conditions. However, combined reforming does not yield as much hydrogen as the steam reforming of methanol.

### *1.2.2 Methanol reaction catalysts*

Low temperature reforming of methanol is required because of its favorable thermodynamics (decreasing CO concentration in the outlet gases). Thus much emphasis has been placed on developing highly active catalysts that can provide the desired fast kinetics at lower temperatures. Most of these investigations have been focused on Cu-based catalysts primarily due to the outgrowth of the extensive use of Cu-based catalysts in methanol synthesis [16]. Since copper has some obvious disadvantages, including deactivation, pyrophoricity, and high-temperature sintering, new approaches have been developed to address these drawbacks: either modification of the Cu-based formulation or development of active and selective formulations from group VIII metals.

1.2.2.1 Copper-based catalysts

For metals, the predominant sintering mechanism in the bulk is vacancy diffusion, which suggests a relationship with cohesive energy. Hughs gave the following increasing order of stability of metals: Ag < Cu< Au< Pd< Fe< Ni< Co< Pt< Rh< Ru< Ir< Os< Re [17]. In this analysis lies the reason why copper-based catalysts are more susceptible to thermal sintering. This also explains why all practical copper catalysts contain one or more metal oxides to minimize thermal sintering. Thus, the copper metal sintering may be considerably reduced by the addition of one or more oxide species, such as ZnO, $Al_2O_3$, or $ZrO_2$.

Numerous investigations have been performed on the Cu/ZnO system, but the nature of the active sites and the reaction mechanism still generates substantial debate. Usually the role of ZnO is considered to be minimal, but it is needed as textural support in segregating the Cu, which minimizes copper sintering. It should come as no surprise that promotional effects of ZnO additives on Cu for the steam reforming reaction have been reported. It has also been suggested that the addition of Zn results in changing the morphology and the structural disorder of the copper particles [18], incorporating of copper into ZnO [19], or forming a Cu-Zn alloy thin layer [20].

The use of alumina provides a high surface area support which serves to increase copper dispersion and decrease its susceptibility to sintering. But at the same time, CuO and $Al_2O_3$ easily form $CuAl_2O_4$, which could decrease the copper dispersion on the surface, resulting in decreased reaction activity. $ZrO_2$ is known to possess oxygen ion vacancies, which can influence the dispersion and alter the morphology of the supported copper metal particle [21]. $ZrO_2$ promotion was shown to increase copper dispersion and weaken the interaction between CuO and $Al_2O_3$, mitigating the generation of $CuAl_2O_4$ spinel type compound [22]. Fisher *et al.* [23] suggest a synergy between Cu and $ZrO_2$, in which all major reaction intermediates are found on $ZrO_2$ and the primary role of copper is to accept the hydrogen released from surface species located on the $ZrO_2$ and subsequent desorption of molecular hydrogen. Velu *et al.* [24] have demonstrated $ZrO_2$ is a more effective support than $Al_2O_3$ to improve Cu reducibility and

dispersion. Furthermore, $ZrO_2$ has also been reported to prevent the sintering of Cu crystallites under reaction conditions, and, thus, it may also be regarded as a structural stabilizer [25].

Ceria is a stable fluorite type oxide, well known for its high oxygen vacancy and mobility properties. The addition of cerium to traditional Cu-based catalysts was reported to enhance activity and selectivity. Patel *et al.* [26] reported that cerium promoted Cu-Zn-Ce-Al oxides have improved activity with suppressed CO concentration when compared to Cu-Zn-Al alone. It is hypothesized that ceria enhances the catalyst stability due to its high oxygen storage capacity; i.e., the partially reduced ceria sites formed under the highly reducing environment of the reforming atmosphere produce mobile oxygen that facilitates coke gasification, inhibiting coke deposition. Additionally, ceria increases the thermal stability of the composite catalyst against sintering. Cheng *et al.* [27] reported addition of yttrium doped ceria (YDC) to $Cu/Al_2O_3$ catalysts drastically enhanced activity, which was attributed to the increase in oxidized copper sites, $Cu^+$. These sites were suggested to be more active than those of metallic copper, $Cu^0$.

The reducibility of ceria can be modified by a dopant. When ceria is doped with divalent ions such as $Mg^{2+}$, $Ca^{2+}$ or trivalent ions such as $La^{3+}$, $Sc^{3+}$, $Y^{3+}$, oxygen vacancies are created in the structure, resulting in high oxygen vacancy concentrations [28]. Liu *et al.* [29] first reported that 3.9 wt% Cu/Ceria catalyst has comparable activity with Cu/ZnO, Cu/Zn(Al)O, and $Cu/Al_2O_3$ in steam reforming of methanol. They suggested that the high activity resulted from highly dispersed Cu metal particles and the $Cu^+$ species were stabilized on the $CeO_2$ surface. A solid solution also forms in the $Ce_{1-x}Cu_xO_{2-x}$ along with $Cu^+$ stabilized by the $Ce^{3+}+Cu^{2+}\rightarrow Ce^{4+}+Cu^+$ redox reaction, which may be the reason for the good performance obtained on these $Ce_{1-x}Cu_xO_{2-x}$ mixed oxides.

Copper has the advantages of being a cheap and efficient catalyst for methanol reactions and efforts to modify copper with other metals that have improved its performance are reviewed here. However, one basic question still remains to be answered: which copper states play a critical role in activity and selectivity?

1.2.2.2 Gold-based catalysts

Bulk metallic gold has been recognized as an inert catalyst. However, innovative research has suggested that nanoscale gold-based catalysts have potential for being effectively employed in fuel cells and related hydrogen fuel processing. Many studies have established that very fine, well dispersed Au particles have high catalytic activity for a number of important reactions, which depends on the size and dispersion of gold or the manner of interaction between gold and support oxides [30-32]. Seminal work by Fu *et al.* [33] demonstrates that the active site appears to be a $Au_n$-O-Ce species, involving gold cations strongly bound with the Ce-O on the ceria surface for the water-gas shift reaction, but not for the low-temperature CO oxidation by oxygen, which is more complex [34].

Few works have focused on the applications of gold supported on oxides as catalysts for the reforming of methanol. Recently, Bowker *et al.* [35] reported that $Au/TiO_2$ prepared by incipient wetness impregnation can photocatalyze the reforming of methanol in aqueous solution. Chang *et al.* [36] reported that $Au/TiO_2$, prepared by a deposition-precipitation method, shows relatively high activity in partial oxidation of methanol, which depends on the particle sizes of metallic gold. Takahashi *et al.* [37] claimed that gold in amorphous $Cu_{50}Zr_{50}$ alloy improves the dispersion of copper effectively for the steam reforming of methanol.

In all these cases, in addition to the choice of support to stabilize gold species, preparation techniques also seem to be very important for determining the catalyst structure and thus the catalytic efficiency. Questions arise then: (1) could gold-ceria be an active catalysts for methanol reaction? If so, which pathway dominates? If not, why is it inert? (2) Could an approach to stabilize gold on ceria with different states be followed, thus discriminating the role of support and gold species for the methanol reaction?

1.2.2.3 Group VIII catalyst --- Pd-Zn Alloy

Cu-based catalysts are active and selective for the methanol steam reforming reaction. However, sintering of the metal at temperatures higher than 280 $^{o}$C and other deactivation issues remain problematic, including its pyrophoric nature when exposed to air. Precious metals and other group VIII metals are active for the conversion of methanol. However, they tend to not be selective for the reforming reaction. Other options include precious metal alloys, not containing copper, with Pd/ZnO being the most active and selective for this type of catalyst.

The direct effect of ZnO support on the methanol steam reforming reactions over Pd/ZnO is minor as concluded from the experimental findings that (1) ZnO itself is inert [38]; (2) the steam reforming activity of the ZnO-free catalyst, Zn-Pd/C, is similar to that of Pd/ZnO catalyst [39]; and (3) a DFT study that suggested that a small amount of CO is produced at the metallic Pd species of the catalysts or at the defect sites of PdZn alloy [40].

Iwasa *et al.* [41] were the first to report that Pd supported on ZnO and reduced at temperatures higher than 300 $^{o}$C has exceptionally high activity and selectivity to $CO_2$ and $H_2$. Combined TPR, XRD, and XPS methods revealed the formation of a PdZn alloy under reduction conditions. But the reaction over catalysts having PdZn alloy phase exhibited reduced selectivity to $CO_2$, comparable to catalysts having metallic Pd phase. This was attributed to the bulk PdZn alloy formed by the spillover of atomic hydrogen from Pd metal to the ZnO, leading to facile reduction of the ZnO and migration of Zn over the metallic surface [42]. Iwasa also expanded their work to other group VIII metals such as Co, Ni, Ru, Ir and Pt on various supports like $In_2O_3$ and $Ga_2O_3$ [38]. It was found that Pd and Pt both formed alloys with In, Ga, Zn and showed improved selectivity to hydrogen in methanol reforming reaction once the alloy was formed. However, of those different compositions, the Pd-Zn alloy appears to be the most active and selective.

Supported Pd-Zn alloy catalysts have also been an interesting topic of research in the past five years. Pd loading and Pd/ZnO ratio optimization studies were performed on $Al_2O_3$-supported catalysts [43]. On a Pd/ZnO/$Al_2O_3$ catalyst, similar activity and selectivity were reported as those for a conventional Cu-ZnO methanol synthesis catalyst at 220 $^{o}$C. Also due to higher

stability of the Pd alloy, much higher operating temperatures can be used and the faster kinetics can be exploited. Studies of Pd/ZnO/$CeO_2$ catalyst showed that it has good thermal stability as well as good activity and selectivity. At an operating temperature of 350 $^oC$, negligible activity loss was observed. Comparatively, 20% loss in hydrogen exit concentration was observed over a Cu/ZnO catalyst under the same conditions [44]. Penner *et al.* [45] reported a highly structured Pd-Zn phase on a mechanically stable $SiO_2$ support. As evidenced by TEM, the PdZn was thermally and structurally stable under reducing conditions up to 600 $^oC$. Suwa *et al.* compared the performance of various supported Pd/ZnO-based catalysts. While much more stable than Cu-based catalysts, deactivation of PdZn catalysts was reported. A Zn-Pd/C catalyst was found to have a much smaller deactivation rate due to the alloy formed between Zn and Pd, which resulted in a smaller amount of surface Zn to form zinc carbonate hydroxide [39].

Furthermore, it was found that larger PdZn particles did not adversely affect the reforming reaction. In fact, an optimum crystallite size which promotes the reforming reaction probably exists over Pd/ZnO type catalysts [46]. Further reports by Agrell [47] confirm a correlation between Pd crystallite size and carbon monoxide selectivity. Karim *et al*. reported crystalline size effects and alloy effects [48]. They found that lower selectivity to hydrogen resulted when small crystallites were formed (~ 1.5nm). However, these small particles were thought to be metallic Pd that was eventually alloyed with Zn upon increasing reduction temperature, resulting in increased selectivity.

The basic phenomenon behind the Pd-Zn surface alloy is that the electron structure is modified. Thus Pd-ZnO alloy has encouraged the following investigations: (1) Can trace amounts of metals be used to modify the surface structure, with the expectation of improving the catalytic performance? and (2) Does the choice of support determine how the active metals are accommodated on the surface?

#### 1.2.2.4 Promotion effects from the addition of alkali metal ions

Recent research has showed that the addition of a third component into Cu-Ceria catalysts can improve its activity for the steam reforming of methanol. Papavasiliou *et al.* [49] claimed that

doping Cu-$CeO_2$ with small amounts of Sm and Zn oxides, which were prepared by urea-nitrate combustion methods, improved the catalytic performance for methanol steam reforming, producing less CO compared to CuO-$CeO_2$. They suggested that dopant cations are incorporated into the $CeO_2$ lattice, leading to solid solution formation, while increasing the dopant loading leads to surface segregation and a decrease in copper oxide dispersion. Oguchi *et al.* [50] reported addition of Zr to Cu-Ceria resulted in copper oxidation, which is the result of a synergistic effect between cerium and zirconia.

According to these authors, ceria alone favors metallic $Cu^0$ formation, but when ceria is combined with $ZrO_2$, copper is in the form of $Cu_2O$. A mixture of both $Cu_2O$ and $Cu^0$ was found when copper was supported on both $ZrO_2$ and $CeO_2$. Ritzkopf *et al.* [51] also confirmed that $Cu^+$ occurs as intermediate species during the reduction of CuO/$ZrO_2$ and may play a role in the steam reforming of methanol. At the same time, $Cu^+$ was observed as a transient species in the reduction of $Cu^{2+}$ to $Cu^0$ in Cu/ZnO, but no activity was attributed to it. Recently, it was found by Chan's group [52] that pure CuO nanoparticles were completely reduced to $Cu_2O$, and this phase can remain stable without further reduction with continued exposure to CO. Thus it may be assumed that $ZrO_2$ is helpful to form stable $Cu^+$ species at the nanoscale.

Furthermore, alkali additives have been reported to improve the catalyst activity for steam reforming of methanol. Qi *et al.* [53] reported that the presence of K(Na) cations can enhance the activity for methanol conversion over Ni,Al layered double hydroxide. And the selectivity to $CO_2$ rather than CO was better with K ions than Na, especially at higher temperatures (*e.g.* 390~400 $^oC$). Koós *et al.* [54] found the K additive increased the adsorption of $CH_3OH$ on $Mo_2C$ and enhanced the production of $H_2$ by steam reforming of methanol. A remarkable feature of the K-promoted $Mo_2C$/C catalyst is its high thermal stability. Houteit *et al.* [55] found that 2 wt% Cs-15wt%Cu-$Al_2O_3$ can reach 94 mol% $CH_3OH$ conversion and $H_2$ selectivity 97 mol% with no detectable formation of CO at 300 $^oC$. The catalysts were prepared by impregnation of $\gamma$-$Al_2O_3$ (133 $m^2/g$) with an aqueous solution of $Cu(NO_3)_2 \cdot 3H_2O$ and $Cs_2CO_3$ respectively. Catalysts were pretreated at 200 $^oC$ under nitrogen and further treated in a gas flow (20%$O_2$/80%$N_2$) before the catalytic test. The authors suggested that the improved activity was due to the fact that cesium prevents the reduction of copper oxide into metallic Cu, and inhibits the formation of $CuAl_2O_4$ spinel upon thermal treatments.

Investigations of the K-modified $Ni/SiO_2$ [56] showed the occurrence of an electron transfer from the promoter to the metal. The electron donation was attributed to the simultaneous effect of the $K^+$ and $O^{2-}$ ions. Additionally, the electron donating character of the potassium and oxygen over layers has also been considered on K/Ru-C [57] and K/Fe [58] catalysts. As a result of this kind of interaction for K-modified $Rh/SiO_2$, the formation of $CO_2^-$ anions bonded to $K^+$ ions was detected [59]. Through simulation, Pala *et al.* [60] claimed that doping the ZnO(10-10) surface with Na or K can significantly alter the chemistry of the surface, and methanol preferred to dissociate into adsorbed HCHO and two surface hydroxyls.

The promotional effect decreases in the order of K > Na >Li over Cu-Cr-Mn catalysts for the methanol decomposition reaction [61]. Although the addition of alkali decreases the surface area, the dispersion of copper was greatly enhanced, thus resulting in significant enhancement in activity and selectivity to CO and $H_2$. The formation of DME was suppressed by the addition of alkali. Interestingly, the activity did not increase linearly with increasing of amount of alkali; the recommended amount of alkali is 1-4 wt%.

Alkali addition is an inexpensive way to modify the surface structure, and has the advantage of an abundant resource. Challenges are to (1) optimize the amount and stabilize active base metals for the methanol reactions with alkali metals instead of other precious metals; (2) understand the mechanism of alkali promotion.

#### 1.2.2.5 Mechanistic considerations for methanol-active catalysts

There has been some debate in the literature concerning the pathway for production of $CO_2$ and $H_2$ by SRM. Much attention has been focused on the mechanism for CO by-product formation, since it will poison the anode catalyst in the present generation proton-exchange membrane PEM) fuel cells. Three different reaction schemes have been suggested:

(a) Decomposition-WGS sequence. In this scheme, CO is believed to be a primary product from methanol decomposition, subsequently converted into $CO_2$ by the WGS reaction, accompanied by more $H_2$ formation. The decomposition step may be the rate-limiting step:

$$CH_3OH(l) \rightarrow CO + 2H_2 \ \Delta H_r^o = 128kJ \cdot mol^{-1}$$

$$CO + H_2O(g) \rightarrow CO_2 + H_2 \ \Delta H_r^o = -41.2kJ \cdot mol^{-1}$$

However, Amphlett *et al.* have noted that carbon monoxide production is less than what is predicted from equilibrium [62] over the commercial $Cu/Zn/Al_2O_3$ catalyst.

As a result, they have revised their reaction scheme to one based exclusively on the steam reforming of methanol, which is written by the following overall reaction,

$$CH_3OH + H_2O \rightarrow CO_2 + 3H_2$$

The ratio of $CO_2/CO$ was adjusted by the reverse WGS reaction, which can happen independently, by the reaction of $CO_2$ and $H_2$, especially at high temperatures.

(b) Methyl formate reaction route, in which no CO takes part.

$$2CH_3OH \rightarrow HCOOCH_3 + 2H_2$$

$$HCOOCH_3 + H_2O \rightarrow CH_3OH + HCOOH$$

$$HCOOH \rightarrow CO_2 + H_2$$

The kinetic study by Jiang *et al.*[63] using $Cu/Zn/Al_2O_3$ catalysts from BASF suggested that methanol dehydrogenation controls the rate of SRM. The little amount of CO in the product was suggested to be produced by decomposition of methyl formate:

$$HCOOCH_3 \rightarrow CO + CH_3OH$$ .

(c) A third scheme was proposed by Takezawa *et al.* [64] to explain the different processes for products obtained over monometallic Pd and alloy PdZn catalysts:

$$CH_3OH \rightarrow HCHO \rightarrow CO \overset{H_2O}{\rightarrow} CO_2 + H_2 \quad \text{(Over Pd)}$$

$$CH_3OH \rightarrow HCHO \overset{H_2O}{\rightarrow} HCOOH \rightarrow CO_2 + H_2 \quad \text{(Over Pd-Zn Alloy).}$$

It is obvious that the difference is due to the difference in the reactivity of the aldehyde intermediate species formed during the course of the reaction.

Figure 1.1 [65] illustrates ways in which $CH_3OH$, in the presence of $H_2O$, can be converted into CO, $CO_2$ and $H_2$.

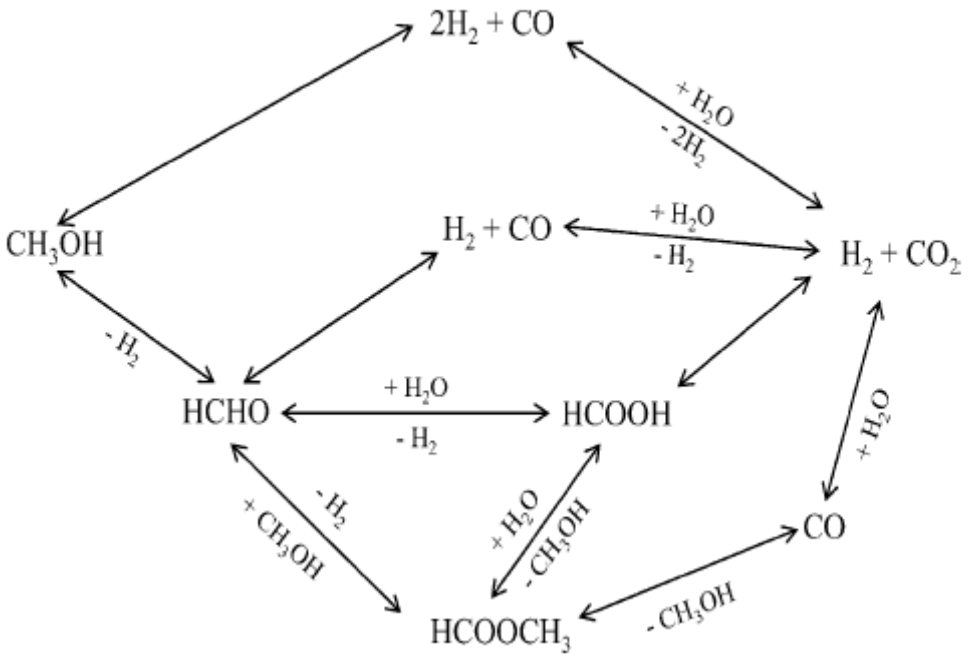


Figure 1.1 Possible reaction pathways for SRM

Furthermore studies in surface science also have revealed that the structures of aldehydes absorbed on IB metals (Cu and Ag) are different from those on Group VIII metals (Rh, Ru, Pt, Pd) [66-69]. They adsorb preferentially in $\eta^1$(O) structure on IB metals, while on Group VIII metals, they exist as $\eta^2$(C, O) structure [70].

It can be seen from the Figure 1.2 that $\eta^1$(O) preserves the molecular identity of HCHO and simply desorbs without decomposition as the temperature is increased. By contrast, the C-C and C-H bonds are rapidly ruptured for $\eta^2$(C, O) structure.

The acid/base surface properties also may have an effect on the reaction pathway. Ranagenethan *et al.* [65] suggested that a Pd/ZnO catalyst favors the reforming reaction due to its higher density of acidic sites. Comparatively, $Pd/CeO_2$ catalyst, which produced a high amount of CO, has a higher density of basic sites, which favors the decomposition reaction. However Niwa *et al.* [71] showed that acidity is a key parameter to control the activity for methanol oxidation. The generated acid sites, possibly Brønsted acid sites, play an important role in the selective oxidation of methanol to formaldehyde. Furthermore, they confirmed that acid sites do not enhance methanol adsorption.

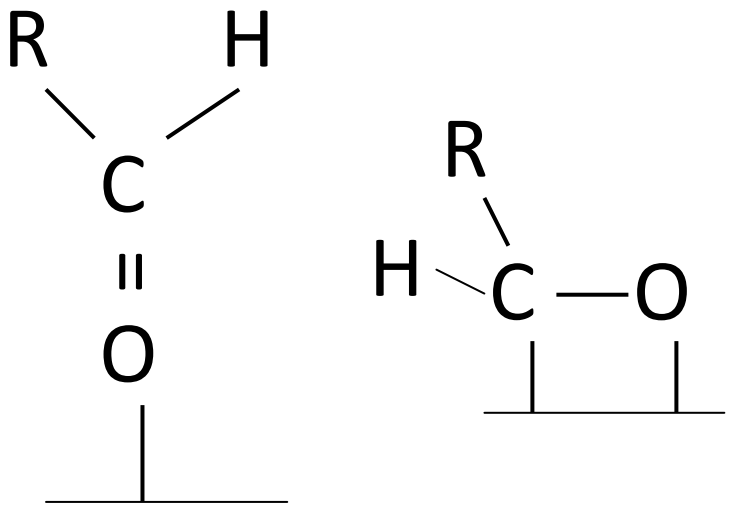


$\eta^1(O)$ $\eta^2(O)$

Figure 1.2 Adsorption structure of $\eta^1(O)$ and $\eta^2(O)$

Regarding the mechanistic investigation of methanol reactions, concerns would be, (1) Whether the methanol pathway is unique to each individual metal; (2) If improved selectivity results through the proper choice of supports or other metal additives, is it a ligand (electronic) or an ensemble (geometric) effect?

### 1.3 Hydrogen production through catalytic decomposition of formic acid

Formic acid is more attractive among various liquid fuels for portable fuel cell equipment. It has better oxidation kinetics, higher theoretical thermodynamic cell potential and less fuel crossover problems in direct formic acid fuel cells than the direct methanol fuel cells [10, 72].

The investigation of decomposition of formic acid goes back to the early part of the last century [73]. In pioneering work, Mailhe and Sabatier studied the formic acid reaction on various oxides and metals [74] . They observed three different pathways for this reaction, shown in Figure 1.3:

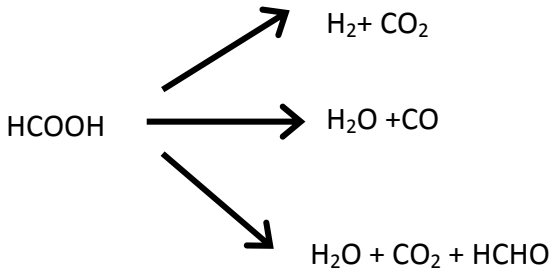


Figure 1.3 Possible reaction pathways in decomposition of formic acid

Since 1936, studies focused on formic acid received wide attention after extensive studies done by Schwab [75] and Rienacker [76], who investigated whether the rate of catalytic reactions on metals was influenced by alloying those metals with others in such a way that the electron concentration increases.

A short review of the literature regarding catalysts for formic acid reaction is presented below. First, the interaction of formic acid with transition metal surfaces in ultrahigh vacuum will be discussed, primarily focusing on Pt, Pd, Au and Cu. Second, catalytic activity of bulk metal oxides will be addressed. Third, metals over metal oxides used for the decomposition of formic acid will be reviewed. While dependent on the experimental conditions, the results vary among groups. Validity or comparison of those results will not be made; rather, the literature will simply be discussed to provide a brief understanding of previous research.

*1.3.1 Formic acid interaction with metals in ultrahigh vacuum*

The reaction of formic acid with metals became a popular topic due to the desire to understand the fundamental aspects of heterogeneous catalysts, for which formic acid decomposition serves as a simple model reaction.

The advantage of an ultrahigh vacuum and its concomitant surface analysis methods allows the exploration of the mechanism and intermediates of these paths at the molecular level under well defined conditions. Thermal desorption of molecular formic acid has been carried out for many metals. Thermal desorption spectroscopy, like temperature programmed desorption, along with temperature programmed reaction spectroscopy, facilitate our understanding of the interaction of the molecule of interest with the surface as a function of surface temperature [77, 78].

The well known volcano- shaped dependence was obtained for the decomposition of formic acid over different metals and activities were correlated with the heats of formation of the corresponding bulk metal formates. Pt and Re are the most active catalysts, followed by Pd, Ru and Ir. Interestingly, gold was found to be weakly active [79]. This weak activity is due to the fact that bulk metallic gold was used instead of highly dispersed gold species. In this section, Pt, Pd, Cu and Au are discussed as relevant to this thesis. Comprehensive reviews have been made by Madix [77] and Thiel [78]

1.3.1.1 Platinum

Formic acid decomposition on clean Pt(100) surface was not found, while $CO_2$ (310 K) and $H_2O$ (180 K, 310 K) were observed on oxygen pre-dosed surfaces [80]. Madix investigated DCOOH absorption with Pt (111) surface and reported the desorption of $CO_2$ (265 K, 361 K, 426 K), $H_2O$, $D_2O$ and HDO (265 K, 295 K), $H_2$, $D_2$ and HD (310 K - 320 K), and CO (473 K, 531 K) from exposure to DCOOH at 195K [81]. Columbia and Thiel reported only $CO_2$ (260 K) and $H_2$

(360 K - 370 K) as desorption products following the adsorption of HCOOH at 130 K [82]. HREEL spectra indicated the formation of bridging formate on Pt (110) and Pt (111) [83-85].

Although Avery *et al.* identified the existence of monodentate formate on oxygen covered Pt (111) after dosing formic acid at 130 K, he also observed the conversion from monodentate to the bridging formate over a short time period [83, 84].

Co-adsorption has also been investigated on Pt surfaces. As mentioned above, the HCOOH adsorption and desorption was enhanced (by a factor of 4-7) over the catalyst pre-dosed with oxygen, or oxygen-covered Pt surfaces [81]. But co-adsorption of other molecules, like $H_2O$ and CO, will suppresses the decomposition of formic acid, because, simply, the sites necessary for deprotonation are blocked [86, 87].

#### 1.3.1.2 Palladium

Pd(100) showed unexpected results: the desorption products are CO and $H_2$. It followed neither the dehydrogenation nor the dehydration pathways [88-90]. The surface spectroscopy investigations failed to agree with each other based on the techniques used. Jorgensen and Madix identified vibrations associated with molecular HCOOH prior to its desorption, a CO loss appears and remains as the only loss after molecular desorption is completed [88]. Solymosi and Kovacs found hydrogen and small amounts of water as desorption products, but their spectroscopic evidence indicated no intermediates existing under these conditions [89]. Sander and Erley reported desorption of small quantities of $CO_2$ and $H_2O$ (180 K), and large amounts of $H_2$ (330 K- 350 K), and CO (480 K), but they failed to track any intermediate through FTIR spectra analysis except for molecular HCOOH vibration [90]. Interestingly, Jorgensen and Madix found the presence of formate on an oxygen-covered Pd (100) surface. Furthermore, they observed the production of $CO_2$ at 265K. Formate was also identified by Photoelectron Spectroscopy (PES) on Pd( 100) covered with Na atoms [91]. This suggests that either oxygen pre-dose or K addition can enhance and stabilize the formate.

#### 1.3.1.3 Copper

$CO_2$ and $H_2$ are the only products from exposure to formic acid of clean Cu(110) at temperatures above 200K. $H_2$ desorbed in two temperature ranges, 270 K - 280 K and 450 K - 475 K; the latter temperature range matched the desorption range of $CO_2$ [92, 93]. Hayden et al. confirmed the bridging formate on Cu (110) by using Infrared Reflection Absorption Spectroscopy (IRAS) [94].

The co-adsorption of atomic oxygen with HCOOH on Cu (110) will increase the amount of formate formed, but inhibit the formation of low-temperature hydrogen since the consumption of protons with oxygen will form water, instead of recombination of protons to form hydrogen [95]. Co-adsorbed C atoms facilitate the decomposition of formate; at the same time, the formation of surface carbonate cannot be avoided at the higher C coverage [96].

The adsorption configuration of formic acid over Cu (100) remains inconclusive. Surface extended and near-edge X-ray analysis of fine structure, combined with photoelectron diffraction showed O atoms pointing toward next-nearest-neighbors [97, 98]. High Resolution Electron Energy Loss Spectroscopy (HREELS) data, as well as theoretical calculations suggested the bridging geometry is dominant [99, 100].

#### 1.3.1.4 Gold

Few studies are available about formic acid adsorption and reaction over gold single crystal surfaces. Outka and Madix reported no formic acid decomposition from clean Au(110). However, desorption of $H_2O$ (200 K, 340 K) and $CO_2$ (340 K), and molecular desorption of formic acid (340 K) were observed on oxygen covered Au(110) [101, 102]. Chtaib *et al.* reported the desorption of $CO_2$ and $H_2$ (180 K) along with the adsorption of HCOOH on polycrystalline Au [103].

Carbon and oxygen XP spectra confirmed the formation of formate species over the gold surface [104]. Similar results were reported by the same group over Au(110) surface through the HREEL spectra [105].

A pressure gap exists between surface science evidence and heterogeneous catalysis, but the fact that group IB and VIII metals are active for formic acid reaction is common to both.

### *1.3.2 Formic acid interaction with metal oxides*

Formic acid has been extensively employed to probe the acidic, basic or redox nature of the surface active sites of oxides. The reason is because of the commonality of the chemisorbed formate intermediate on almost every surface. Although formic acid will tend to be transformed because of its ability to dimerize, the dissociative adsorption is unimolecular and has a similar bonding structure over most oxides [106].

Systematic investigations of more than 40 metal oxides in power form were conducted by Fein and Wachs [107]. They proposed that there are almost no correlations between the following chemical properties; $H_2$-TPR onset temperature and the enthalpies of formation of bulk metal oxides; TOFs and $H_2$-TPR onset temperature; and TOFs and the isotopic dioxygen exchange rates with the metal oxide lattice oxygen. Weakly inverse correlations were found for TOFs versus the enthalpies of formation of bulk metal oxides. They also demonstrated a strong inverse relationship between TOFs and the surface formate decomposition temperature.

Ceria has a fluorite-type crystal lattice [108]. $CeO_2$ (111) and (100) surfaces are shown in Figure 1.4. The large shaded spheres represent oxygen anions, and the smaller unshaded spheres represent $Ce^{4+}$ cations [109].

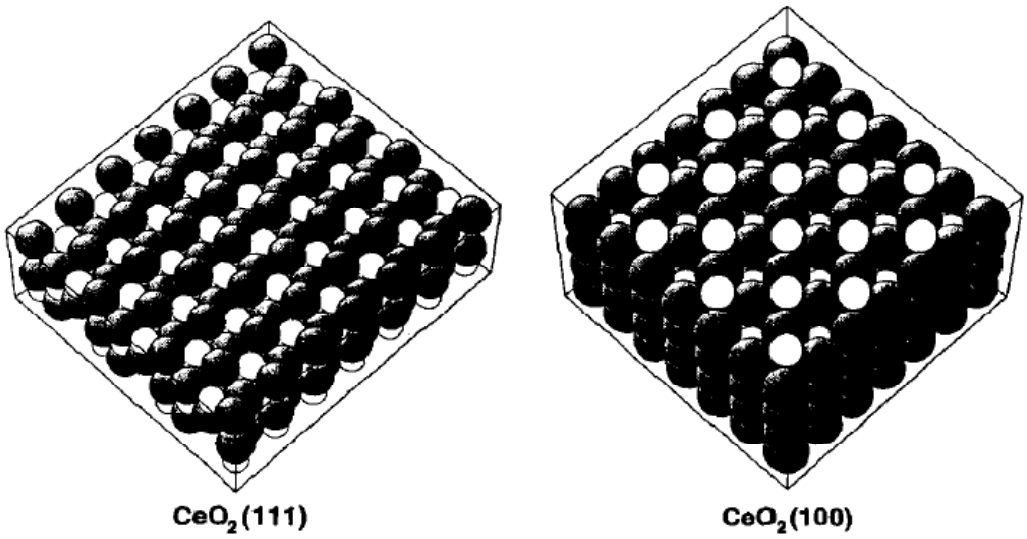


Figure 1.4 Schematic diagrams of the ideal terminations of the $CeO_2$ (111) and $CeO_2$ (100) surfaces

$CeO_2$ (111) surface has hexagonal symmetry and is composed of an outer layer of $O^{-2}$ anions. The second layer of $Ce^{4+}$ cations are also exposed on the surface. Both cations and anions individually have one vacany in their coordination spheres relative to that in the bulk. The $CeO_2$ (100) surface has fourfold symmetry and also has cations and anions exposed. However, the $O^{-2}$ anions are fully coordinated, while the $Ce^{4+}$cations have four coordination vacancies. TPD and HREELS study of formic acid dosed on $CeO_2$ (111) and $CeO_2$ (100) was carried out to check whether the ease of reduction of oxide is the principal factor to determine the product distribution. Vohs's group [109] concluded that desorption of formic acid is similar on both $CeO_2$ surfaces, as well as the presence of monodentate formate is found on both. $CO_2$, CO, $H_2O$ and trace amounts of formaldehyde were produced, according to the dehydration pathway. Further studies investigating pre-treatment effects on $CeO_2$ (111) were extended to fully oxidized and highly reduced $CeO_2$ (111). Senanayake *et al.* [110] suggested that on oxidized $CeO_2$ (111) surface, besides the formation of water, $H_2$ and $CO_2$ are formed at 350 K and, predominantly, CO is produced above 400 K. On reduced $CeO_2$ (111), only CO and $H_2$ were the dominant products, as found by using various characterization methods, like C soft X-way Photoelectron Spectroscopy (sXPS) , temperature programmed desorption and Near Edge X-ray Absorption

Fine Structure (NEXAFS). Similar results were further confirmed through Reflection Absorption Infrared Spectroscopy (RAIRS) and DFT calculations [111].

### *1.3.3 Decomposition of formic acid over supported metal catalysts*

Nickel- and copper- based catalysts have been studied for formic acid decomposition. Iglesia and Boudart carried out a detailed investigation of decomposition of formic acid using Ni, Cu and Ni/Cu catalysts. They suggested that over copper catalysts, the turnover frequency for formic acid decomposition was independent of the concentrations of the decomposition products (CO, $CO_2$ and $H_2$), the metal loading, the metal dispersion and the choice of supports ($SiO_2$ and $Al_2O_3$) [112-114]. Falconer *et al.* studied the formic acid decomposition reaction over Ni/$SiO_2$ at atmospheric pressure, and they indicated that the metal oxides followed the same reaction pathway as seen for single nickel crystals in an ultrahigh vacuum system [115]. Solymosi and Erdohelyi performed a detailed study of the formic acid reaction over Rh supported catalysts. They observed that hydrogen selectivity was higher for Rh on $Al_2O_3$, MgO and $SiO_2$, compared with that on $TiO_2$. They also reported that the reaction order was equal to one, which indicated that adsorption of formic acid was the rate determining step [116].

Besides oxides, other supports like carbon and carbide were also reported for formic acid reaction. Ross *et al.* reported that Pd/C is more active than Au/$TiO_2$ for decomposition and reforming of formic acid, with selectivity of 95-99% above 400 K [117]. Zhou *et al.* observed that the addition of Pd to Au/C and Ag/C would enhance the activity and selectivity; simply explaining it as the formation of a surface alloy [118]. Pioneering work from Boudart reported platinum-like activity of $Mo_2C$ [119]. Koos *et al.* reported that the $Mo_2C$ prepared by the reaction of $MoO_3$ with multiwalled carbon nanotubes displayed higher activity [120]. Also Mullins reported that a new pathway exists over Pt modified $Mo_2C$ [121]. Hydrogen production that is free of CO was also obtained in the reforming of formic acid over Ir/Carbon from 383 K to 473 K [122].

Bimetallic catalysts were also widely investigated in formic acid reaction under liquid phase conditions. Recently Ag-Pd core-shell nano-catalysts were reported to catalyze formic acid

decomposition at room temperature. By controlling the layer of Pd atoms on Ag core, the palladium shell contains terrace sites that are electronically enhanced by the Ag core [123].

Few reports exist for gold-based catalysts. Ojeda and Iglesia recently showed that gold nanoparticles with the average particle size around 3-5 nm supported on alumina had significant higher activity compared with platinum nanoparticles on the same support [124]. But they attributed the activity to TEM-invisible sub-nm gold clusters on the alumina surface. Gazsi *et al.* examined gold deposited selectivity to $CO_2$ was enhanced with the addition of water, since the water gas shift reaction was on six different supports ($SiO_2$, $CeO_2$, $Al_2O_3$, ZSM-5, $TiO_2$ and carbon), and concluded that the reaction pathways of the decomposition of formic acid were influenced by the nature of the supports: dehydrogenation pathway is dominant over gold deposited on $SiO_2$, $CeO_2$ and carbon[125]. Bulushev *et al.* investigated the formic acid reaction over Au/C and Au/$TiO_2$ and claimed that needed [117].

### *1.3.4 Mechanistic investigation on decomposition of formic acid*

Although the formation of formate species was independent of the surface properties, three surface bonding structures of formates have been reported [107] : monodentate, bidentate, and surface bridging configuration, shown in Figure 1.5.

As indicated above, decomposition of formic acid follows two principal pathways, (i) dehydrogenation, $HCOOH \rightarrow CO_2 + H_2$ and (ii) dehydration, $HCOOH \rightarrow CO + H_2O$.

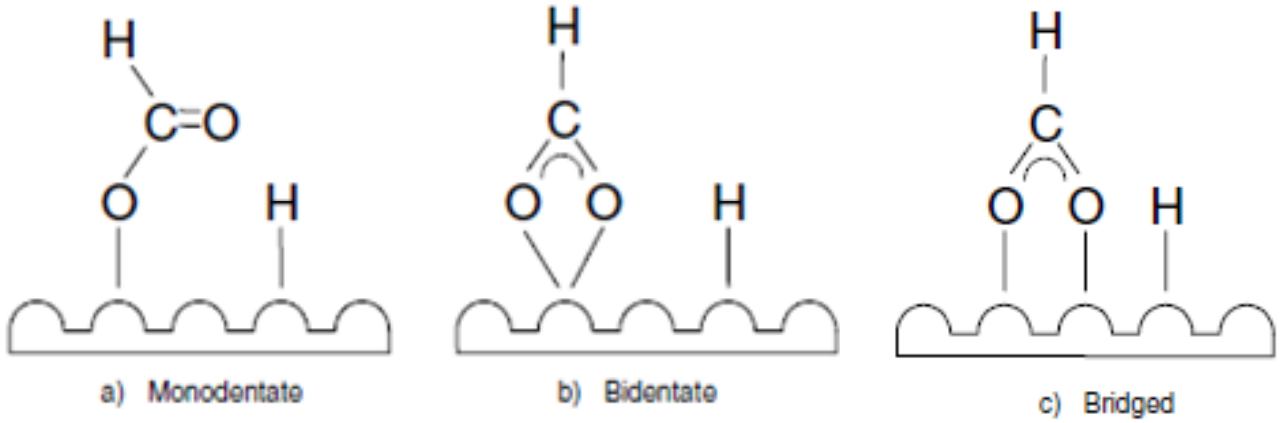


Figure 1.5 Scheme of dissociative adsorption of formic acid on the catalyst surface

In general, on metals, the dehydrogenation reaction is observed almost exclusively. On metal oxides, the reaction pathway more or less depends on the properties of the oxides. On $Al_2O_3$ [126] and $SiO_2$ [127], the dehydration pathway prevails; while on MgO [128] and $ZrO_2$ [129], the dehydrogenation pathway dominates. On $Cr_2O_3$ [130] and $Fe_2O_3$ [131], the reaction pathway becomes complicated since both pathways take place simultaneously. Considerable progress has been made to elucidate the reaction mechanism using many characterization methods such as infrared spectroscopy, isotopic kinetic studies, and adsorption measurements during surface reactions.

IR spectroscopy coupled in many cases with isotope use, as with deuterated formic acid (DCOOD, DCOOH, and HCOOD), has been widely used to reveal some aspects of mechanism of the catalytic reactions. The IR spectra on those oxides, recorded at room temperature, showed the existence of adsorbed formic acid as well as the characteristic formate species, their bands disappearing as temperature was increased [132]. Also the IR study of decomposition of gaseous HCOOD on ZnO and MgO surface shows that only HD is present in the gas phase. Also due to the instability of the C-H bond in the formate species, it has been suggested that the desorption of $CO_2$ from the surface is the slowest step in the formate decomposition [129].

Although IR spectroscopy has demonstrated different adsorbed species, it can not be used to prove the participation in rate-determining steps. Kinetic investigations should complement these studies. One way is to compare the rate of decomposition of formic acid with the thermal

decomposition of the corresponding metal formate. Mars *et al.* [133] found approximately linear relationship between the thermal stability of the formate and the temperature at which decomposition rate of the formic acid on the corresponding oxide reached a fixed value (1.6 X $10^{14}$ molecules/cm$^2$/sec). There are two drawbacks of this approach. First, the temperature at which the decomposition of a salt began was not a reliable indication of its thermodynamic stability [134]. In some cases, the reaction is thermodynamically favored but cannot be observed, because of kinetics limitations. Second, depending on different reaction sequences, various rates should have been selected for comparison. However, correlation came from using the temperature at which the decomposition of formic acid over different catalysts reached pre-established values.

The kinetic isotope effect (KIE) is the ratio of reaction rates of two different isotopically labeled molecules in a chemical reaction. A KIE involving hydrogen and deuterium is represented as:

$$KIE = \frac{k_H}{k_D}$$

Here $k_H$ and $k_D$ are reaction rate constants.

The term, primary isotope effect, is used when the isotopic replacement is in a chemical bond that is broken or formed in a rate limiting step during which isotopic substitution can significantly modify the reaction rate. Conversely, a smaller rate change will occur if the substitution is not involved in the bond that is breaking or forming, which is called the secondary isotope effect. Also, the magnitude of the kinetic isotope effect can be used to elucidate the reaction mechanism. However, if other steps are partially rate-determining, the effect of isotopic substitution will be masked; this approach only works well for simple molecules [135].

The kinetic isotope effect has been widely used by Iglesia's group [124, 136-138]. They extended this approach to almost every simple but significant reaction they investigated, like methane activation, NO oxidation, and methanol reactions. Recently, they used this approach to investigate formic acid decomposition on Au-$Al_2O_3$ and concluded that the dehydrogenation pathway prevailed over this catalyst [124].

As discussed here, although formic acid is a very simple molecule, it is still difficult to clearly elucidate the mechanism without the help of comprehensive characterization, and we cannot expect one technique alone to delineate the reaction pathways for this system.

### 1.4 Thesis rationale and objectives

The general goals of my dissertation were: (1) to design precious metal clusters (Au, Pt and Pd) for the activation reaction of methanol and formic acid; and (2) to elucidate the role of supports (especially $CeO_2$) in stabilizing these metal clusters. The following objectives have been addressed in detail:

(a) Develop gold-ceria as a new catalyst for the steam reforming of methanol; elucidate the reaction pathway over gold-based catalysts; and compare the differences between Group IB metals (Au, Cu) with Group VIII metals (Pd, Pt) supported on ceria for the methanol reactions

(b) Investigate alkali effects on methanol and formic acid reactions over platinum supported on inert supports ($SiO_2$)

(c) Identify the role of metal clusters: One is well dispersed IB metals (Au, Cu) on ceria, and the other is sodium stabilized platinum on silica for methanol and formic acid reactions; and explore the common features between those two catalyst types and their catalytic activity/selectivity.

(d) Conduct extensive parametric studies with selected catalyst compositions, determining the effect of preparation methods, addition of a promoter, and feed gas composition on the activity and selectivity of the catalysts.

(e) Propose a mechanism for methanol steam reforming and decomposition of formic acid over gold-based and platinum-based catalysts.

## 1.5 References


[1] N. Armaroli, V. Balzani, *Angew. Chem. Int. Ed*. 46 (2007) 52.

[2] A. Gore, *Our Choice: A Plan to Solve the Climate Crisis*, Rodale Inc. New York, 2009.

[3] *New Science for a Secure and Sustainable Energy Future,* Department of Energy, 2008.

[4] C. H. Bartholomew, R. J. Farrauto, *Fundamentals of Industrial Catalytic Processes*, Wiley, 2006.

[5] R. M. Navarro, M. C. Alvarez-Galván, J. A. V. de la Mano, S. M. Al-Zahrani, J. L. G. Fierro, *Engergy Envrion. Sci.* 3 (2010) 1865.

[6] R. M. Navarro, M.A. Peña, J. L. G. Fierro, *Chem. Rev.* 107 (2007) 3952.

[7] Information from World LP Gas Association. Available link through: *www. Worldlpgas.com*

[8] A. Haryanto, S. Fernando, N. Murali, S. Adhikari, *Energy Fuels* 19 (2005) 2098.

[9] D. R. Palo, R. A. Dagle, J. D. Holladay, *Chem. Rev.* 107 (2007) 3992.

[10] X. Yu, P. G. Pickup, *J. Power Sources* 182 (2008) 124.

[11] M. Peters, B. Köhler, W. Kuckshinrichs, W. Leitner, P. Markewitz, T. E. Müller, *ChemSusChem* 4 (2011) 1216.

[12] S. Enthaler, *ChemSusChem* 1 (2008) 801.

[13] J. Agrell, B. Lindström, L. J. Pettersson, S. G. Järås, Chapter 3, *Catalysis*, Vol.16, The Royal Society of Chemistry, 2002.

[14] M. Badlani, I. E. Wachs, *Catal. Lett.* 75(2001) 137.

**[**15] P. J. de Wild, M. J. F. M. Verhaak, *Catal. Today* 60 (2000) 3.

[16] S. Sá, H. Silva, L. Brandão, J. M. Sousa, A. Mendes, *Appl. Catal. B* 99 (2010) 43.

[17] S. Hughs, *Deactivition of Catalysts*, Academic Press, New York, 1994.

[18] P. L. Hansen, J. B. Wagner, S. Helveg, J. R. Rostrup-Nielsen, B. S. Clausen, H.Topsøe, *Science* 295 (2002) 2053.

[19] K. Kiler, *Appl. Surf. Sci.* 19(1984) 267.

[20] J. Nakamura, I. Nakamura, T. Uchijima, T. Wantanabe, T. Fujitani, *Stud. Surf. Sci. Catal.* 101 (1996) 1389.

[21] W. Dow, W. Y. Wang, T. Huang, *J. Catal.* 184(1999) 357.

[22] Y. F. Li, X. F. Dong, W. –M. Lin, *Int. J. Hydrogen Energy* 29(2004) 1617.

[23] I. A. Fisher, A. T. Bell, *J. Catal.* 184 (1999) 357.

[24] S. Velu, K. Suzuri, M. Okazaki, M. P. Kapoor, T. Osaki, D. Ohashi, *J. Catal.* 194 (2000) 373.

[25] W. H. Cheng, I. Chen, J. Liou, S. S. Lin, *Top. Catal.* 22 (2003) 225.

[26] S. Patel, K.K. Pant, *J. Power Sources* 159 (2006) 139.

[27] W. Cheng, I. Chen, J. Liou, S. Lin, *Top. Catal.* 22(2003) 225.

[28] A. Trovarelli, *Catalysis by Ceria and Related Materials*. Imperial College Press, 2002.

[29] Y. Liu, T. Hayakawa, K. Suzuki, S. Hamakawa, T. Tsunoda, T. Ishii, M. Kumagai, *Appl.Catal. A* 223 (2002) 137.

[30] P. Pyykkö, *Angew. Chem. Int. Ed*. 43 (2004) 4412.

[31] A. S. K. Hashmi, G. J. Hutchings, *Angew. Chem. Int. Ed*. 45 (2006) 7896.

[32] G. C. Bond, C. Louis, D. T. Thompson*, Catalysis by Gold*, ImperialCollege Press, 2006.

[33] Q. Fu, H. Saltsburg, M. Flytzani-Stephanopoulos, *Science* 301(2003) 935.

[34] W. Deng, C. Carpenter, N. Yi, M. Flytzani-Stephanopoulos, *Top. Catal*. 44 (2007) 199.

[35] M. Bowker, L. Millard, J. Greaves, D. James, J. Soares, *Gold Bulletin* 37 (2004) 170.

[36] F. W. Chang, H. Y. Yu, L. S. Roselin, H. C. Yang, *Appl. Catal. A* 290 (2005) 138.

[37] T. Takahashi, M. Inoue, T. Kai, *Appl. Catal. A* 218 (2001) 189.

[38] N. Iwasa, N. Takezawa, *Top. Catal.* 22 (2003) 215.

[39] Y. Suwa, S. Ito, S. Kameoka, K. Tomishige, K. Kunimori, *Appl. Catal. A* 267 (2004) 9.

[40] K. H. Lim, Z. X. Chen, K. M. Neyman, N. Rösch, *J. Phys. Chem. C* 110(2006) 14890.

[41] N. Iwasa, S. Masuda, N. Ogawa, N. Takezawa, *Appl. Catal. A* 125 (1995) 145.

[42] N. Iwasa, T. Mayanagi, N. Ogawa, K. Sakata, N. Takezawa, *Catal. Lett.* 54(1998) 119.

[43] G. Xia, J. D. Holladay, R. A. Dagle, E. O. Jones, Y. Wang, *Chem. Eng. Technol*. 28 (2005) 515.

[44] N. Iwasa, T. Mayanagi, N. Wataru, M. Arai, T. Takewasa, *Appl. Catal. A* 248(2003) 153.

[45] S. Penner, B. Jenewein, H. Gabasch, B. Klotzer, D. Wang, A. Knop-Gericke, R. Schlogl, K. Hayek, *J. Catal.* 241(2006) 14.

[46] R. A. Dagle, A. Platon, D. R. Palo, A. K. Datye, J. M. Vohs, Y. Wang, *Appl. Catal. A* 342 (2008) 63.

[47] J. Agrell, G. Germani, S. Jaras, M. Boutonnet, *Appl. Catal. A* 242 (2003) 233.

[48] A. Karim, T. Conant, A. Datye, *J. Catal.* 243 (2006) 420.

[49] J. Papavasiliou, G. Avgouropoulos, T. Ioannides, *Appl. Catal. B* 69 (2006) 226.

[50] H.Oguchi, T. Nishiguchi, T. Matsumoto, H. Kanai, K.Utani, Y. Matsunura, S. Imamure, *Appl. Catal. A* 281(2005) 69.

[51] I. Ritzkopf, S. Vukojević, C. Weidenthaler, J. –D Grunwaldt, F. Schüth, *Appl. Catal. A* 302(2006) 215.

[52] J. Pike, S.-W. Chan, F. Zhang, X.-Q. Wang, J. Hanson, *Appl. Catal. A* 303(2006) 273.

[53] C. Qi, J. C. Amphlett, B. A. Peppley, *J. Power Sources* 171 (2007) 842.

[54] A. Koós, R. Barthos, F. Solymosi, *J. Phys.Chem. C* 112 (2008) 2607.

[55] A. Houteit, H. Mahzoul, P. Ehrburger, P. Bernhardt, P. Légaré, F. Garin, *Appl. Catal. A* 306(2006) 22.

[56] H. Praliaud, M. Primet, G. Martin, *Appl. Surf. Sci*. 17(1983) 107.

[57] K. Urabe, K. Aika, A. Ozaki, *J. Catal*. 32 (1974) 108.

[58] Z. Paál, G. Ertl, S. B. Lee, *Appl. Surf. Sci*. 8 (1981) 231.

[59] F. Solymosi, H. Knözinger, *J. Catal*. 122 (1990) 166.

[60] R.G.S. Pala, H. Metiu, *J. Catal.* 254 (2008) 325.

[61] W. H. Cheng, C. Y. Shiau, T. H. Liu, H. L. Tung, J. F. Lu, C. C. Hsu, *Appl. Catal. A.* 170 (1998) 215.

[62] J. C. Amphlett, R. F. Mann, B. A. Peppley, *Stud. Surf. Sci. Catal.* 81 (1994) 409.

[63] C. J. Jiang, D. L. Trimm, M. S. Wainwright, N. W. Cant, *Appl. Catal. A* 97(1993) 145.

[64] N. Takezawa, N. Iwasa, *Catal. Today* 36(1997) 45.

[65] E. Ranganathen, S. Bej, L. Thompson, *Appl. Catal. A* 289(2005) 153.

[66] B. A. Sexton, *Surf. Sci.* 102 (1981) 271.

[67] I. E. Wachs, R. J. Madix, *J. Catal*. 53 (1978) 208.

[68] H. Luth, G. W. Rubloff, W. D. Grobman, *Surf. Sci*. 63 (1977) 325.

[69] B.J. Xu, X.Y. Liu, J. Haubrich, R. J. Madix, C. M. Friend, *Angew. Chem. Int. Ed*. 48 (2009) 4206.

[70] E. Jeroro, J. M. Vohs, *J. Am. Chem. Soc.* 130 (2008) 10199.

[71] M. Niwa, J. Igarashi, *Catal. Today* 52(1999) 71.

[72] S. Uhm, H. J. Lee, J. Lee, *Phys. Chem. Chem. Phys*. 11(2009) 9326.

[73] P. Mars, J. J. F. Scholten, P. Zwietering, *Advances in Catalysis and Related Subjects*, Vol. 14, Academic Press, 1963.

[74] A. Mailhe. P. Sabatier, *C. R. Acad. Sci., Paris*, 152 (1911) 1212.

[75] G. M. Schwab, *Trans. Faraday Soc*. 42 (1936) 689

[76] G. Rienãcker, B. Barry, *Z. Inorg. Chem.* 257 (1948) 41.

[77] R. J. Madix, *Adv. Catal*. 29 (1980) 1.

[78] M. R. Columbia, P. A. Thiel, *J. Electroanalytical Chem*. 369 (1994) 1.

[79] W. J. M. Rootsaert, W. M. H. Sachtler, *Z. Phys. Chem*. 26 91960) 16.

[80] N. Kizhakevariam, E. M. Stuve, *J. Vac. Sci. Technol. A* 8 (1990) 2557.

[81] N. Abbas, R. J. Madix, *Appl. Surf. Sci*. 16 (1983) 424.

[82] M. R. Columbia, P. A. Thiel, *Surf. Sci*. 235(1990) 53.

[83] N.R. Avery, *Appl. Surf. Sci.* 14 (1982-1983) 149.

[84] N. R. Avery, *Appl. Surf. Sci.* 11-12 (1982) 774.

[85] M. R. Columbia, A. M. Crabtree, P. A. Thiel, *J. Am. Chem. Soc*. 114(1991) 1231.

[86] M. R. Columbia, P. A. Thiel, *Surf. Sci*. 235(1990) 53.

[87] M. R. Columbia, A. M. Crabtree, P. A. Thiel, *J. Electroanal. Chem*. 345(1993) 93.

[88] S. W. Jorgensen, R. J. Madix, *J. Am. Chem. Soc*. 110 (1988) 397.

[89] F. Solymosi, I. Kovacs*, Surf. Sci.*259(1991) 95.

[90] D. Sander, W. Erley, *J. Vac. Sci. Technol. A* 8 (1990) 3367.

[91] C. Egawa, I. Doi, S. Naito, K. Tamaru*, Surf. Sci.* 176 (1986) 491.

[92] M. Bowker, R. J. Madix, *Surf. Sci.* 102(1987) 542.

[93] M. Bowker, E. Rowbotham. F. M. Leibsle, S. Haq, *Surf. Sci*. 349 (1996) 97.

[94] B. E. Hayden, K. Prince, D. P. Woodruff, A. M. Bradshaw, *Surf. Sci*. 133 (1983) 589.

[95] S. Poulston, E. Rowbotham, P. Stone, P. Parlett, M. Bowker, *Catal. Lett*. 52 (1998) 63.

[96] F. C. Henn, J. A. Rodriguez, C. T. Campbell, *Surf. Sci*. 236 (1990) 282.

[97] D. A. Outka, R. J. Madix, J. Stohr, *Surf. Sci*. 164 (1985) 235.

[98] M. D. Crapper, C. E. Riley, D. P. Woodruff, *Phys. Rev. Lett*. 57 (1986) 2598.

[99] S. P. Mehandru, A. B. Anderson, *Surf. Sci*. 219 (1989) 68.

[100] A. Puschmann, J. Haaase, M. D. Crapper, C. E. Riley, D. P. Woodruff, *Phys. Rev. Lett*. 54 (1985) 2250.

[101] D. A. Outka, R.J. Madix, *Surf. Sci*. 179 (1987) 361.

[102] D. A. Outka, R. J. Madix, *J. Am. Soc. Chem*. 109 (1987) 1708.

[103] M. Chtaib, J. P. Delrue, R. Caudano. *Phys. Scr.* T4 (1983) 133.

[104] R. W. Joyner, M. W. Roberts, *Prod. R. Soc. London, Ser A*, 359 (1976) 107.

[105] M. Chtaib, P. A. Thiry, J. P. Delrue, J. J. Pireaux, R. Caudano, *J. Eletron. Spectrosc*. 29 ( 1983) 293.

[106] P. Zielke, M. A. Suhm, *Phys. Chem. Chem. Phys.* 9 (2007) 4528.

[107] D. E. Fein, I. E. Wachs, *J. Catal.* 210 (2002) 242.

[108] Z. L. Wang, X.-D. Feng, *J. Phys.Chem. B* 107(2003) 13563.

[109] J. Stubenrauch, E. Brosha, J. M. Vohs, *Catal. Today* 28 (1996) 431.

[110] S. D. Senanayake, D. R. Mullins, *J. Phys. Chem. C* 112(2008) 9744.

[111] W. O. Gordon, Y. Xu, D. R. Mullins, S. H. Overbury, *Phys. Chem. Chem. Phys.* 11 (2009) 11171.

[112] E. Iglesia, M. Boudart, *J. Catal*. 81 (1993) 214.

[113] E. Iglesia, M. Boudart, *J. Catal*. 81 (1993) 224.

[114] E. Iglesia, M. Boudart, *J. Catal*. 88 (1993) 325.

[115] J. L. Falconer, L. C. Burger, I. P. Corfa, K. G. Wilson, *J. Catal.* 104 (1987) 424.

[116] F. Solymosi, A. Erdohelyi*, J. Catal*. 91 (1985) 327.

[117] D. A. Bulushev, S. Beloshapkin, J. R. H. Ross, *Catal. Today* 154 (2010) 7.

[118] X. Zhou, Y. Huang, W. Xing, C. Liu, J. Liao, T. Lu, *Chem. Commun*. (2008) 3540.

[119] B. Levy, M. Boudart, *Science* 181(1973) 547.

[120] A. Koos, F. Solymosi, *Catal. Lett*. 138 (2010) 23.

[121] D. W. Flaherty, S. P. Berglund, C. B. Mullins, *J. Catal.* 269(2010)33.

[122] F. Solymosi, A. Koos, N. Liliom, I. Ugrai, *J. Catal.* 279 (2001) 213.

[123] K. Tedsree, T. Li, S. Jones, C. W. A. Chan. K. M. K. Yu, P. A. Bagot, E. A. Marquis, G. D. W. Smith, S. C. E. Tsang, *Nat. Nanotech*. 6 (2011) 302.

[124] M. Ojeda, E. Iglesia*, Angew. Chem. Int. Ed.* 48 (2009) 4800.

[125] A. Gazsi, T. Bansagi, F. Solymosi, *J. Phys. Chem. C* 115 (2011) 15459.

[126] G. Patermarakis, *Appl. Catal. A* 252 (2003) 231.

[127] K. Fukuda, Y. Noto, T. Onishi. K. Tamaru. *Trans. Faraday Soc.* 63 (1967) 3072.

[128] H. Nakatsuji, M. Yoshimoto, M. Hada, K. Domen, C. Hirose, *Surf. Sci*. 336(1995) 232.

[129] Y. Noto, K. Fukuda, T. Onishi, K. Tamaru, *Trans. Faraday Soc.* 63 (1967) 3081.

[130] G. M. Schwab, E. Schwab-Agallidia, *J. Am. Soc. Chem*. 71 (1949) 1806.

[131] S. A. Halawy, S. S. Al-Shihry, M. A. Mohamed, *Catal. Lett*. 48 (1997) 247.

[132] P. G. Harrison, B. Maunders, *J. Chem. Soc. Faraday Trans*. 81 (1985) 1345.

[133] P. Mars, J. J. F. Scholten, P. Zwietering, *Advan. Catal.* 14 (1963) 35.

[134] J. M. Trillo, G. Munuear, J. M. Criado, *Catal. Rev*. 7 (1972) 51.

[135] G. M. Schwab, A. M. Watson, *Trans. Faraday Soc. 60*(1964) 1833.

[136] J. Wei, E. Iglesia, *J. Catal.* 224 (2004) 370.

[137] D. K. Kim, E. Iglesia*, J. Phys. Chem. C* 112(2008)17235.

[138] Y. H. Chin, C. Buda, M. Neurock, E. Iglesia, *J. Am. Chem. Soc.* 133 (2011) 15958.

# Chapter 2: Experimental Methods and Procedures

## 2.1 Catalyst preparation

### *2.1.1 Ceria based catalysts*

#### 2.1.1.1 Synthesis of nanoscale ceria

Ceria nanoshapes were prepared by precipitation followed by hydrothermal methods. Typically, 4.5 mmol $Ce(NO_3)_3 \cdot 6H_2O$ (99.5%, Alfa) was dissolved in a 90 mL aqueous NaOH (98%, Alfa) solution with an appropriate concentration ($C_{NaOH}$). The stock solution in a Teflon bottle was stirred at room temperature for 10 min and then sealed tightly in a stainless steel vessel autoclave. The hydrothermal treatment was carried out at different temperatures ($T$) for 24 h. After being cooled down, the obtained white precipitates were collected, washed with deionized (DI) water, and then dried in vacuum at 70 –80 °C overnight. The as-dried yellow powders were air-calcined at 400 °C for 4 h. The applied values of $C_{NaOH}$ and $T$ were varied according to the target crystal shape: (1) Rod: $C_{NaOH}$ = 6 mol/L, $T$ = 100 °C; (2) Cube: $C_{NaOH}$ = 6 mol/L, $T$ = 180 °C; (3) Polyhedron: $C_{NaOH}$ = 0.1 mol/L, $T$ = 180 °C.

#### 2.1.1.2 Synthesis of gold-ceria

3 g $CeO_2$ in powder form was slurred in 150 mL DI water under stirring. 75 mL $(NH_4)_2CO_3$ aqueous solution (1 mol/L) was added. Then, 0.174 mmol $HAuCl_4 \cdot 3H_2O$ (99.99%, Alfa) was dissolved in 75 mL DI water and added into the above solution dropwise. The pH was kept at 8 – 9 during the whole process. The resulting precipitates were aged at room temperature for 1 h and then filtered, washed for three times by DI water at 60 – 70 °C. The product was dried in

vacuum at 70 −80 °C overnight, and then air-calcined at 400 °C for 4 h. The NaCN-leaching was done in 2%NaCN-NaOH (pH 12) aqueous solution at room temperature.

2.1.1.3 Synthesis of platinum-ceria

3 at%Pt-Ceria was prepared by impregnation method using $H_2PtCl_6$ as precursor and choosing different ceria nanoshapes as supports. The product was dried in vacuum at 70 −80 °C overnight, and then air-calcined at 400 °C for 4 h.

2.1.1.4 Synthesis of copper-ceria

Copper-ceria was prepared with the Urea Gelation Co-precipitation (UGC) methods. Typically, take 10%copper-ceria for example, 1.8g copper (II) nitrate (Johnson Matthey Electronics) and 41.1 g ammonium cerium(IV) nitrate (Aldrich) were mixed and dissolved in 600 mL DI- water. This gives an atomic ratio of Ce/Cu of 9:1. Excess urea (72g) was added into the solution under constant stirring and boiling over a hot plate. After the precipitant was produced, DI-water was added to 800 mL, and the solution was kept boiling for 8 h. The precipitate was filtered, washed twice, then dried in vacuum at 120 $^oC$ for 12 h, and crushed to powder before calcination. Samples were heated to 400 $^oC$ in air at 2 $^oC$/min, holding at the final temperature for 4 h.

Another set of copper-ceria was prepared by deposition-precipitation method. Ceria nanorods and nanocubes were chosen as supports. Typically, ceria nanopowders (3 g) were added in 150 mL DI water under stirring. $Cu(NO_3)_2{\cdot}2.5H_2O$ (3.08 mmol, 0.716 g) was dissolved in 75 mL DI water and added into the above $CeO_2$ solution dropwise. The pH was adjusted to 9 during the whole process by adding freshly made sodium carbonate ($Na_2CO_3$, 99.5%, Alfa) buffering solution (0.5 M) dropwise. The resulting precipitates were aged at room temperature for 1 h and then filtered, washed three times with DI water at room temperature. The product was dried in

vacuum at 70 °C overnight, and then air-calcined at 400 °C for 4h. In all air calcinations, the heating rate was 2 °C/min.

An aqueous solution of ammonium carbonate ($(NH_4)_2CO_3$, 2 mol/L) was also used as leaching agent. It was reported that copper oxide would dissolve into ammonium solution, thus it helps to elucidate which copper species is active for the reactions. The $(NH_4)_2CO_3$-leached samples were dried at 120 °C overnight, and then air-calcined at 400 °C for 2h. Hence, these samples were exposed at 400 °C for twice as long as the corresponding parent samples.

*2.1.2 Alkali modified platinum-$SiO_2$*

Pt-$SiO_2$ was prepared by incipient wetness impregnation (IMP) method. $Pt(NH_3)_4(NO_3)_2$ as the precursor was added into $SiO_2$ (Sigma-Aldrich, fumed, $S_{BET}$=243 $m^2/g$, pore volume: 3 ml/g) drop-dip. Sodium was added to the dried and uncalcined sample also by IMP method by using sodium nitrate as precursor. To check the effect of Pt/Na loading sequence, Na was added before/after loading Pt or was co-impregnated with Pt. It was found that there is no difference in catalytic performance by changing the loading sequence. The as-prepared samples were dried at 60 $^oC$ in vacuum overnight and calcined in air at 400 $^oC$ for 4 h.

To investigate the influence of temperature on the Na removal, some samples were washed with deionized-water at 70 $^oC$ for 60 min. This was followed by filtering the suspension and drying the solid at 60 oC in vacuum overnight, further calcining it in static air at 400 $^oC$ for 4 h before testing. A heating rate of 2 $^oC$/min from RT to 400 $^oC$ was used.

## 2.2 Catalyst Characterization

### *2.2.1 Composition*

Bulk composition analysis of the catalysts was conducted in an inductively coupled plasma optical emission spectrometer (ICP-OES, Leeman Labs Inc.).

### *2.2.2 Surface area*

The BET surface area was determined by single-point $N_2$ adsorption/desorption cycles in a Micromeritics AutoChem II 2920. The as-calcined (400 °C, air) samples were pretreated in He at 300°C for 0.5 h before tests.

The physical properties along with the synthesis methods of the samples investigated in this thesis are listed in Table 2.1

### *2.2.3 X-ray Photoelectron Spectroscopy (XPS)*

A Kratos AXIS Ultra Imaging X-ray Photoelectron Spectrometer (XPS) with a resolution of 0.1 eV was used to determine the atomic metal ratios of the surface region and the metal oxidation states. Samples in powder form were pressed on a double-sided adhesive copper tape for analysis. All measurements were carried out at room temperature without any sample pre-treatment. An Al Kα X-ray source was used in this work. All binding energies were calibrated with the C 1s peak at 285.0 eV.

*2.2.4 Electron microscopy*

Transmission electron microscopy (TEM) and high-resolution TEM (HREM) were performed on a JEOL 200cx and JEOL 2010 at 200 kV, respectively. The TEM samples were prepared by drying an ethanol suspension containing dispersed catalyst powders on carbon film-coated copper grids.

HAADF images were done with an aberration-corrected STEM fitted with an electron monochromator, a Zeiss Libra 200-80 MC operating at 200kV with the detector acceptance angle for the imaging of 24 mRad at the Center for Nanoscale Systems, Harvard University. The samples were suspended in n-hexane and loaded on carbon grids.

*2.2.5 X-ray Absorption Spectroscopy(XAS)*

X-ray absorption near edge spectroscopy (XANES) was employed to examine the oxidation state of various gold-ceria under different conditions. XANES was conducted over selected gold-ceria samples under the methanol and pre-reduction conditions. The spectra were collected using the beamline X18B of the National Synchrotron Light Source (NSLS) at Brookhaven National Laboratory (BNL). For the fresh sample, each catalyst sample was pressed on a Kapton tape as a thin film. In the *ex-situ* experiments, the sample was loaded into polyimide tube microreactor ( 0.123 I.D.) with quartz blocking both ends of catalyst bed to prevent the catalyst powder's movement, only allowing gas to flow through the tube. The spectra were taken in the "fluorescence-yield model" by a Ge 13-element detector. The detector was placed at a position 90 degrees with respect to the incident beam. The sample was placed at 45 degrees both to the incident beam and the Ge detector. The reported XANES data are the averages of three scans (lasting approximately 30 min/scan), and no changes were detected between the first and the last scan.

*2.2.6 Temperature Programmed Desorption (TPD)*

Samples were first pre-reduced in 20%$H_2$-He flowing at 70 mL·min$^{-1}$. Different absorbents (methanol, formic acid, carbon monoxide or carbon dioxide) were introduced into the system by flowing the mixture of absorbent and pure helium. Until completion of the adsorption, the samples were purged with pure helium to clean the residual gases before each test. The temperature was heated from RT to final temperature with a heating rate of 5 $^{o}$C/min in the pure helium. The different adsorbents are 5%CO/He, 2%$CO_2$/He, 16%$CH_3OH$/He (generated from the methanol bubbler), 3.3% HCOOH/He and 2.0%$CH_3OH$/2.6%$H_2O$/ He (generated by the mixture of corresponding higher purity liquid solution and injected by a syringe pump).The outlet gas was analyzed on-line by a quadruple residual gas analyzer (MKS model RS-1).

*2.2.7 Temperature Programmed Surface Reactions (TPSRs)*

Samples were pretreated as TPD tests. In $CH_3OH$-TPSR, the mixture of methanol was produced by flowing pure helium through methanol bubbler which was kept at 25 $^{o}$C. In HCOOH-TPSR, 3.3% formic acid was injected into the pre-heated pure helium stream by liquid pump. In $CH_3OH$+$H_2O$-TPSR, the mixture of methanol and water was also generated by flowing pure helium through a liquid bubbler filled with methanol and water. The outlet gas was also analyzed on-line by a quadruple residual gas analyzer (MKS model RS-1).

**2.3 Activity evaluation**

All catalytic performance evaluations were performed in a home-made microreactor at atmospheric pressure with a loading of 100 mg catalyst powders. To avoid undesired hot spots in the catalytic bed, the catalysts were diluted with quartz powder. In typical catalytic tests, the total flow rate was set as 70 mL·min$^{-1}$, giving a space velocity (GHSV) of 42,000 h$^{-1}$ in most light-off tests. In catalytic performance test, temperature was kept at each temperature for 1.5

hours before heating up. The kinetics measurements were operated by keeping methanol or formic acid conversion below 15%. The adjustable parameters were either the loading amount of sample or the flow rate, depending on the test temperature. The feed and product gases were analyzed on-line by a residual gas analyzer (MKS model RS-1).

*2.3.1 Decomposition of methanol*

The feed was constituted of a mixture of $CH_3OH$ /He with a molar ratio of 16/84 and was generated by flowing pure helium through methanol bubbler, which was kept at 25 $^oC$. The change of methanol concentration was modulated by changing the flow rate through liquid pump. The conversion of methanol was calculated by the equation:

$$CH_3OH_{conversion} = \frac{P_0 - P_T}{P_0} \times 100$$

, where $P_0$ is the initial partial pressure of methanol which was calibrated daily before testing, and $P_T$ is the partial pressure of methanol at a given temperature.

*2.3.2 Steam reforming of methanol*

A mixture of methanol and water was injected into the flowing gas by a syringe pump and vaporized in the heated gas line before entering the reactor. The feed gas comprised of a mixture of $CH_3OH/H_2O$/He with a molar ratio of 2/2.6/95.4.

*2.3.3 Decomposition of formic acid*

3.3 mol% HCOOH balanced with pure helium was generated by injecting formic acid (Acros, 99% pure) into the pre-heated gas line through liquid pump. The effect of water or carbon

monoxides was carried out by maintaining the formic acid concentration at 3.3 mol %. The same flow rate of pure helium was replaced by either 3%$H_2O$/Helium (by flowing pure helium through water bubbler at room temperature) or 5%CO/Helium (Airgas premixed gases).

**Table 2.1 Physical properties of ceria- and silica- based materials**

| Samples | $S_{BET}$ ($m^2 \cdot g_{cat}^{-1}$) | Metal Concentration (at%)[a] | Preparation methods |
|---|---|---|---|
| Ceria (Rod) | 105 (54) [b] | N/A | Hydrothermal |
| Ceria (Cube) | 27 (27) [b] | N/A | Hydrothermal |
| Ceria (UGC) | 140 | N/A | UGC |
| 1%Au-Ceria(Rod) | 100 | 0.9(0.5[c]) | Deposition-Precipitation |
| 1%Au-Ceria(Rod) | 24 | 0.9(0.03[c]) | Deposition-Precipitation |
| 15%Cu-Ceria(Rod) | 95 | 14.9(4.5[d]) | Deposition-Precipitation |
| 15%Cu-Ceria(Cube) | 28 | 14.7(6.5[d]) | Deposition-Precipitation |
| 5%Cu-Ceria(UGC) | 115 | 4.6 | UGC |
| 3%Pt-Ceria(Rod) | 98 | 2.9 | IMP |
| 3%Pt-Ceria(Cube) | 23 | 2.7 | IMP |
| 3%Pt-Ceria | 128 | 2.8 | IMP |
| 1%Pd-Ceria | 95 | 0.9 | Coprecipitation |
| $SiO_2$ | 243 | N/A | Sigma-Aldrich[f] |
| 1%Pt-$SiO_2$ | 187 | 1.0 (0.9 [e]) | IMP |
| 3Na-1%Pt-$SiO_2$ | 158 | 1.0 | IMP |

[a] Designed concentration confirmed by ICP-OES analyses;

[b] Specific surface areas in parentheses were calculated based on the nanoparticle size and shape;

[c] After aq. NaCN-leaching;

[d] After 2M $Na_2CO_3$ aq. solution washing;

[e] After DI water washing;

[f] Commercial catalyst (Sigma-Aldrich, fumed).

# Chapter 3: Decomposition of methanol over Group IB and Group VIII metals supported on ceria

The adsorption of methanol over catalysts is the first step of the methanol interaction with the catalyst surface, regardless of whether this occurs through physical or chemical interaction. Decomposition of methanol not only can help us understand the interaction between methanol and catalyst surfaces, but it can also discriminate the different roles of methanol and water in the methanol steam reforming reaction. Temperature programmed reaction couple with mass spectrometry (TPD/MS) was primarily used here, which is a useful approach to elucidate the stable intermediates during the dynamic process and to investigate the surface reactions under realistic conditions [1]. Group IB (Au and Cu) and Group VIII (Pd and Pt) metals supported on ceria were chosen with the goal to discriminate the chemistry between Group IB and Group VIII metals.

## 3.1 Methanol desorption from ceria

The interaction between methanol and single crystal ceria nanoshapes was investigated by $CH_3OH$-Temperture Programmed Desorption (TPD). The ceria nanoshapes (rods and cubes) were prepared by a hydrothermal technique as described in Chapter 2. As shown in Figure 3.1(a), hydrogen and carbon monoxide were eluted simultaneously on the ceria nanorods, which comprise {110} and {100} surfaces. Apparently, these products were due to the decomposition of the methoxy group formed upon adsorption of methanol on the ceria surfaces. On the other hand, weak hydrogen desorption was observed over the {100} ceria cube faces as shown in Figure 3.1(b). Thus, there are different interactions between the {110} and {100} surfaces of ceria with methanol.

Siokou *et al*. [2] studied $CH_3OH$ adsorbed at 300 K on $CeO_2$ films grown on Cu(111). The main desorption products were CO and $H_2$, which desorbed near 580K with smaller amounts of $H_2O$, HCHO, $CH_3OH$ and $CO_2$. It was suggested that the decomposition of a single surface

intermediate, $CH_3O$, gave the products. They also claimed that on a pre-oxidized annealed film, $CO_2$ was formed from the decomposition of HCOO intermediate; however, according to their IR data, they did not find any OH species on the oxide surface.

The reaction of $CH_3OH$ on several different ceria-based model catalysts has been studied extensively. Single crystal $CeO_2(111)$ was made by growing $CeO_2$ on yttria-stabilized zirconia and ceria films on $Al_2O_3$ (0001). Ferrizz *et al.*[3] suggested that the reaction of $CH_3OH$ on ceria surface is highly structure sensitive and depends on the crystallographic orientation, the concentration of surface oxygen vacancies, as well as the oxidation state of surface cerium cations. Methoxide intermediates adsorbed on surface oxygen vacancy sites will dehydrogenate to produce HCHO and surface hydroxyls. The surface hydroxyl will either react with additional methoxides to reform $CH_3OH$ or react to produce $H_2O$. On the other hand, methoxides adsorbed on partially reduced ceria surfaces, possibly on $Ce^{3+}$ sites, undergo complete dehydrogenation to CO and $H_2$.

Mullins *et al.* [4] investigated $CeO_2$ thin films deposited on Ru (0001). sXPS and TPD data showed the relationship between desorption products and Ce oxidation states. $CH_3OH$ reacts at low temperatures with fully oxidized $CeO_2$ to produce $H_2O$ at 200K, but HCHO and $CH_3OH$ desorb near 560K. On reduced $CeO_2$, adsorption of methanol is strong and it undergoes more extensive decomposition producing CO and $H_2$ near 640K, in addition to HCHO and $H_2O$.

Also it is documented that different ceria surfaces have different bonding characteristics, namely the very stable and neutral (111) surface, the less stable, slightly puckered (110) surface, and the higher energy (100) surface [5]. It is generally the case that a less stable surface will be more favorable for the formation of oxygen vacancies and thus more catalytically active. While this is true for (111) and (110) surfaces [6], activity is not necessarily determined by the stability of the pure surfaces. Physically the defective type (100) surface would be unstable and thus undergoes significant rearrangements, which results in a greater energy gain due to the relaxation. According to the model proposed by Wang *et al.* [7], the surface density of atoms in the corresponding planes follows the order of (111) > (100) > (110). The enthalpy of the formation of oxygen vacancies follows the same order [8].

The results indicated that the nanostructure of ceria plays an important role in the interaction between ceria and methanol. Since $CeO_2$ (110) has lower enthalpy of formation of oxygen vacancies, this surface can stabilize a higher number of intermediate methoxy species, compared with $CeO_2$ (100). This result agrees with previous work which used hydrogen as a probe molecule [9] to identify the difference between ceria nanorods comprising (110) and (100) surfaces, and ceria nanocubes, bound by (100) planes.

## 3.2 Methanol decomposition over Group VIII metals (Pd, Pt) on ceria

### *3.2.1 Platinum-ceria: support effect*

The interaction between methanol and ceria was enhanced by the addition of platinum. As shown in Figure 3.2, stronger desorption peaks of carbon monoxide and hydrogen were observed from the Pt-Ceria(rod) at lower temperatures compared with pure ceria. Carbon dioxide desorption also took place. Because of the existence of surface oxygen species, which could be stabilized by the interaction between platinum and ceria [10], the formation of carbon dioxide is attributed to CO oxidation over Pt-Ceria. This is confirmed by the fact that carbon dioxide elution is directly related to carbon monoxide. The desorbed products distribution was the same over Pt-ceria (cube), the only difference being the lower light-off temperature on the Pt-Ceria (rod). This difference may be due to the different availability of active platinum sites on the {100} and {110} surfaces of ceria.

Temperature programmed surface reaction (TPSR) was used to further study the interaction between the reactant and catalyst surface. As shown in Figure 3.3, carbon monoxide and hydrogen formed simultaneously during $CH_3OH$-TPSR over the ceria nanorods. The data suggest that the methoxy group is the intermediate, and it decomposed into CO and $H_2$.

The same experiment was carried out over Pt-ceria, as shown in Figure 3.4. It was observed that the addition of platinum greatly enhanced the lower-temperature activity. The onset temperature for the formation of carbon monoxide and hydrogen shifted to as low as 150 $^oC$, and total

methanol conversion occurred at 300 $^{o}$C. This indicates that Pt-ceria and ceria share the same intermediate, the methoxy group, in the methanol decomposition reaction. It also confirmed the results from $CH_3OH$-TPD study regarding the onset temperature for methanol conversion.

Surface analysis methods, such as high resolution electron energy loss spectroscopy (EELS) [11] and surface temperature programmed desorption [12] were applied to investigate the existence of various species on the platinum surface. Only physical adsorption was observed on a clean platinum surface; however, it is widely agreed that methanol decomposes over oxygen-covered platinum to form adsorbed CO and hydrogen atoms [13].

Different methods [13, 14] were reported to oxidize the platinum surface with the goal of activating the methanol molecule. For example, Sexton *et al.* [13] applied oxygen pre-treatment to prepare oxygen-covered platinum surfaces. In the current study, it is believed that ceria is the reservoir of oxygen and the interaction between platinum and ceria creates the Pt-$O_x$ active sites on the ceria surfaces.

### *3.2.2 Palladium-ceria: palladium loading and pretreatment effects*

Palladium is in the same group as platinum and is also much cheaper than platinum. Furthermore, palladium shows reasonable CO resistance compared with platinum [15], thus it is worth to extend the study of methanol reactions to palladium supported on ceria.

Palladium-loaded ceria was provided by Prof. Chan's group at Columbia University. They used a co-precipitation method with palladium nitrate and hexamethylenetetramine (HMT) as precursors to prepare different palladium loadings in ceria. Figure 3.5 shows $CH_3OH$-TPSR over 1%Pd-$CeO_2$. The profile is similar to what was observed over Pt-Ceria. Carbon monoxide and hydrogen were the dominant products as methanol was consumed. This indicates that Pd and Pt may share the same intermediates and go through the same pathway. Based on $CH_3OH$-TPSR, the effect of various palladium loadings on methanol decomposition was evaluated, and the results indicated that there was no significant difference with the various palladium loadings.

This suggested that only a limited amount of palladium was effectively dispersed on the ceria surface and that only that part of palladium participated in the methanol reaction.

The application of Pd-$CeO_2$ to other environmental catalytic processes like NO reduction with CO [16] and methanol synthesis reactions [17], has been widely investigated. The formation of a partial solid solution is well documented. The choice of precursors and pre-treatment methods (atmosphere and temperatures) plays an important role in the interaction between palladium and ceria, thus affecting the catalytic performance [18, 19, and 20]. In the case of benzene dehydrogenation reaction, the chloride precursor prevented the activity loss at high temperatures compared with the nitrate precursor, because the formation of stable ceria oxychloride facilitated the irreversible reduction of $Ce^{4+}$ to $Ce^{3+}$ [18]. Shen *et al.* [20] reported the choice of palladium precursor among chloride, acetate and nitrate, affected the final size distribution of palladium, resulting in different interactions between palladium and ceria.

We furthered our study by changing the pretreatment conditions. For example, 1% Pd-$CeO_2$ was pretreated with 20%$H_2$/He at 300 $^oC$ and 500 $^oC$, respectively, and then tested in the decomposition of methanol. The methanol conversion along with the methane generation rate varied with the pre-reduction temperature although carbon monoxide and hydrogen were the main products. After the higher temperature treatment, lower amounts of methane were produced as shown in Figure 3.6. At 250 $^oC$, the rate of formation of methane over 1% Pd-$CeO_2$ is 5.8 $\mu mol/s \cdot g_{cat}$ for the 300 $^oC$ pretreatment, and 2.9 $\mu$ $mol/s \cdot g_{cat}$ for the 500 $^oC$ pretreatment.

The structure of 1%Pd-$CeO_2$ was also characterized by TEM. In Figure 3.7, three typical images are shown: the fresh calcined at 350 $^oC$ , $H_2$-reduced at 300 $^oC$ and used in methanol reaction, and $H_2$-reduced at 500 $^oC$ and used in methanol reaction. The average particle size of ceria is 8 nm in all the samples. The morphology of the used sample is like that of the fresh sample, being roughly octahedral in shape. But a more rounded shape was observed after the higher temperature reduction treatment. Herrmann *et al*. [21] measured the electron conductivity of Pd-$CeO_2$ during hydrogen reduction process. They suggested that the formation of oxygen vacancies and the subsequent electron transfer from reduced ceria to palladium were a function of the reduction temperature. In our study, CO and $H_2$ were produced by methanol

decomposition reaction. The higher temperature treatment may inhibit the dissociation of CO and the methanation reaction through $CO + 3H_2 \rightarrow CH_4 + H_2O$.

### *3.2.3 The similarity between Pd and Pt*

We compared the activity between Pt-ceria and Pd-ceria under the same test conditions, shown in Figure 3.8, and observed that Pt-ceria has slightly higher activity than Pd-ceria. Given those two Pd- and Pt-ceria samples were prepared by optimized methods, they also exhibited the best activity among samples. Although there is a slight difference in activity, the same reaction pathway to produce carbon monoxide and hydrogen as products was observed over group VIII (Pd, Pt) metals on ceria. The findings agree with previous results which used platinum or palladium supported on different oxides [22, 23]. HREELS and isotopic labeling experiments have shown that methanol decomposition proceeds by initial cleavage of the O-H bond on these metals to form methoxy ($CH_3O$) intermediates [15, 24]. It is also worthwhile to mention that the stability of methoxy plays an important role in deciding the reaction pathway in methanol decomposition, which will be addressed more in the following sections. Barteau has identified a linear correlation between the decomposition temperature and the enthalpy of formation of the corresponding metal oxides [25]. This idea was applied to Group VIII (Pt, Pd) and IB (Cu, Au) metals with separate linear equations. In the case of Pd and Pt, because platinum has low $-\Delta H_f$ value for the formation of oxides compared with that of palladium, Pt-$O_x$ would have a higher activity than Pd-$O_x$ on ceria as we observed here, Figure 3.8. From this analysis, it would be apparent that the role of ceria is to provide its oxygen to the Pt, Pd metals and stabilize them in their active Pt-$O_x$ and Pd-$O_x$ form for the methanol decomposition reaction at low temperatures.

## 3.3 Methanol decomposition over Group IB metals (Cu, Au) supported on ceria

### *3.3.1 Gold-ceria : methanol coupling reactions*

On the Au-ceria samples, no CO elution was observed; only $CO_2$ and $H_2$ were produced, as shown in Figure 3.9. If the intermediate was the methoxy species, which is the same species as that on ceria, the simultaneous desorption of CO and $H_2$ should be observed instead of $CO_2$ and $H_2$. Thus, the formation of $CO_2$ and hydrogen indicated that methanol decomposition on gold-ceria may follow a different pathway [26, 27]. Indeed, methyl formate intermediate on the Au-ceria was found, but not on ceria during $CH_3OH$ – TPSR.

In $CH_3OH$-TPSR over the 1%Au-Ceria(Rod), hydrogen was formed starting at ~ 175 $^oC$ (Figure 3.10, Temp. I). Carbon dioxide and methane were also detected in the outlet gas, which are the products from the decomposition of methyl formate [28].

$$HCOOCH_3 \rightarrow CO_2 + CH_4$$

At the same time, small amounts of methyl formate and formic acid were observed in the effluent gas along with hydrogen, as shown in the inset of Figure 3.10. This indicates that decomposition of methanol follows the methyl formate pathway [28, 29]

$$2CH_3OH \rightarrow HCOOCH_3 + 2H_2.$$

The formation of formic acid can be attributed to the conversion of dioxymethylene, $H_2COO$,

$$2H_2COO_{(a)} \rightarrow 2HCOO_{(a)} + H_{2(g)}.$$

The short-lived species, dioxymethylene, was also reported on ceria thin films [4].

The temperature for CO formation was higher than that for the other species. Hence, CO may derive from the decomposition of methyl formate, but it competes with the formation of $CO_2$ and $CH_4$ [30, 31]. Another possibility is that CO may derive from the reverse water-gas shift reaction, from the $CO_2$ and $H_2$ formed.

It has been found that methanol adsorbs weakly and molecularly on a clean gold surfaces [32, 33]. However, on oxygen-covered gold (111) surfaces, the formation of small gold clusters [34] takes place, and stronger adsorption of methanol [32-34] has been reported. In the present work, ceria can provide the active oxygen to the small gold clusters stabilized on its surface. The different crystal planes of ceria have different energetics towards oxygen vacancy formation, the {110} being the most favorable [35, 36].

Previous work has shown that ceria plays an important role in stabilizing gold clusters and controlling the gold oxidation state. It was found that cerium oxide with the highest surface area and highest number of surface oxygen species retains the highest amount of gold [9, 37]. A strong crystal plane effect of ceria on the gold- ceria activity has been identified in the WGS reaction [9]. Thus, ceria nanorods facilitate the dispersion of gold on their {110} surfaces; while gold could not be dispersed on the {100} surfaces. As a result, the 1%Au-Ceria(Cube) material was not active for the WGS reaction [9].

Based on previous studies [32, 38] formaldehyde is stable on gold surfaces and can then easily continue to react with methoxy or other sources of oxygen to form methyl formate or formate groups. However this path leads to CO and $H_2O$ instead of $CO_2$ and $H_2$. As found here the methyl formate and hydrogen appear together and $H_2$ and $CO_2$ are the dominant species; hence, the decomposition of formate on gold can be ruled out.

In summary, a cooperative mechanism for the methanol decomposition on Au-Ceria has been found in this thesis work, as depicted by Scheme 3.1. Reduced ceria adsorbs methanol as methoxy which combines with the formaldehyde adsorbed on gold to form methyl formate. The role of water in the reactions of methanol, namely under methanol steam reforming conditions, will be addressed in Chapter 4.

### *3.3.2 Copper-ceria: methanol dehydrogenation reaction*

Copper-ceria was studied for the methanol decomposition reaction simply because copper- based catalysts are the active catalysts for the methanol synthesis reaction [39]. However, detailed

studies relying on the temperature programmed reactions to elucidate the mechanism are absent in the literature. Methanol, methyl formate, and formic acid were chosen as probe molecules to understand the methanol reaction pathway over copper-ceria.

5%Cu-Ceria and ceria were prepared by the Urea Gelation Co-precipitation (UGC) method and calcined at 400 $^{o}$C before any further tests. Similar to what was observed on other ceria sources, hydrogen and carbon monoxide were produced simultaneously around 300 $^{o}$C over the polycrystalline ceria prepared by the UGC method, as shown in Figure 3.11(a). Once again, the decomposition of methoxy group is surmised to produce CO and $H_2$.

On the other hand, on Cu-Ceria, the desorption profile of hydrogen showed one main peak at 245 $^{o}$C with a shoulder peak at 275 $^{o}$C as shown in Figure 3.11(b). Carbon dioxide showed a main peak around 275 $^{o}$C with the onset temperature *ca*. 245 $^{o}$C. Water and methanol have a broader desorption peak below 300 $^{o}$C, and no carbon monoxide was observed. It is clear that copper addition facilitates the adsorption of methanol on the surface, and changes the reaction pathway. As discussed in the case of gold-ceria, if the intermediate is the methoxy group, simultaneous desorption of CO and $H_2$ should be observed instead of $CO_2$ and $H_2$. Thus, a different pathway for the decomposition of methanol has opened, and we need to identify the intermediates involved.

To explore the possible intermediates when methanol was adsorbed on copper-ceria, $CH_3OH$-TPSR was carried out over the Cu-Ceria samples. As shown in Figure 3.12, it was found that the onset temperature for hydrogen and carbon dioxide production is around 205 $^{o}$C, which is close to the desorption temperature of those species observed by $CH_3OH$-TPD. Furthermore, methyl formate was produced with carbon monoxide and trace amounts of methane at 250 $^{o}$C.

Given the presence of larger amounts of hydroxyl groups and/or trace amounts of oxygen on the ceria surface, it is possible that stabilized methoxy groups would react with either of them to form formaldehyde. Poulston *et al.* [40] suggested that the surface oxygen would facilitate the transition of methoxy to formaldehyde over Cu-$SiO_2$. The occurrence of a coupling reaction between methoxy and formaldehyde would then lead to the formation of methyl formate. Finally, reaction of methyl formate with surface hydroxyls would lead to formic acid whose

dehydrogenation would produce hydrogen and carbon dioxide. If this pathway is followed, we should observe it under steam reforming conditions, as we will see in Chapter 4.

The formation of methyl formate over copper-ceria catalysts was confirmed. In order to further investigate its role in the conversion of methanol to $CO_2$ and $H_2$, formate- based molecules, like methyl formate ($HCOOCH_3$) and formic acid (HCOOH), were chosen as probe molecules.

The desorption profiles during $HCOOCH_3$-TPD over 5%Cu-Ceria (UGC) are shown in Figure 3.13. Carbon dioxide and hydrogen are the main desorption species, along with the formation of methane. The desorption peak temperature (*ca.* 225 $^{o}$C) is the same for carbon dioxide and methane, while the hydrogen peak temperature is slightly higher (*ca.* 235 $^{o}$C).

Idem *et al.* suggested that on copper surfaces [30], decomposition of methyl formate may follow the following two possible pathways:

$$HCOOCH_3 \rightarrow CO_2 + CH_4$$

or

$$HCOOCH_3 \rightarrow CO + CH_3OH\ .$$

Since the formation of $CO_2$ and hydrogen are simultaneous, this suggests that the first pathway occurs at the beginning of the desorption period. The formation of carbon dioxide and hydrogen also shows that absorbed methyl formate will undergo further reactions. One possibility is through the hydrolysis route to form formic acid [31, 41], given the existence of large amounts of surface hydroxyls:

$$HCOOCH_3 + H_2O \rightarrow HCOOH + CH_3OH\ .$$

Indeed, formic acid was produced during this experiment. The decomposition of formic acid through the dehydrogenation route explains well the product distribution

$$HCOOH \rightarrow H_2 + CO_2 .$$

We also used formic acid as a reactant to confirm the dehydrogenation assumption. As shown in Figure 3.14, carbon dioxide and hydrogen were the main desorption species, which have the

main peak around 230 $^{o}$C along with a shoulder peak at 305 $^{o}$C. Based on these findings, we concluded that the dehydrogenation pathway is followed over Cu-Ceria. Also there are two sets of desorption peaks that can be attributed to different adsorbed formates [42]. The first type uses two oxygen to stabilize over the copper surface (bidentate), while the second uses one oxygen to bind on the surface (monodentate) [43, 44].

### 3.4 Active species in the decomposition of methanol

The above findings provide strong evidence that the dehydrogenation of methanol takes place over the ceria supported group IB metals (Cu and Au), producing $CO_2$ and $H_2$. It remains to be shown what the active metal sites are for this reaction. We examine this separately for gold and copper on ceria in the following sections.

#### *3.4.1 Gold-ceria: Au-[$O_x$]-Ce*

Since the pioneering work by Haruta [45] and Hutchings [46] drew attention to the attractive catalytic prosperities of nano-sized gold, nano gold has been demonstrated to catalyze many gas phase and even liquid phase reactions, and the gold particle size is believed to play a critical role in the enhanced catalytic performance [47]. Recent work from Lambert's group has demonstrated Sonogashira cross coupling of iodobenzene with phenylacetylene using supported $Au/La_2O_3$ and reported that large gold particles (around 28 nm) had higher activity and selectivity compared to small gold particles (around 3 nm) [48] . For the epoxidation of styrene, however, the same group showed that gold clusters, $Au_{55}$, were active, while nanoparticles were totally inactive [49]. Earlier work from Fu *et al.* which used NaCN leaching to remove gold particles and clusters from the surface of ceria clearly showed that atomically dispersed gold species are active for the water gas shift reaction [50]. This breakthrough finding was supported later by TEM characterization [51] and DFT calculations[52] , whereby gold ions stabilized with

surrounding oxygens over an oxygen vacancy on $CeO_2$ (111) would have good activity for the WGS reaction.

The same approach to investigate the role of nano gold particles and atomically dispersed gold was used in this thesis. The removal of gold nanoparticles was done by aqueous 2M NaCN solution at pH=12, room temperature. After this treatment, only Au-$O_x$ species strongly bound on ceria were left on the ceria surface. As mentioned above, these species and ceria produce methyl formate in a cooperative way, involving the surface oxygen of ceria close to the gold centers, as shown in Scheme 3.1. It was also found that gold nanoparticles (3 nm avg. size) on the ceria nanocubes are too big to be activated by the ceria surface oxygen. This is why removal of the gold nanoparticles by NaCN leaching, does not reduce the activity of the Au-ceria nanocubes, containing now just ~0.03%Au, probably fully dispersed and stabilized on the ceria (100) surfaces. More detailed discussion of this will be presented in Chapter 4. However, the results so far demonstrate that Au-$O_x$-Ce species are active for the methanol decomposition reaction. Thus, the reaction mechanism is concluded to involve Au-O and O-Ce sites on both the {110} and the {100} ceria surfaces.

### *3.4.2 Copper-ceria: Cu-[$O_x$]-Ce active sites*

Copper supported on ceria was reported to be a good catalyst for methanol reactions by Liu *et al.* in 2002 [52]. They also suggested that $Cu^+$ is active for methanol steam reforming simply because of the $Ce^{3+}+Cu^{2+}\rightarrow Ce^{4+}+Cu^+$ redox reaction. For methanol decomposition reaction, there are few reports addressing the active species. The various copper species on ceria mainly depend on the copper loading amount and the preparation methods [54, 55]. The active copper species is a subject of debate, not only because different reactants exist in different reaction systems, such as in a more reductive or more oxidative atmosphere, but also because of the evolution of copper species under reaction conditions [56, 57]. However, it is generally accepted that there are four different copper species demonstrated through $H_2$-TPR or CO-TPSR techniques, namely, highly dispersed $CuO_x$ species on ceria, strongly bound Cu–[$O_x$]–Ce surface species, $Cu^{2+}$ ion dopants in the ceria lattice (solid solution) and CuO particles [58, 59 ] .

In order to investigate which copper species is active for methanol reactions, we followed here the controlled species isolation method. This is a two-step approach. First copper was deposited on ceria nanorods and nanocubes. As discussed before, different ceria nanoshapes have different abilities to stabilize metal ions. Highly dispersed copper species on ceria nanorods and copper nanoparticles on ceria nanocubes were obtained. Second, ammonia carbonate solution was used to leach the copper samples. It is documented that ammonia washing is an efficient way to dissolve copper oxides [60, 61]. This method was applied with the goal of diminishing the contribution from copper oxides. CO-TPR was also used to titrate the different oxygen species on the surface.

The evolution of $CO_2$ desorption from CO-TPR is plotted as a function of temperature in Figure 3.15, curves (a) and (b) for the $CO_2$ signal from the parent and ammonia- washed copper-ceria (rod), respectively. This clearly showed that after leaching, the desorption peak below 200 $^oC$ disappeared. Similarly the first peak ($H_2O$ formation) disappeared when checked by $H_2$-TPR results, so we can conclude that this peak is due to highly dispersed $CuO_x$ species on ceria. However, the peaks between 200 $^oC$ and 300 $^oC$ were maintained. There are two kinds of copper species in this temperature range, namely strongly bound Cu–[$O_x$]–Ce surface species and $Cu^{2+}$ ion dopants in the ceria lattice. In the case of copper-ceria (cube), shown in curves (c) and (d) of Fig. 3.15, the intensities of all $CO_2$ desorption peaks decreased after ammonia leaching. This suggests that the interaction between copper and ceria cubes is less strong than that of copper and ceria nanorods. The detailed $CO_2$ desorption analysis is shown in Table 3.1.

Confirmed through $CH_3OH$-TPSR experiments, the leached copper-ceria samples, irrespective of the ceria nanoshape used, were active between 150 $^oC$ – 300 $^oC$. Additionally, the same product distribution was found as for the parent samples. The formation of methyl formate and hydrogen was also identified on the leached samples. Furthermore, catalytic evaluations for the decomposition of methanol were carried out over the parent and leached copper-ceria samples. The reaction rates were in the same temperature range over the different sets of copper ceria parent and washed samples, as shown in Figure 3.16. The parent copper-ceria (rod) has the highest reaction rate among all copper-ceria samples that were investigated, apparently because of higher number of active sites. That is the reaction mechanism is presumed to be the same, and indeed the same activation energies ($E_a$= 112 ± 3 kJ/mol) were measured for all copper-ceria

catalysts. We suggest here that the active copper species for the methanol decomposition reaction is the strongly bonded Cu-[$O_x$]-Ce surface species, while the other copper species on the surface of ceria, i.e. $CuO_x$ clusters, $Cu^{2+}$ ion dopants in the ceria lattice, and CuO nanoparticles are spectator species. The same conclusion was recently reached for the water gas shift reaction on copper-ceria [59].

### *3.4.3 Copper-Zinc-Alumina: ZnO decorating the copper surface*

Cu-ZnO-$Al_2O_3$ ( $\geq$ 37.0 wt% CuO, $\geq$ 37.0 wt% ZnO, balance $Al_2O_3$, supplied by BASF) is one of the robust commercial catalysts, which has been used successfully for the water gas shift and methanol synthesis reactions. In this section, the leaching approach that was applied to copper-ceria was extended to this commercial catalyst, with the goal of examining the active amount of copper needed for the methanol decomposition reaction.

As demonstrated by the $H_2$-TPR profiles (Fig. 3.17), after applying the ammonia leaching method, the hydrogen consumption peaks over the leached samples all decreased, compared with those of the parent. The contribution of each peak to the total peak areas was analyzed, and the results are shown in Table 3.2. It was found that the percentage of species reduced in the medium temperature range ( 125 $^oC$ - 175 $^oC$) increased after leaching. Although the position of peaks depended upon the supports, the sequence of copper reduction is independent of the supports.

Furthermore, the catalytic performance of leached and parent commercial copper catalyst (Cu-Zn-$Al_2O_3$) in methanol decomposition reaction was evaluated. It is interesting to observe that the washed samples were much more active than the parent samples in the decomposition of methanol as shown in Figure 3.18. Previous results [39] suggested that copper surface area is an important factor to improve the activity, and the role of ZnO is believed to increase the dispersion of copper. Wainwright *et al.* [62] investigated the effect of NaOH leaching in Raney copper-zinc alloy in methanol synthesis and the water gas shift reactions. They demonstrated that the improved activity was due to the enhanced Cu-ZnO interface. Friedrich *et al.* [63] suggested the increased surface area and concentration of zinc oxides on the catalyst surface

could help to increase the activity of Raney copper in methanol synthesis reaction. The same group later showed that the addition of small amounts of metal oxides (ZnO for example) to skeletal copper significantly improved activity in methanol synthesis. Most recently, Tanabe *et al.* [64] proposed iron species in the leached layer of Al-Cu-Fe quasicrystal showed high activity for methanol steam reforming. Here the commercial copper catalyst investigated has 37 wt%-45 wt% copper oxides and 37 wt% zinc oxide. Ammonia carbonate would also dissolve zinc oxide in the leaching process. Two possibilities exist. One is that zinc complexes in the solution may redeposit and decorate the copper surface, improving the interaction between copper and zinc after calcination. The second, zinc oxides may be attracted away from the bulk catalysts, changing the porosity of the copper catalyst. Enhancement of diffusion would explain the difference in methanol decomposition if the reaction is very fast. Although further work needs to be done to better understand the morphology change between leached and parent commercial copper samples, the preliminary results reported here still point out one of the possible directions to decrease the usage of copper while maintaining or enhancing the catalytic performance in methanol reactions. This approach is also useful for indentifying the reaction- relevant copper species for mechanistic interpretation.

### 3.5 Examination of gold structures in methanol decomposition

The transformation of the gold oxidation state and structure during the reaction is critical for identifying the active species. Along with this information, one should know whether these structural changes are accompanied by catalyst deactivation. In this work, we used X-ray absorption near-edge structure (XANES) spectroscopy at the synchrotron facility of the Brookhaven National Laboratory to characterize the gold-ceria samples under methanol decomposition reaction conditions. The methanol decomposition reaction was conducted over 1%Au-Ceria (Rod) at different reaction temperatures in a gas mixture of 16%$CH_3OH$-He at the total flow rate of 50 mL/min. XANES spectra over the 1%Au-Ceria (Rod) were collected after 1.5 h reaction at different temperatures (150 $^oC$ , 225 $^oC$ and 300 $^oC$ respectively), as shown in Figure 3.19. The shift of the white line energy (Au $L_{III}$ edge) over the fresh gold sample indicated that gold was mainly cationic. This agrees with previous results through XPS

characterizations: ionic gold ($Au^{+}$ and $Au^{3+}$) are the main species in the gold-ceria nanorods or polyhedra [26]. The evolution of the white line feature after reaction showed a drop of the normalized intensity of the white line. Thus, some of the oxidized gold was reduced during the methanol decomposition reaction. The question then is whether the reduced gold state or the remaining oxidized gold species are the active sites. If the latter is true, the overall activity of the catalyst should be lower after 1.5 h of reaction at each of the two temperatures tested. Of course, if not all the initially oxidized gold is in active Au-$O_x$-Ce association with ceria, we would expect a fraction of it to easily reduce and form gold clusters and particles with heating and time-on-stream [65-67]. From leaching experiments, we know that only 0.5%Au is in active state on the 1%Au-Ceria(rod) sample [9]; hence, we expect that the non associated, inactive gold species will be reduced and grow and mask the results.

In order to further elucidate the evolution of gold state, R-space EXAFS data analysis was performed and is shown in Figure 3.20. For the fresh 1%Au-Ceria (Rod), the first shell radial distance at 1.60 Å and the third shell radial distance at 3.12 Å indicated the existence of Au-O bonds in the fresh sample, which agree with results over 0.5AuCe(La)$O_x$ reported by Deng *et al.* [65]. The second shell radial distance at 2.5 Å is the typical value of Au-Au bond [66]. The Au-Ce distance at 3.79 Å was obtained, which was consistent with DFT calculation by Tibiletti *et. al* [68]. They reported a similar value with the model that gold was assumed to fill a cerium ion vacancy site on the $CeO_2$ (111) plane. The differences between fresh sample and used sample after methanol decomposition reaction with different temperatures ( 150 $^{o}$C and 225 $^{o}$C) are: (a) the Au-Au contribution is dominant after reaction. Two larger peaks, which are located at 2.3 Å and 3.0 Å respectively and resulted from the splitting of single Au-Au path contribution, were also observed. These could be explained as the Ramsauer-Townsend resonance at a single energy in the backscattering amplitude of Au [67]; (b) the intensity of peak attributed to Au-O decreased. This indicates that reduction of gold species occurred during the methanol reaction. It is also corroborated by the XPS analysis of the gold-ceria samples after reaction. But as discussed before, oxygen-covered gold surface is a prerequisite for the methanol activation reaction.

### 3.6 Comparison between group VIII metals (Pd, Pt) and IB metals (Cu, Au) in methanol decomposition

A detailed study for methanol decomposition reactions over Group IB (Cu and Au) and VIII (Pt and Pd) metals supported on ceria has been carried out. The results showed that all these catalysts enhanced the low temperature methanol decomposition compared with pure ceria. The significant difference between Group IB and Group VIII metals is the product distribution; hence their hydrogen selectivity. Through temperature programmed reactions, the importance of the stability of methoxy groups was confirmed. Takezawa *et al.* [69] and Chung *et al.* [70] have suggested that the absorption bands due to CH asymmetric stretching vibration in a terminal methyl group are strongly influenced by the nature of metal oxides when surface normal alcoholates are formed on the oxides. Also they used the parameter *F*, electronegativity, to quantify the difference between metal oxides.

$$F = {I_p \cdot (Z^2 / R^3)^{3/4}} \Big/ {1000}$$

Here, $I_p$ is the ionization potential (in volts); $Z$ is the cation charge; and $R$ is the radius (Å) of the metal ion of charge $Z$. The higher the value of $F$, the less stable the alcoholate.

The different strengths of the C-H bond of the methoxy groups when adsorbed on the support reflects the stability of methoxy groups [71]. Thus we adapt this parameter to correlate our results in methanol decomposition. This is a reasonable assumption, since the reaction regimes can be regarded as the M-O region, i.e. metals in oxidized states. As shown in Table 3.3, Pt has the highest $F$ value compared with Pd and Au. This agrees with our observation that the methoxy group was unstable on the Pt-ceria catalyst, decomposing into carbon monoxide and hydrogen.

### 3.7 Summary

In this chapter, Group VIII (Pt, Pd) and Group IB (Au, Cu) metals supported on ceria were investigated for the methanol decomposition reaction. Since the stability of methoxy group is different between those two groups of metals, a different reaction pathway in methanol decomposition was identified. The stability of the methoxy group was proposed to be quantitatively related to the electronegativity of the oxides.

For Group VIII (Pt, Pd) metals, the dehydrogenation pathway, which follows the formation of carbon monoxide and hydrogen, was observed. In the case of Pt-ceria, the support effect was investigated by using different ceria nanoshapes as supports. An indirect shape effect was found, whereby the pre-exponential factors (i.e. the number of active sites) of the reaction rates only differ as a function of ceria nanoshapes; while the apparent activation energies were similar for all the Pt-ceria samples investigated. In the case of Pd-ceria, the amount of palladium loading and reduction temperature were investigated. The results indicated the amount of palladium in the bulk had a minor effect on the activity performance. However, more methane was produced over Pd-ceria after 500 $^{o}$C reduction pre-treatment compared with that of 300 $^{o}$C reduction. The reason could be the formation of bigger palladium particles after 500 $^{o}$C pretreatment.

For Group IB (Au, Cu) metals, the methanol coupling pathway which produced methyl formate and hydrogen was observed. Temperature programmed reactions using different molecules ($CH_3OH$, $HCOOCH_3$, and HCOOH) elucidated the role of methyl formate in the product distribution in methanol decomposition over these IB metals. Through leaching process, strongly bonded and highly dispersed IB metal species were identified as the active sites for methanol reactions. The XANES data further confirmed the existence of oxidized gold species during the methanol decomposition reaction.

### 3.8 References


[1] J. L. Falconer, J. A. Schwarz, *Catal. Rev. Sci. Eng*. 25 (1983) 141.

[2] A. Siokou, R. M. Nix*, J. Phys. Chem. B* 103 (1999) 6984.

[3] R. M. Ferrizz, G. S. Wong, T. Egami, J. M. Vohs, *Langmuir* 17 (2001) 2464.

[4] D. R. Mullins, M. D. Robbins, J. Zhou, *Surf. Sci.* 600 (2006) 1547.

[5] A. Trovarelli, *Catalysis by Ceria and Related Materials*. Imperial College Press, 2002.

[6] J. C. Conesa, *Surf. Sci*. 339 (1995) 337.

[7] Z. L. Wang, X.-D. Feng, *J. Phys.Chem. B* 107(2003) 13563.

[8] T. X. T. Sayle, S. C. Parker, C. R. A. Catlow, *J. Chem. Soc. Chem. Commun*. (1992) 977.

[9] R. Si, M. Flytzani-Stehphanopoulos, *Angew. Chem. Int. Ed.* 47 (2008) 2884.

[10] J. S. Shyu, K. J. Otto, *J. Catal.*115 (1989) 307.

[11] K. Franaszczuk, E. Herrero, P. Zelenay, A. Wieckowski, J. Wang, R. I. Masel, *J. Phys. Chem.* 96 (1992) 8509.

[12] R. W. McCabe, D. F. McCready, *J. Phys. Chem*. 90 (1986) 1428.

[13] B. A. Sexton, *Surf. Sci.* 102 (1981) 271.

[14] C. G. Freyschlag, R. J. Madix, *Mater. Today* 14 (2011) 134.

[15] J. A. Gates, L. L. Kesmodel, *J. Catal.*83 (1983) 437.

[16] S. Roy, M. S. Hegde, *Catal. Commun.* 9 (2008) 811.

[17] Y. Matsumura, W. Shen, Y. Ichihashi, M. Okumura, *J. Catal.*197 (2001) 267.

[18] L. Kepliński, M. Wolcyrz, J. Okai, *J. Chem. Soc. Faraday Trans.* 91 (1995) 507.

[19] N. Tsubaki, K. Fujimoto, *Top. Catal.* 22 (2003) 325.

[20] W. Shen, Y. Matsumura, *Phys. Chem. Chem. Phys*. 2 (2000) 1519.

[21] J. M. Herrmann, C. H. Van, L. Dibansa, R. Harvolona, *J. Catal*. 159 (1996) 361.

[22] J. R. Croy, S. Mostafa, J. Liu, Y. Sohn, H. Heinrich, B. R. Cuenya, *Catal. Lett*. 119 (2007) 209.

[23] K. Sun, W. Lu, M. Wang, X. Xu, *Appl. Catal. A* 268 (2004) 107.

[24] D. H. Ehilers, A. Spitzer, H. Lüth, *Surf. Sci*. 160 (1985) 57.

[25] M. A. Barteau, *Catal. Lett.* 8 (1991) 175.

[26] N. Yi, R. Si, H. Saltsburg, M. Flytzani-Stephanopoulos, *Appl. Catal. B* 95 (2010) 87.

[27] N. Yi, R. Si, H. Saltsburg, M. Flytzani-Stephanopoulos, *Energy Environ. Sci*. 3 (2010) 831.

[28] A. Gazsi, T. Bánsági, F. Solymosi, *Catal. Lett*. 131 (2009) 33.

[29] K. Takahashi, N.Takezawa, H. Kobayashi, *Appl. Catal.* 2 (1982) 363.

[30] R.O. Idem, N.N. Bakhshi, *Ind. Eng. Chem. Res.* 33 (1994) 2056.

[31] K. Takahashi, H. Kobayashi, B. Takezawa, *Chem. Lett*. (1985) 759.

[32] D.A. Outka, R.J. Madix, *J. Am. Chem. Soc*. 109 (1987) 1708.

[33] J. L. Gong, D.W. Flaherty, R.A. Ojifinni, J.M. White, C.B. Mullins, *J. Phys. Chem. C* 112 (2008) 5501.

[34] B. J. Xu, X.Y. Liu, J. Haubrich, R.J. Madix, C.M. Friend, *Angew. Chem. Int. Ed*. 48

(2009) 4206.

[35] A. Trovarelli, *Catal. Rev. Sci. Eng.* 38 (1996) 439.

[36] M. Nolan, S.C. Parker, G.W. Watson, *Phys. Chem. Chem. Phys.* 8 (2006) 216.

[37] Q. Fu, W. Deng, H. Saltsburg, M. Flytzani-Stephanopoulos, *Appl. Catal. B* 56 (2005)

57.

[38] D. A. Outka, R.J. Madix, *Surf. Sci.* 179 (1987) 361.

[39] D. R. Palo, R. A. Dagle, J. D. Holladay, *Chem. Rev*. 107 (2007) 3992.

[40] S. Poulston, E. Rowbotham, P. Stone, P. Parlett, M. Bowker, *Catal. Lett.* 52 (1998) 63.

[41] C. J. Jiang, D. L. Trim, M. S. Wainwright, N. W. Cant, *Appl. Catal. A* 97 (1993) 145.

[42] G. J. Millar, C. H. Rochester, K. C. Waugh, *J. Chem. Soc. Faraday Trans*. 87(1991) 1491.

[43] G. J. Millar, C. H. Rochester, K. C. Waugh, *J. Chem. Soc. Faraday Trans*. 87 (1991) 2795.

[44] C. Li, K. Domen, K. Maruya, T. Onishi, *J. Catal.*125 (1990) 445.

[45] M. Haruta, T. Kobayashi, H. Sano, N. Yamada, *Chem. Lett*. 16 (1987) 405.

[46] G. J. Hutchings, *J. Catal*. 96 (1985) 292.

[47] A. S. K. Hashmi, G. J. Hutchings, *Angew. Chem. Int. Ed*. 45 (2006) 7896.

[48] G. Kyriakou, S. K. Beaumont, S. M. Humphrey, C. Antonetti, R. M. Lambert, *ChemCatChem* 2 (2010) 1444.

[49] M. Turner, V. B. Golovko, O. P. H. Vaughan, P. Abdulkin, A.Berenguer-Murcia, M. S. Tikhov, B. F. G. Johnson, R. M. Lambert, *Nature* 454 (2008) 981.

[50] Q. Fu, H. Saltsburg, M. Flytzani-Stephanopoulos, *Science* 301 (2003) 935.

[51] T. Akita, K. Tanaka, M. Kohyama, *J. Mater. Sci.* 43 (2008) 3917.

[52] Z. P. Liu, S. J. Jenkins, D. A. King, *Phys. Rev. Lett*. 94 (2005) 196102.

[53] Y. Liu, T. Hayakawa, K. Suzuki, S. Hamakawa, T. Tsunoda, T. Ishii, M. Kumagai, *Appl.Catal. A* 223 (2002) 137.

[54] P. Bera, K. R. Priolkar, P. R. Sarode, M. S. Hegde, S. Emura, P. Kumashiro, N. P. Lalla, *Chem. Mater.* 14 (2002) 3591.

[55] Y. Li, Q. Fu, M. Flytzani-Stephanopoulos, *Appl. Catal. B* 27 (2000) 179.

[56] X. Wang, J.A. Rodriguez, J.C. Hanson, D. Gamarra, M. Fernandez-Garcia, A. Martinez-Arias, *J. Phys. Chem. B* 109 (2005) 19595.

[57] P. Djinović, J. Batista, A. Pintar*, Appl. Catal. A* 347 (2008) 23.

[58] W. Liu, M. Flytzani-Stephanopoulos, *J. Catal.* 153 (1995) 317; ibid 304.

[59] R. Si, J. Raitano, N. Yi, L. Zhang, S. –W. Chan, M. Flytzani-Stephanopoulos, *Catal. Today* 180 (2012) 68.

[60] Q. Luo, R. A. Mackay, S. V. Babu, *Chem. Mater.* 9 (1997) 2101.

[61] L. Li, Y. Zhan, Q. Zheng, Y. Zheng, C. Chen, Y. She, X. Lin, K. Wei, *Catal. Lett*. 130 (2009) 532.

[62] M. S. Wainwright, D. K. Trimm, *Catal. Today* 23 (1995) 29.

[63] J. Friedrich, D. J. Young, M. S. Wainwright, *J. Catal*. 80 (1983) 14.

[64] T. Tanabe, S. Kameoka, A. P. Tsai, *Appl. Catal*. 384 (2010)241.

[65] W. Deng, A. I. Frenkel, R. Si, M. Flytzani-Stephanopoulos, *J. Phys. Chem. C* 112(2008) 12834.

[66] Y. Guan, E. J. M. Hensen, *Phys. Chem. Chem. Phys.* 11 (2009) 9578.

[67] V. Aguilar-Guerrero, R. J. Lobo-Lapidus, B. C. Gates, *J. Phys. Chem. C* 113 (2009) 3259.

[68] D. Tibiletti, A. Amieiro-Fonseca, R. Burch, Y. Chen, J. M. Fisher, A. Goguet, C. Hardacre, P. Hu, D. Thompsett, *J. Phys. Chem. B* 109 (2005) 22553.

[69] N. Takezawa, H. Kobayashi, *J. Catal*. 25 (1972) 179.

[70] J. S. Chung, C. O. Bennett, *J. Catal*. 92 (1985) 173.

[71] F. S. Feil, J. G. Ommen, J. R. H. Ross, *Langmuir* 3(1987) 668.

**Table 3.1 Carbon dioxide ($CO_2$) analysis in CO-TPR**

| Sample | Temperature ($^oC$) | $CO_2$ Amount ( μ mol/g) |
|---|---|---|
| 15%Cu-$CeO_2$(Rod) | 124 | 1055 |
| | 176 | 1008 |
| | 221 | 1513 |
| Leached 15%Cu-$CeO_2$(Rod) | / | / |
| | 175 | 1146 |
| | 240 | 642 |
| 15%Cu-$CeO_2$(Cube) | / | / |
| | 165 | 596 |
| | 208 | 1375 |
| Leached 15%Cu-$CeO_2$(Cube) | / | / |
| | 162 | 596 |
| | 204 | 875 |

**Table 3.2 Peak analysis over commercial Cu-Zn-$Al_2O_3$ in $H_2$-TPR**

| Sample | Temperature / $^oC$ (Peak Percentage%) |
|---|---|
| Cu-ZnO-$Al_2O_3$ | 135 $^oC$ ( 10.7%) |
| | 159 $^oC$ (26.7%) |
| | 175 $^oC$ (62.6%) |
| Leached Cu-ZnO-$Al_2O_3$ | 135 $^oC$ (18.0%) |
| | 153 $^oC$ (40.5%) |
| | 175 $^oC$ (41.5%) |

**Table 3.3 The value of electronegativity (*F*) over precious metals**

| Metal | Cation Charge | Radius ($\AA$) | Ionization Potential ( $eV$) | $F^{\#}$ |
|---|---|---|---|---|
| Pd | +2 | 0.86 | 19.63 | 0.0779 |
| Pt | +2 | 0.80 | 18.56 | 0.0867 |
| Au | +1 | 1.37 | 9.23 | 0.0045 |
| Ce | +3 | 1.01 | 20.2 | 0.1026 |

# based on the references [69, 70] in Chapter 3.

**Scheme 3.1 Proposed cooperative reaction scheme for methanol coupling over Au-Ceria.**

**The active gold structure is a cluster of gold atoms of sub-nm size.**

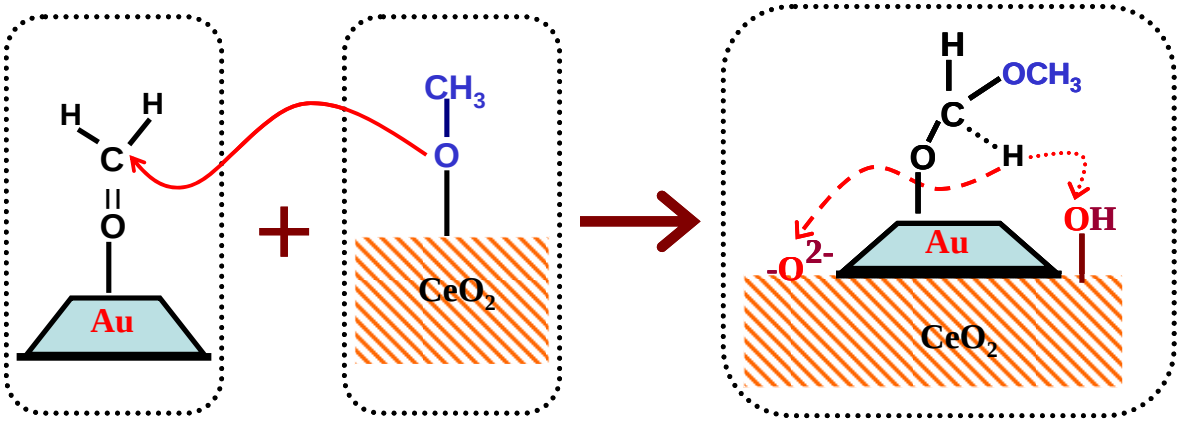

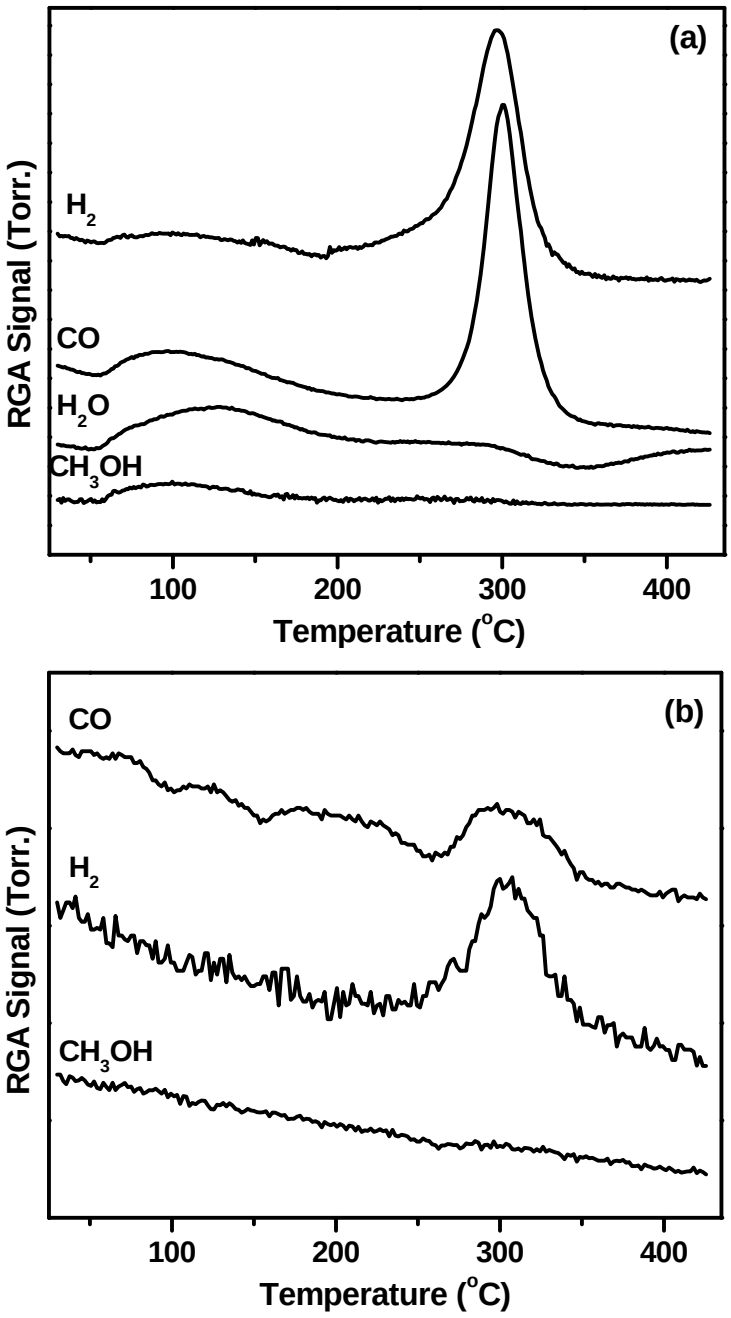


Figure 3.1 $CH_3OH$-TPD profiles over (a) Ceria (Rod) and (b) Ceria (Cube)

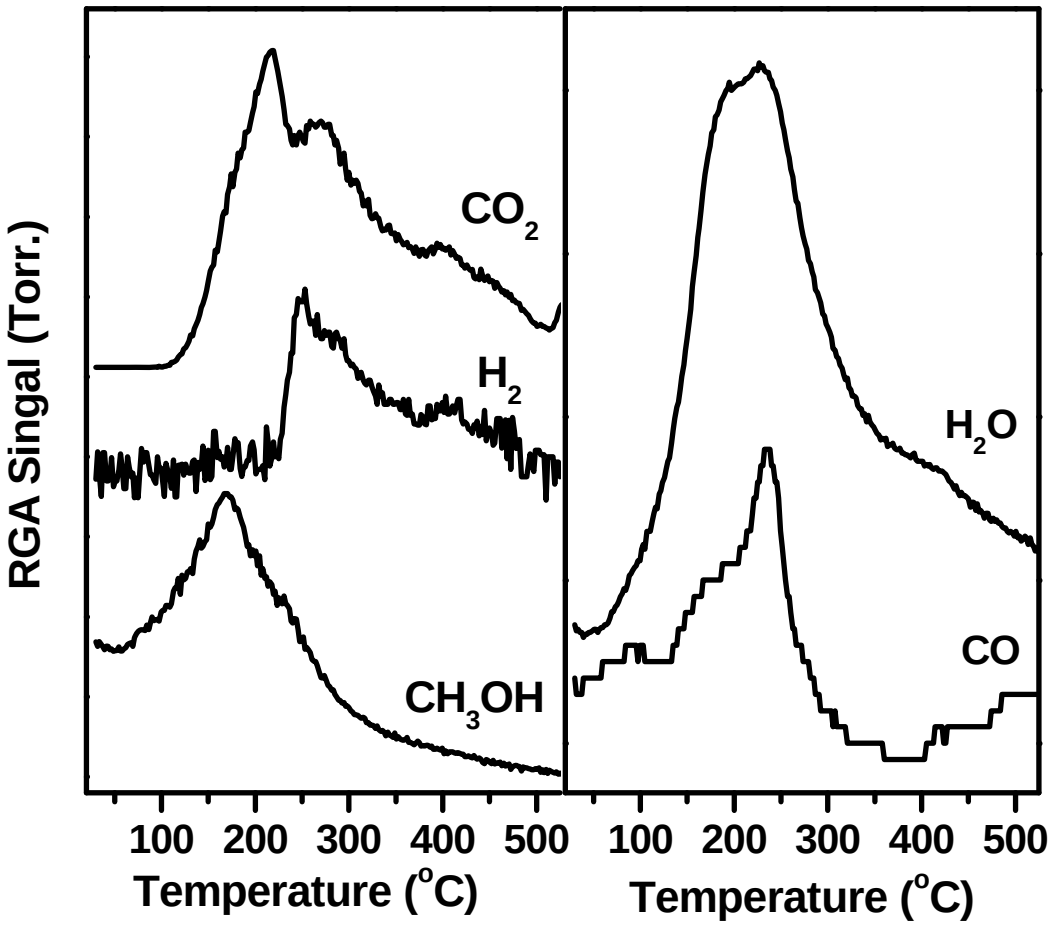


Figure 3.2 $CH_3OH$-TPD profiles over 3% Pt-Ceria (Rod)

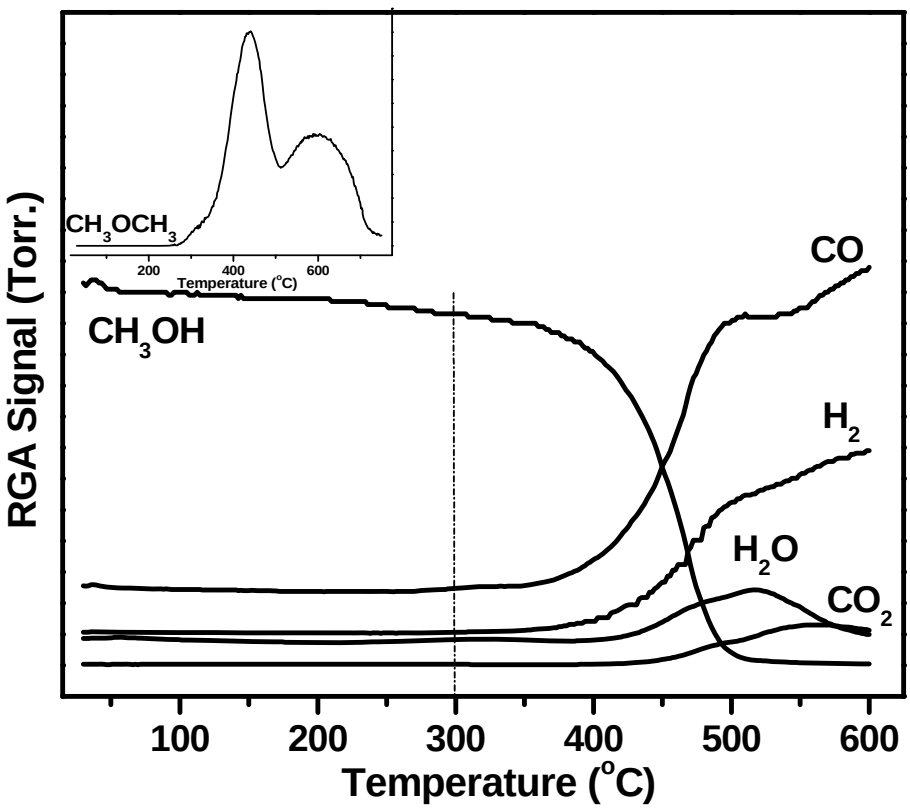


Figure 3.3 $CH_3OH$-TPSR profile over Ceria (Rod)

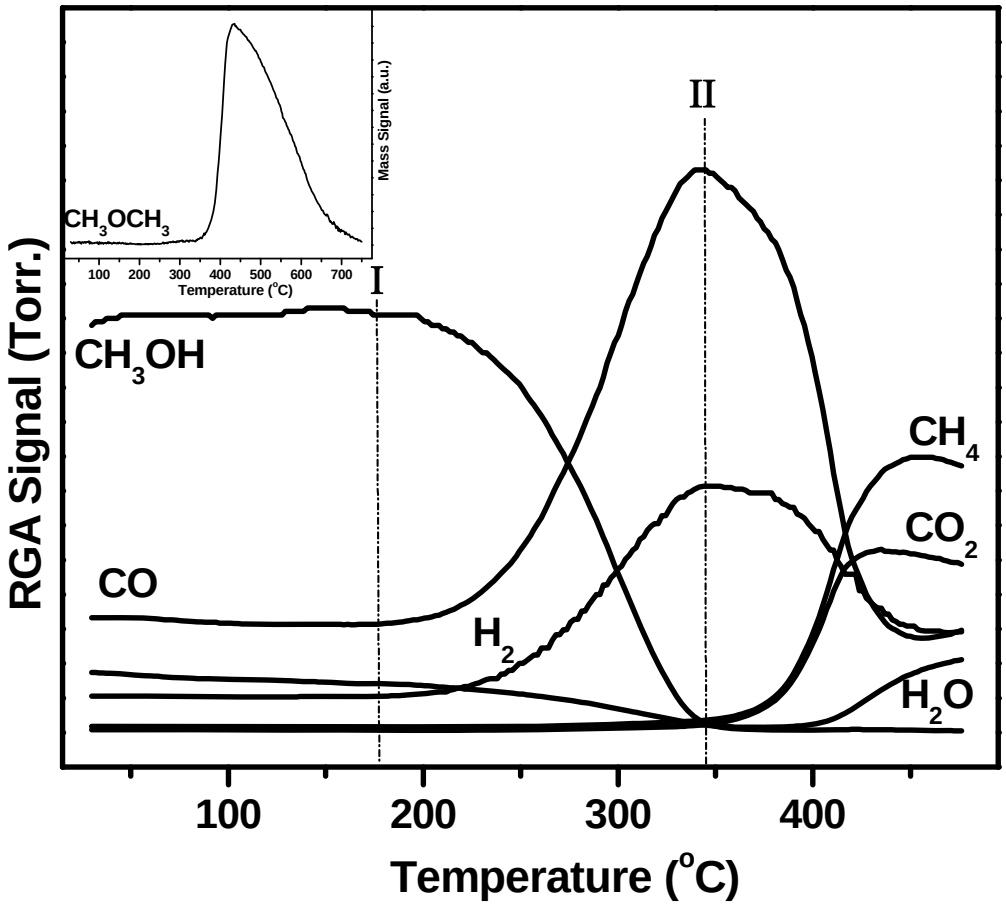


Figure 3.4 $CH_3OH$-TPSR profiles over 3% Pt-Ceria (Rod)

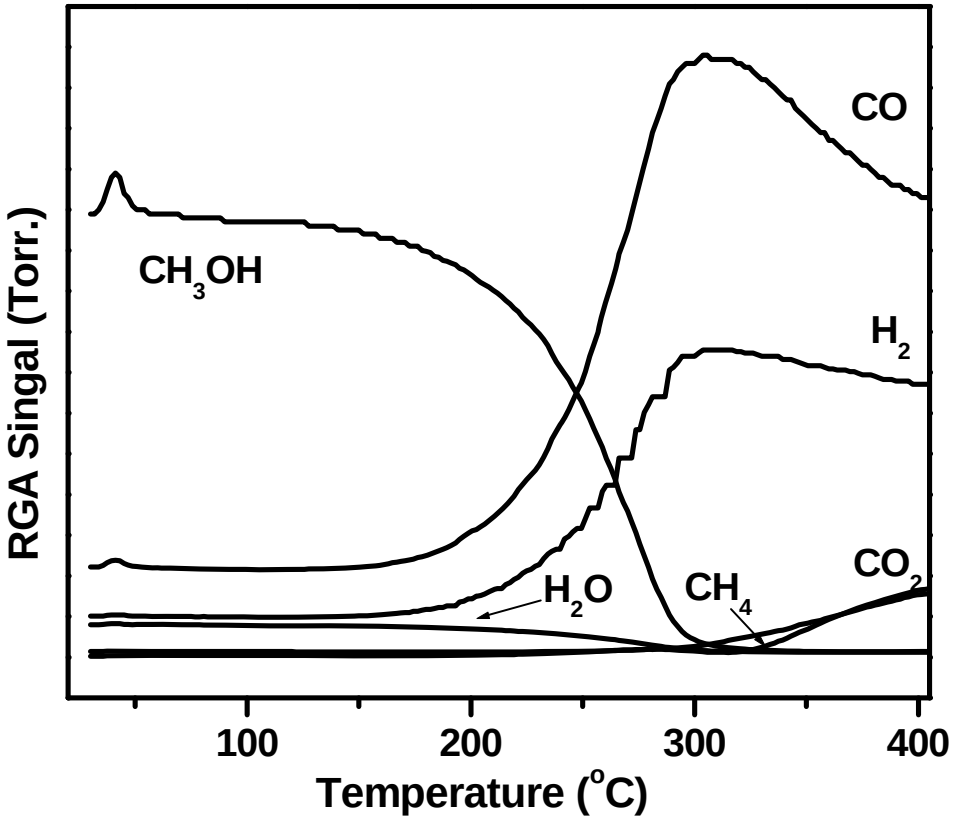


Figure 3.5 $CH_3OH$-TPSR profile over 1% Pd-Ceria

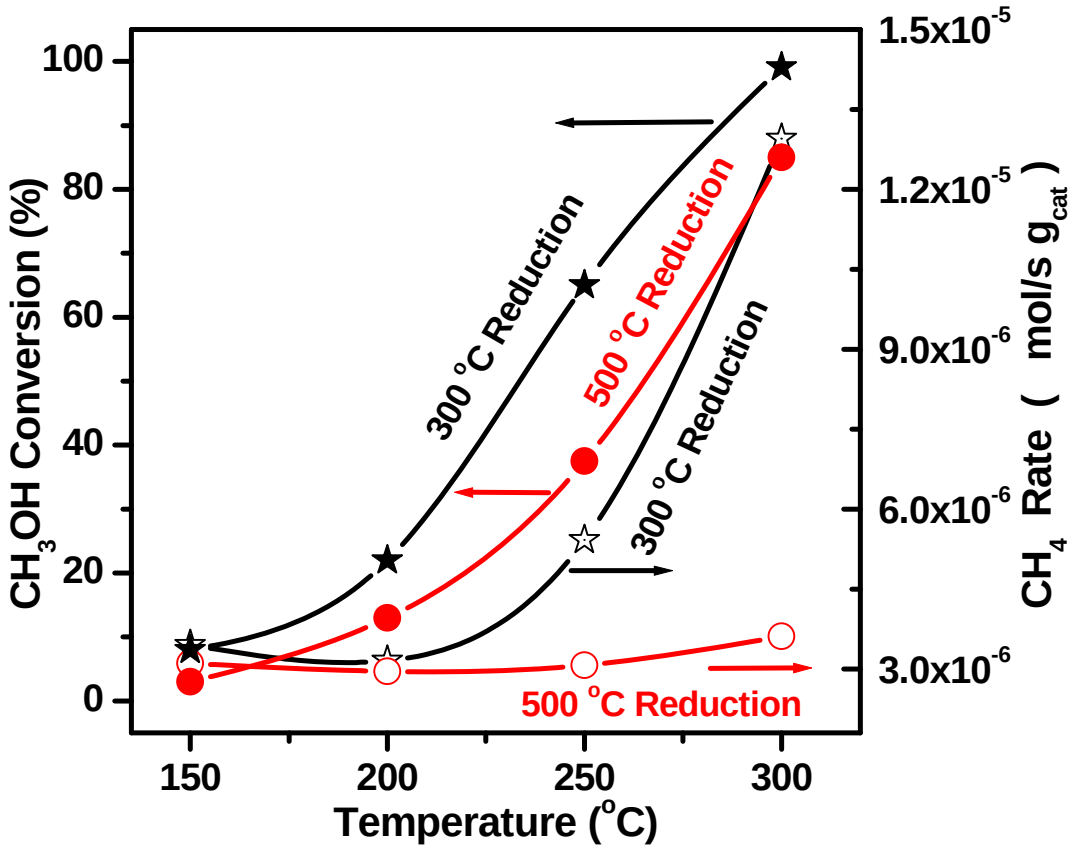


Figure 3.6 Methanol conversion (%) and methane formation rate over 1%Pd-Ceria pre-reduced at two different temperatures

Gas composition: 16%$CH_3OH$/bal. He; GSHV= 42,000 $h^{-1}$

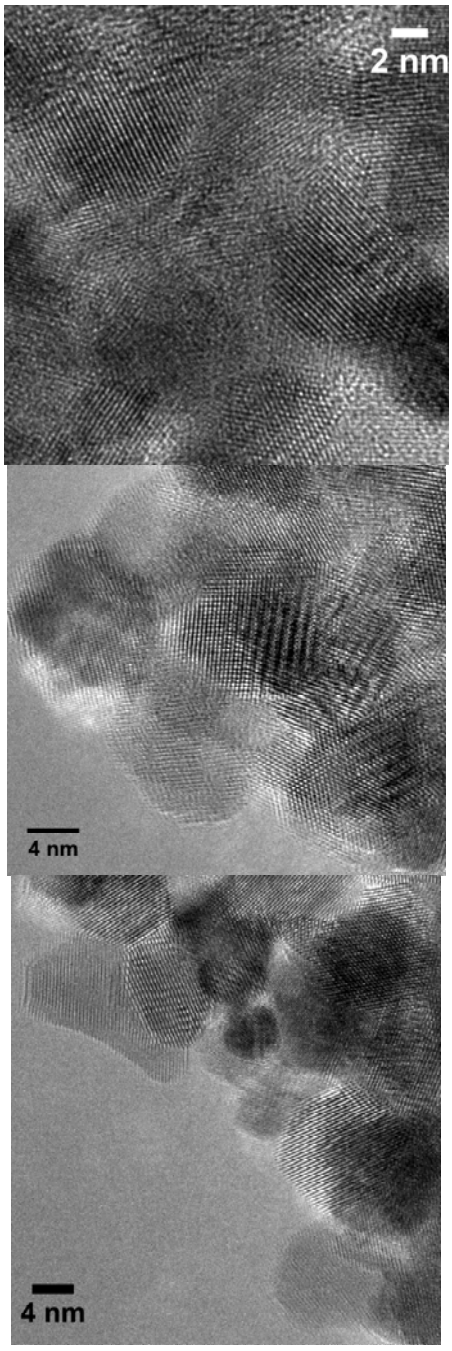


Figure 3.7 TEM images over (a) fresh 1%Pd-Ceria (top); (b) used under 300 $^{o}$C pre-reduced (middle); (c) used under 500 $^{o}$C pre-reduced (bottom)

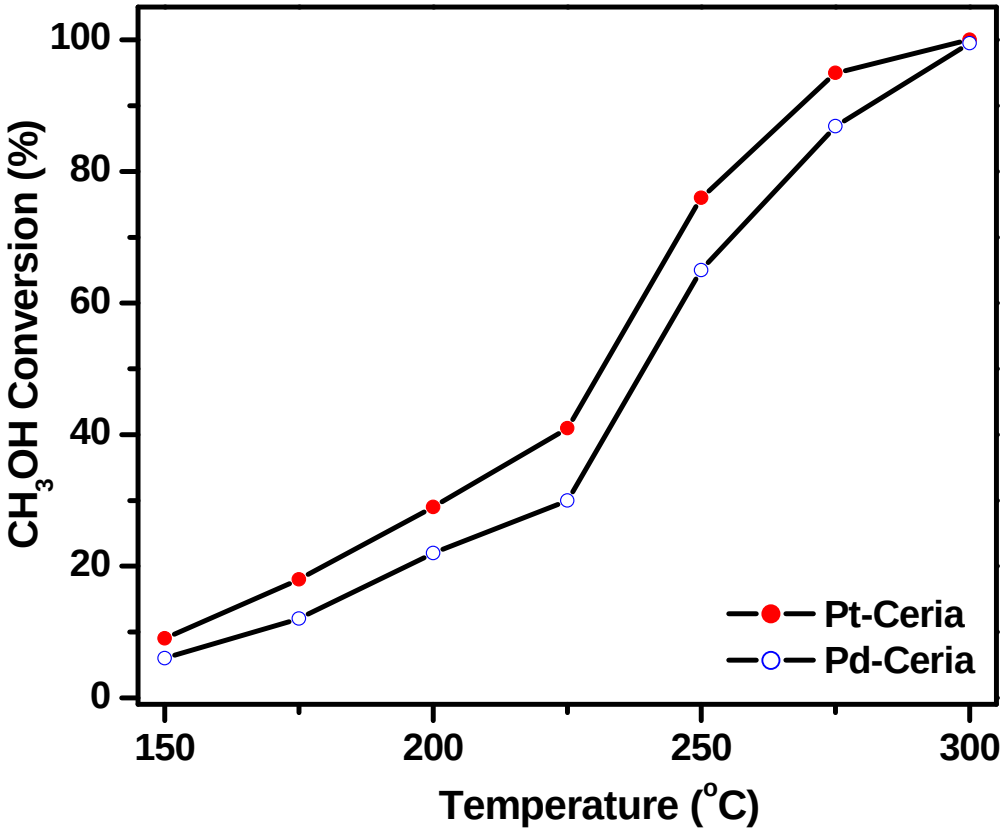


Figure 3.8 Methanol conversion (%) over 3% Pt-Ceria(Rod) and1% Pd-Ceria

Gas composition: 16%$CH_3OH$/bal. He; GSHV= 42,000 $h^{-1}$

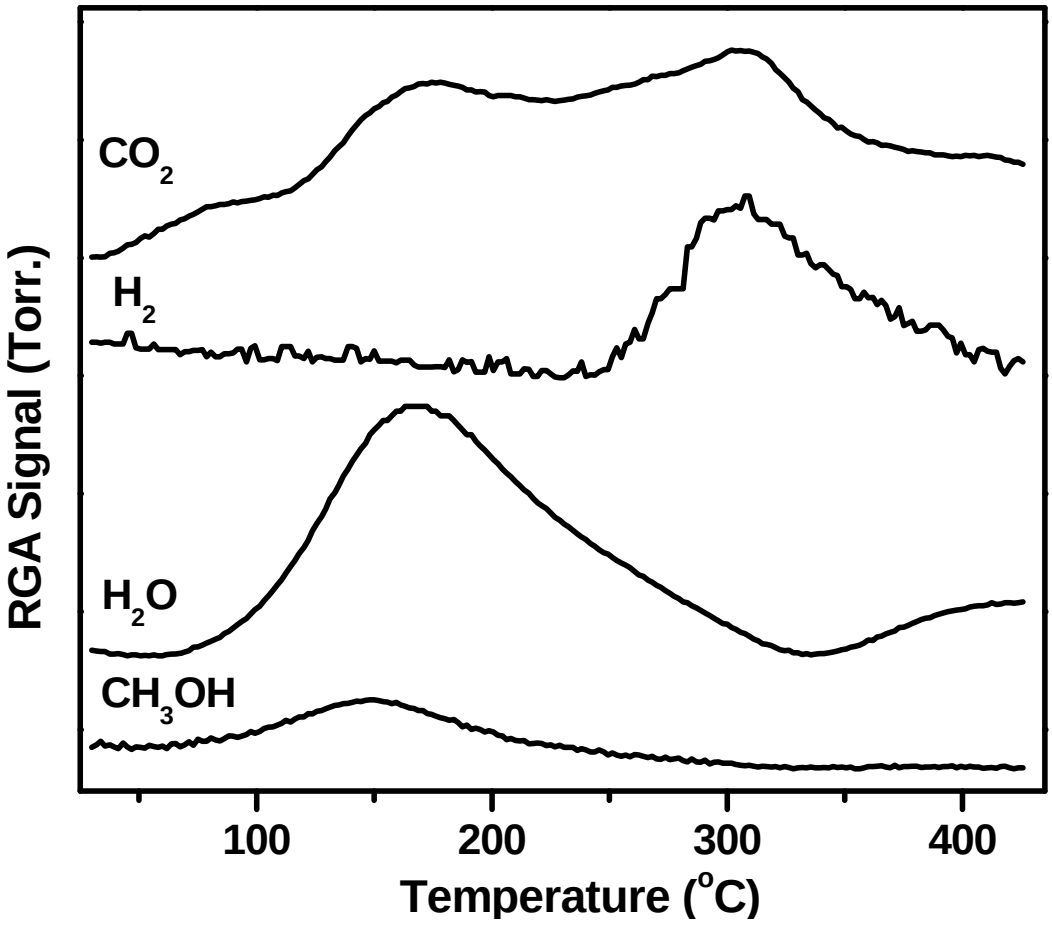


Figure 3.9 $CH_3OH$-TPD profile over 1%Au-Ceria (Rod)

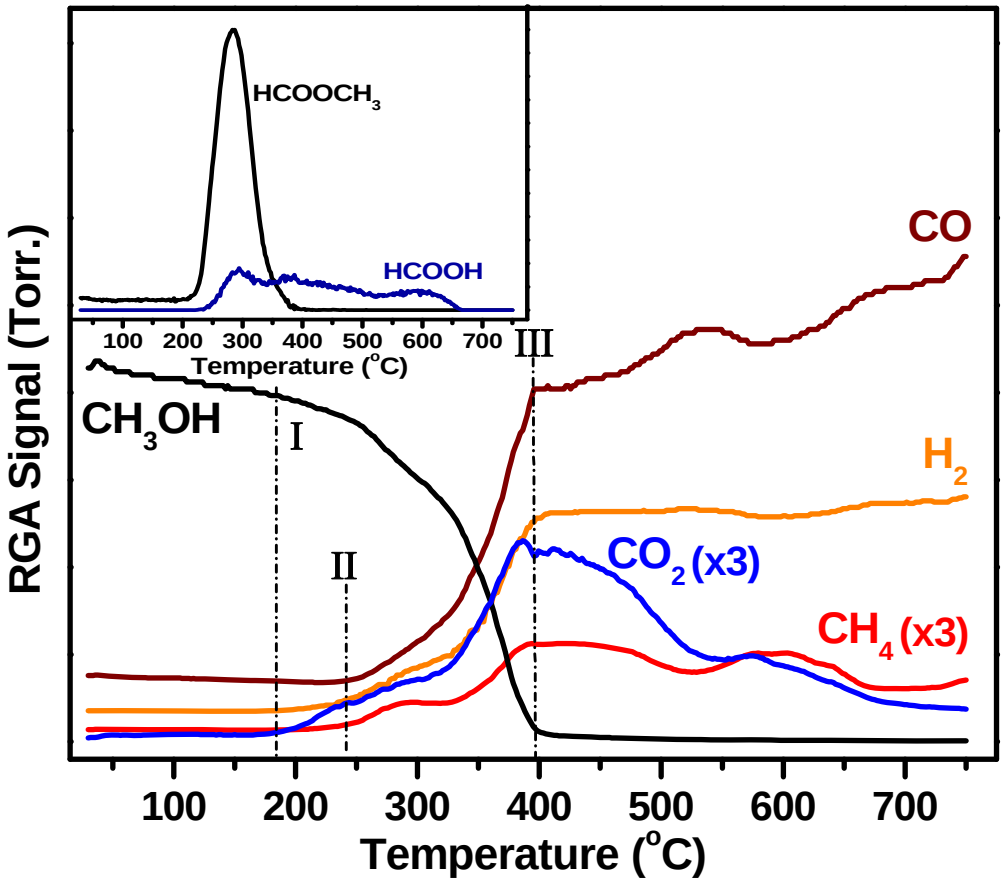


Figure 3.10 $CH_3OH$-TPSR profile over 1% Au-Ceria (Rod)

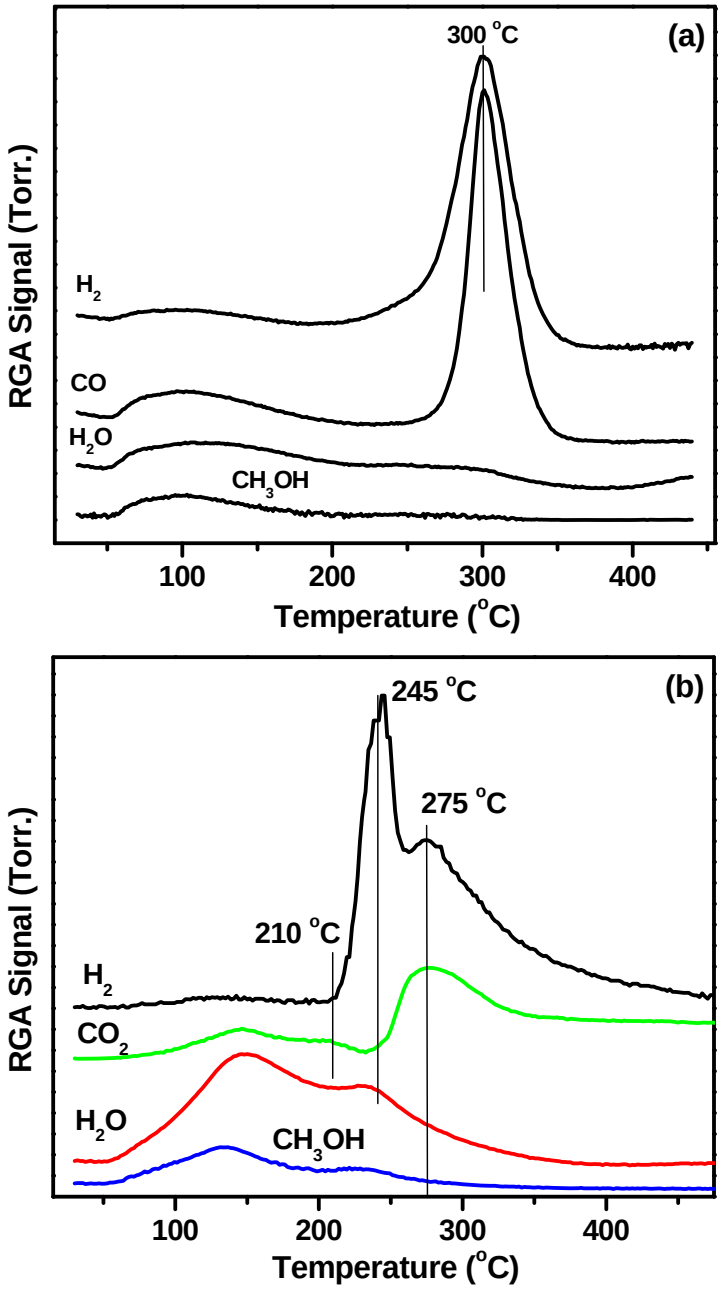


Figure 3.11 $CH_3OH$-TPD profiles over (a) Ceria (UGC) and (b) 5%Cu-Ceria (UGC)

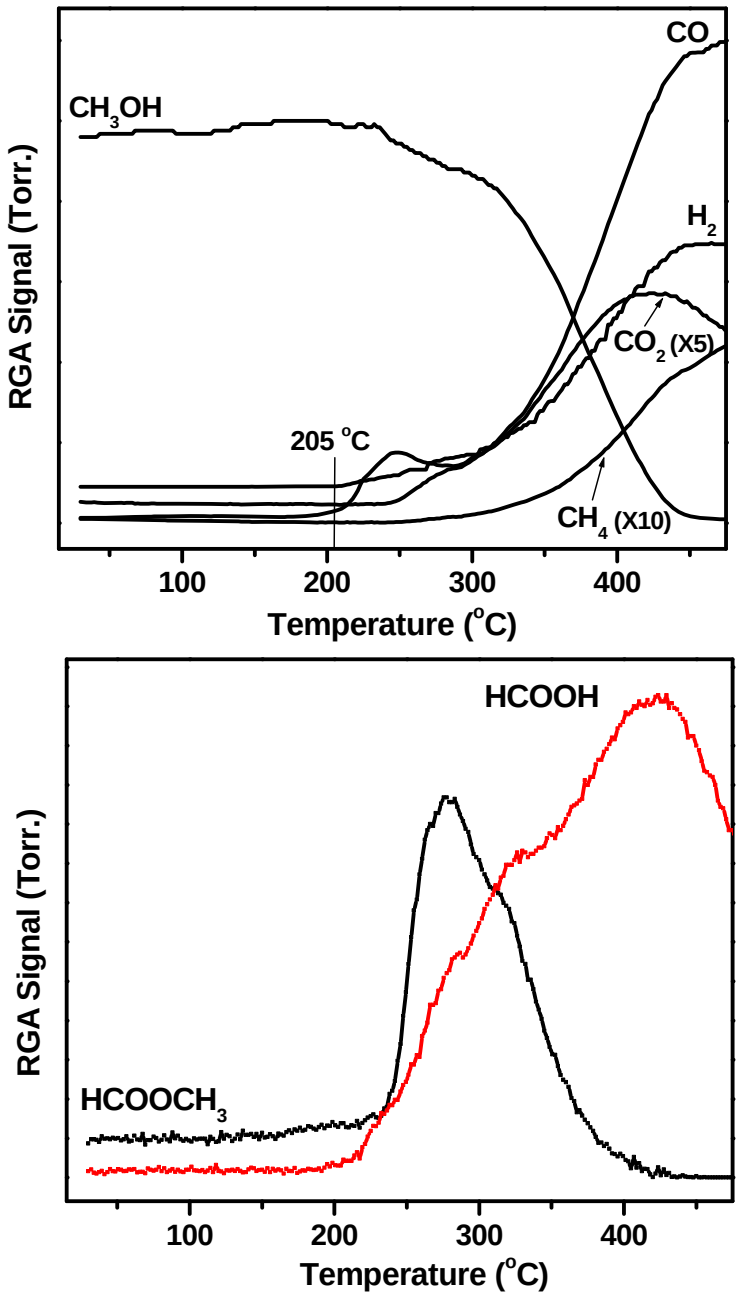


Figure 3.12 $CH_3OH$-TPSR profile over 5%Cu-Ceria (UGC)

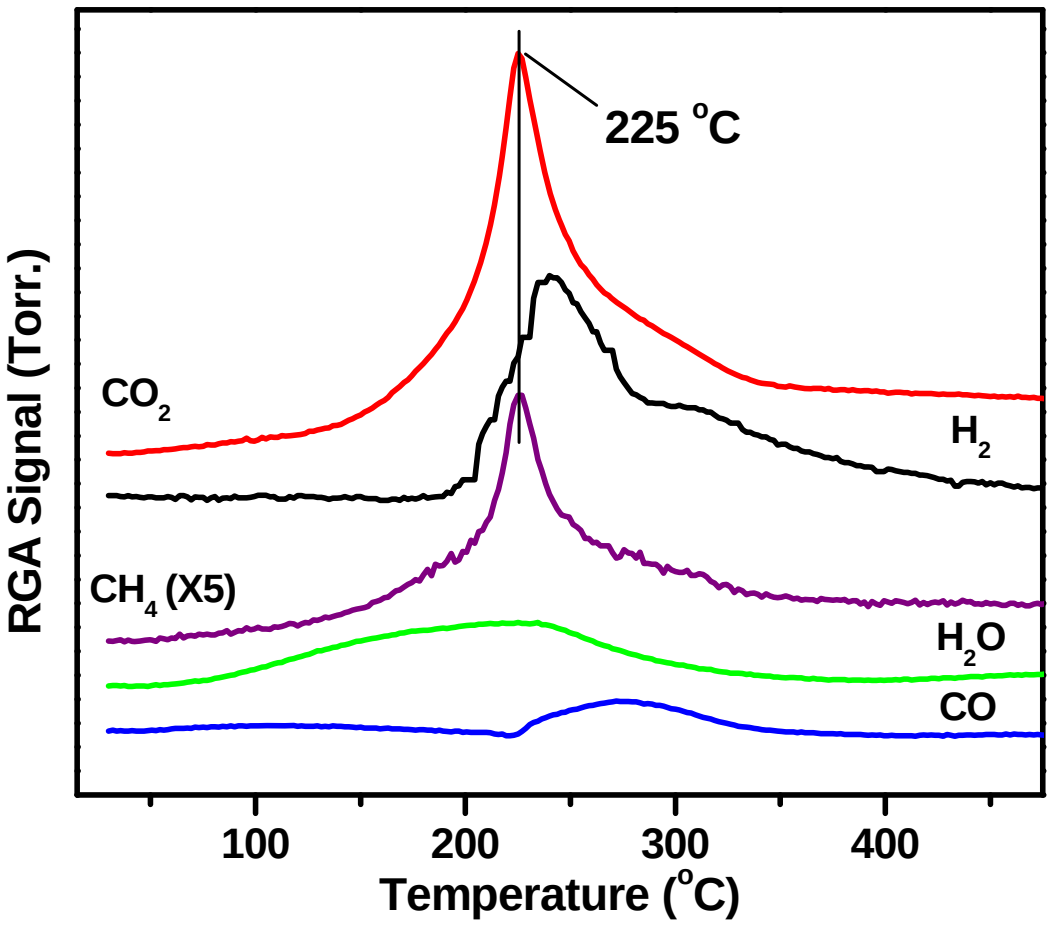


Figure 3.13 HCOOH-TPD profile over 5%Cu-Ceria(UGC)

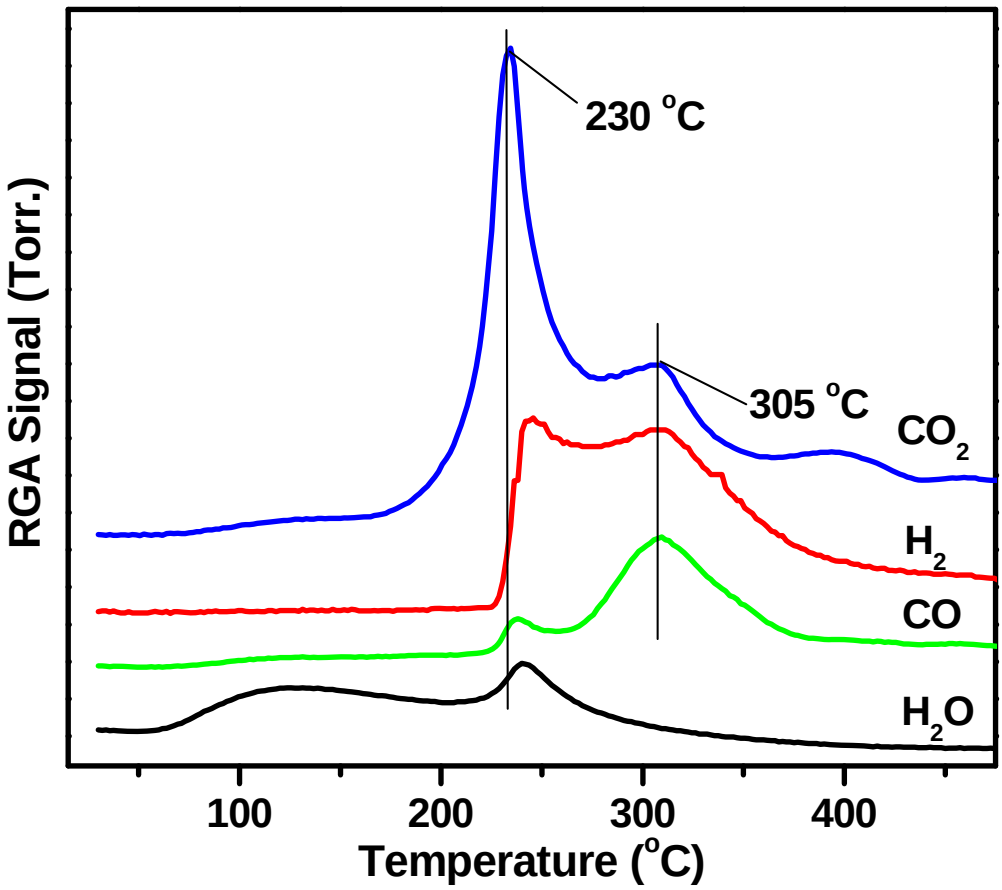


Figure 3.14 HCOOH-TPSR profile over 5%Cu-Ceria(UGC)

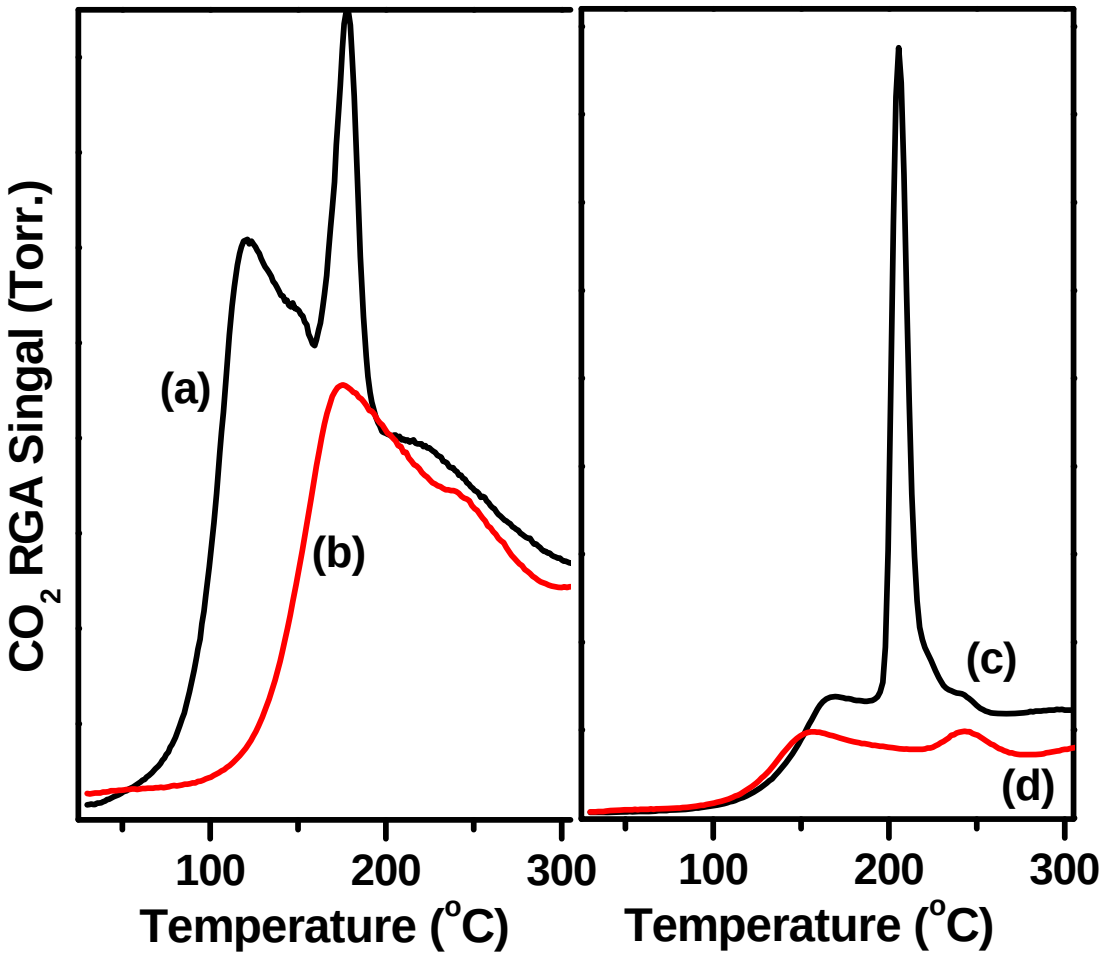


Figure 3.15 $CO_2$ desorption profiles from CO-TPR over (a) 15%Cu-$CeO_2$(Rod); (b) Leached 15%Cu-$CeO_2$(Rod); (c) 15%Cu-$CeO_2$(Cube); and (d) Leached 15%Cu-$CeO_2$(Cube)

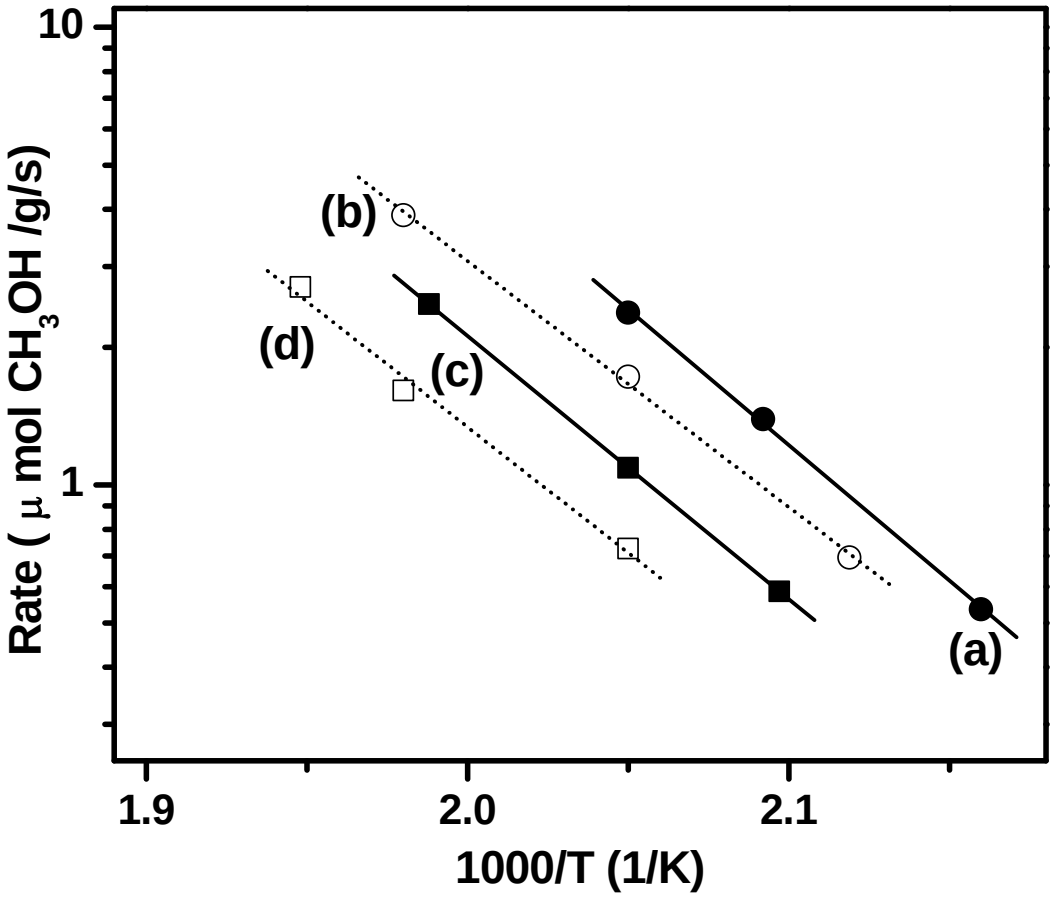


Figure 3.16 Methanol decomposition rates over Cu-$CeO_2$ catalysts: (a) 15%Cu-$CeO_2$(Rod); (b) Leached 15%Cu-$CeO_2$(Rod); (c) 15%Cu-$CeO_2$(Cube); and (d) Leached 15%Cu-$CeO_2$(Cube)

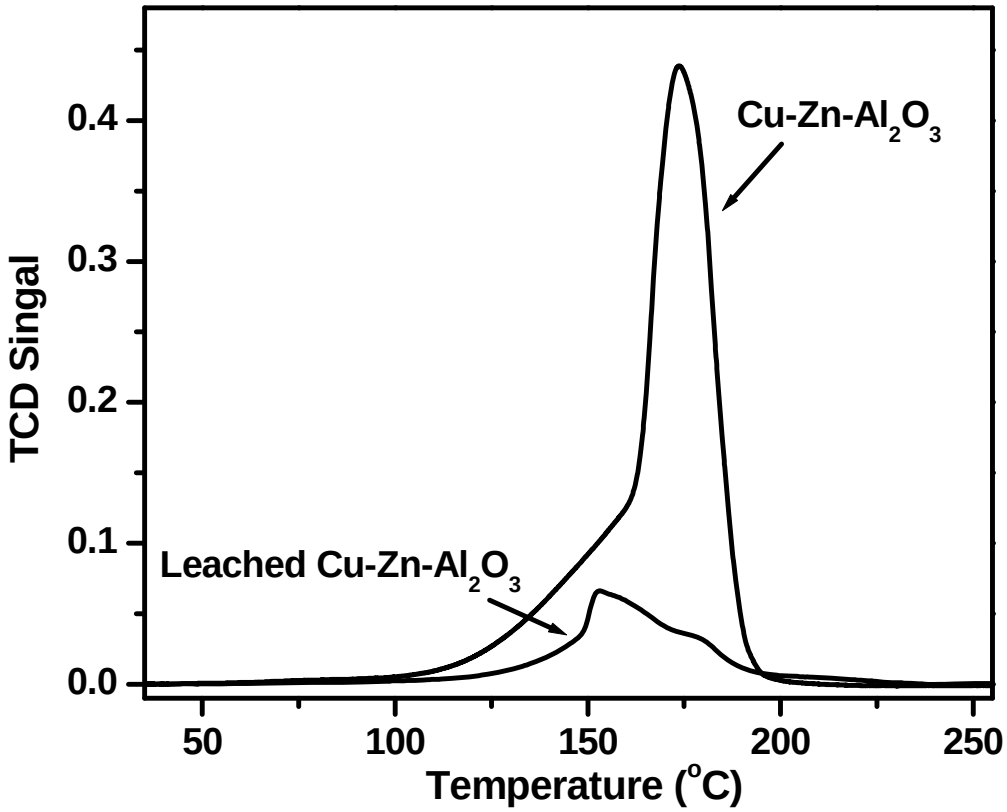


Figure 3.17 $H_2$-TPR profiles over commercial Cu-Zn-$Al_2O_3$ catalysts (parent and leached)

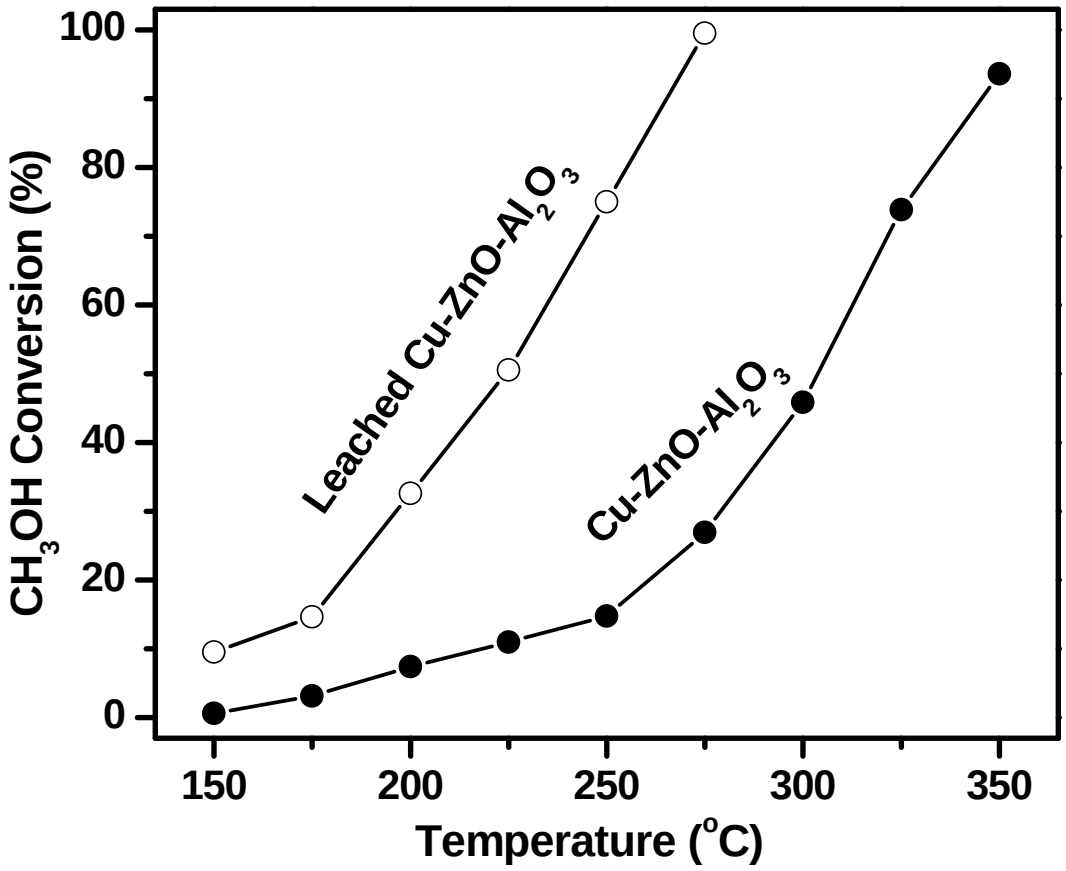


Figure 3.18 Methanol conversion (%) over commercial Cu-Zn-$Al_2O_3$ catalysts (parent and leached)

Gas composition: 16%$CH_3OH$/bal. He; GSHV= 42,000 $h^{-1}$

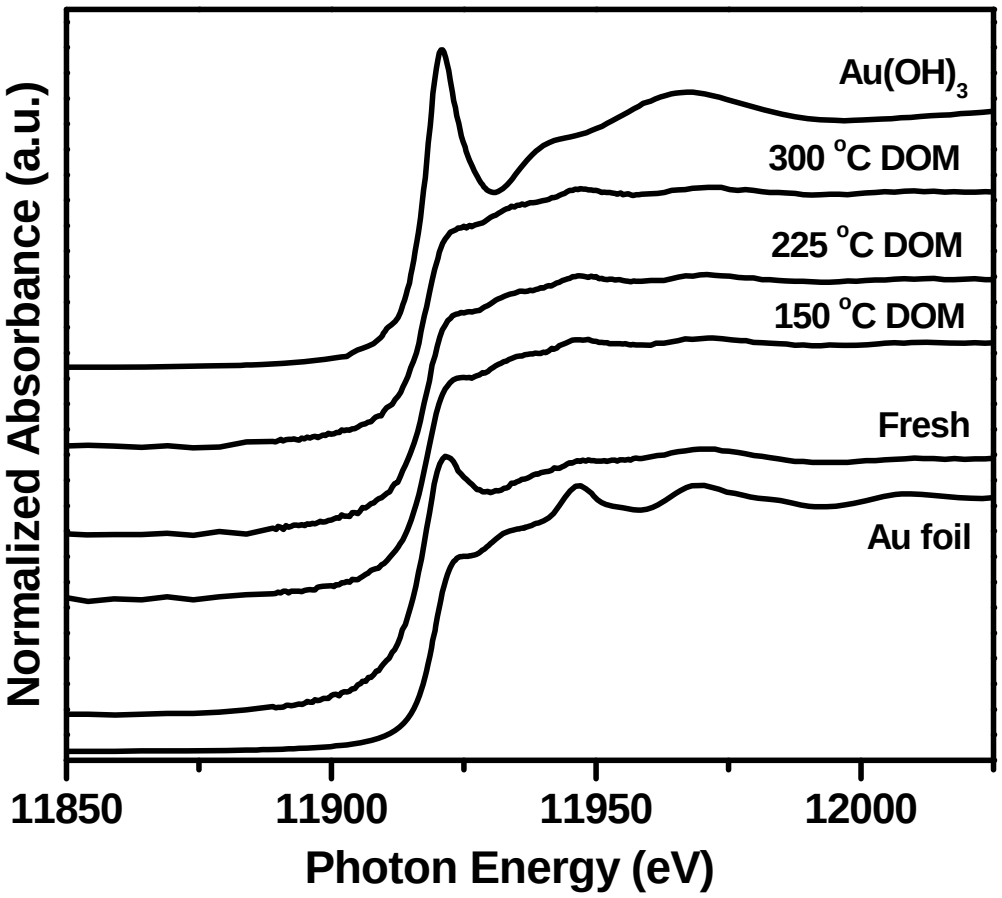


Figure 3.19 Au $L_{III}$-edge XANES spectra of 1% Au-Ceria(Rod) under various conditions

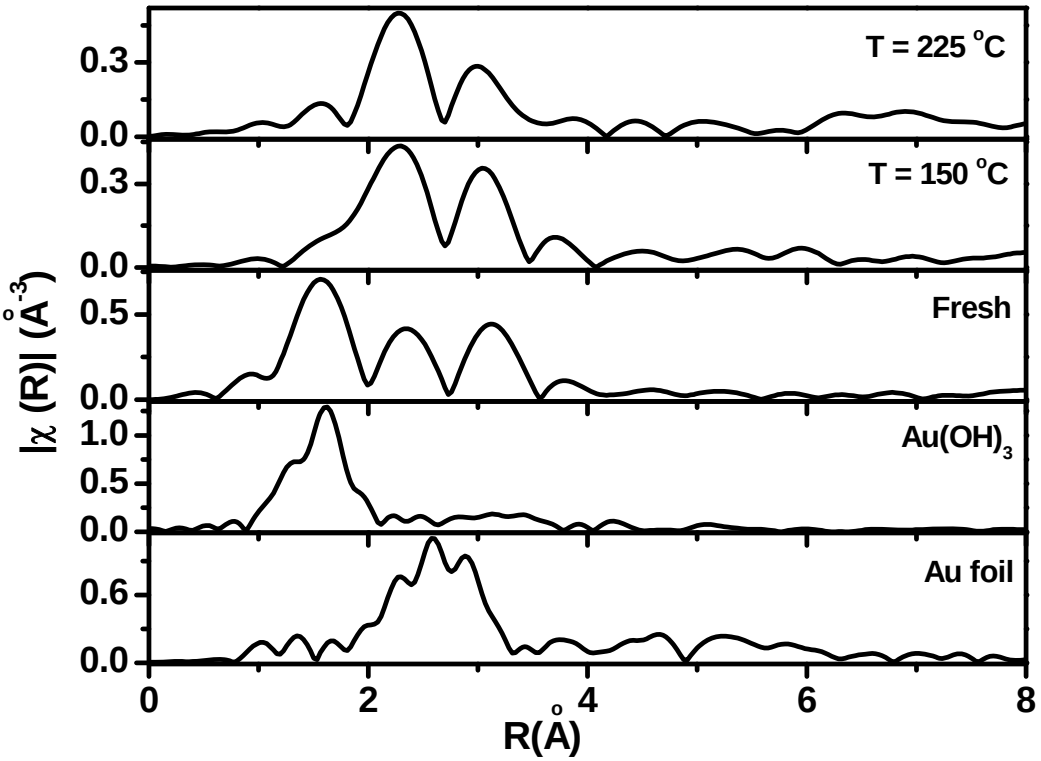


Figure 3.20 EXAFS analysis of 1%Au-Ceria(Rod) under various conditions (as-prepared and used in methanol decomposition for 1.5 h at 150 °C and 225 °C) in the R space

# Chapter 4: Steam reforming of methanol over gold and platinum dispersed on oxide surface

Steam reforming of methanol (SRM), which produces hydrogen and carbon dioxide by reacting a methanol and water (steam) mixture, is one of the significant catalytic processes to produce hydrogen in different scales. Steam reforming of methanol produces the highest amount of hydrogen among all hydrogen-producing reactions using methanol as reactant. Practically, this reaction is pursued as a source of on-board hydrogen production for fuel cells. This solves the problem of storing pressurized hydrogen on-board which is not a viable solution for passenger vehicles. Methanol is not an exotic fuel; rather it can be found in many gas stations, and is also one of the logistics fuels used by the US military. SRM may be the preferred option for small portable fuel cells used either commercially or for soldier power. Fundamentally, mechanistic studies followed by the exploration of new types of low temperature catalysts for steam reforming of methanol, would provide insights to optimize the operation conditions based on the choice of catalysts.

We have addressed the different chemistry in methanol decomposition between Group IB metals (Cu and Au) and Group VIII metals (Pt and Pd) in Chapter 3. In this Chapter, gold and platinum are chosen as representative of those two groups of metals and are used to explore gold-based and platinum-based catalysts for low temperature (< 300 $^{o}$C) steam reforming of methanol. First different approaches aimed at optimizing and maximizing the active sites were investigated. Second, the role of water was investigated to build the link between methanol decomposition and methanol steam reforming. Third, stability tests along with parametric studies at different operation conditions were carried out to check the potential of these catalysts for practical applications.

## 4.1 Au-Ceria as low-temperature methanol steam reforming catalyst

For the methanol decomposition reaction, different pathways between Pt, Pd-Ceria and Au-Ceria were identified through temperature programmed reactions. Similar to copper, gold catalyzes the formation of methyl formate over gold-ceria. Because no carbon monoxide was produced at low temperatures over gold-ceria, it could be a potential catalyst itself or used as a suitable catalyst component for methanol steam reforming with excellent selectivity to $CO_2$.

### *4.1.1 Low temperature activity*

Steam reforming of methanol (SRM) was studied over gold-ceria and pure ceria. Pure ceria was prepared by a hydrothermal method, and gold was added through the deposition precipitation (DP) method at 80 $^{o}$C. More detailed preparation procedures are available in Chapter 2. Samples were reduced with 20%$H_2$/He at 300 $^{o}$C before each activity test. Typical test conditions are: 2.0%$CH_3OH$/2.6%$H_2O$ balanced with helium. The steady-state SRM reaction rates were measured by keeping each temperature constant for 1.5 h. Methanol conversion was followed as a function of temperature over the 1%Au-$CeO_2$ and gold-free ceria samples. Addition of gold improved the activity of the undoped ceria dramatically, as shown in Figure 4.1. The 1%Au-Ceria (Rod) catalyst achieved full methanol conversion at ~300 $^{o}$C, and no hysteresis or deactivation was observed upon cooling to lower temperatures. Even after three cycles, including heating to 300 $^{o}$C in the reaction gas mixture, cooling to room temperature in He, and reheating to 300 $^{o}$C in the reaction gas mixture, the Au-Ceria (Rod) sample retained its fresh-state activity. The same was also true for the 1%Au-Ceria (Cube) catalyst. Hence, the SRM stability of Au-Ceria is promising for potential practical application. More detailed stability testes will be addressed in the following section.

It was observed that the reaction rates were much lower on the 1%Au-Ceria (Cube) than on the 1%Au-Ceria (Rod). At 250 $^{o}$C, the rate was 12.3 μmol·gcat$^{-1}$·s$^{-1}$ over Au-Ceria(Rod) and 0.2 μmol ·gcat$^{-1}$·s$^{-1}$ over Au-Ceria(Cube). However, the apparent activation energies were the same, ~ 110 kJ/mol, as shown in Figure 4.2. The apparent activation energy of SRM over Au-Ceria catalysts is close to values obtained on Cu/ZnO/$Al_2O_3$ catalysts, 105 kJ·mol$^{-1}$ [1]. Much higher $E_{app}$ values were found for the undoped ceria nanocubes, 168 ± 2.3 kJ·mol$^{-1}$, and ceria nanorods, 136 ± 2.7 kJ·mol$^{-1}$ (Table 1). Methanol decomposition on ceria has been reported as a structure-sensitive reaction [2]. Thus, the two different $E_{app}$ values found here for SRM on gold-free ceria are indicative of a similar structure sensitivity of the SRM reaction on ceria {100} and {110} surfaces.

Although gold on ceria nanocubes was much less active than that over ceria nanorods, we cannot attribute the difference to the small difference (2x) of the specific surface area of the two ceria nanoshapes, Table 2.1. What appears to be an important difference is that in the case of gold on the ceria nanorods, the size of the gold clusters remained < 1 nm (invisible by HRTEM). After leaching the calcined parent sample using NaCN solution, the 1%Au-Ceria (Cube) had very little (~0.03% by ICP) residual gold. The SRM activity of this leached sample was the same as that of the parent sample. Hence, the 3 nm gold nanoparticles are not active for the SRM reaction, and in the 1%Au-Ceria (Cube) all the catalysis is done by the interaction of the residual gold and ceria. The residual gold on ceria was 0.5 at.%Au for the rod and 0.03 at.%Au for the cube, which can be counted as the active sites. Turnover frequencies can then be calculated by properly scaling the measured reaction rates, assuming 100% gold dispersion in the leached samples. The TOFs thus calculated were similar for both samples, *e.g.*, the TOF ~ 0.42 s$^{-1}$ at 250 $^{o}$C for both types of Au-Ceria samples. These results strongly suggest that the low-temperature SRM reaction mechanism over the Au-Ceria {110} and {100} surfaces is the same; *i.e.*, the reaction is structure insensitive.

All evidence (same activation energies and same TOF values), and as will be discussed below, same $CO_2$ selectivities and same reaction intermediates, point to a structure-insensitive SRM reaction on Au-Ceria, which was also observed on other ceria- supported catalysts, like gold-ceria and copper-ceria for the water gas shift reaction. Also, this indicates that Au-$O_x$ species stabilized on the reduced ceria sites, catalyze the reaction on both the {100} and {110} ceria

surfaces by the same reaction pathway. Thus, ceria does not appear to play a role in the low-temperature SRM pathway, opened by the Au-$O_x$ active sites. The number of the latter of course is determined by the availability of anchoring sites (binding sites) on ceria, which differs for the two different surfaces of ceria used here. The preparation conditions, especially calcination temperature and oxygen potential can also affect the number of binding sites on these surfaces.

Methanol conversion over pre-reduced Au-Ceria was compared to pre-oxidized samples, and the results are shown in Figure 4.3. It was found that the pre-reduced samples showed much higher activity in SRM. However, once the reaction achieved full conversion, the same shape of methanol conversion was observed when the reaction was cooled down to lower temperature in the mixture of methanol and water (2.0 %$CH_3OH$/ 2.6% $H_2O$/He). Thus, the reaction conditions determine the steady-state active structure of the catalyst. The reduction treatment has been proposed to be beneficial to gold added to a support oxide by deposition-precipitation method. Indeed, the oxidation-reduction treatment is considered better than air calcination to disperse the gold particles on the support. Here this protocol was not followed and all samples were typically calcined in air at 400 $^oC$ after drying. However, reduction at 300 $^oC$ leads to gold-assisted surface reduction of ceria [3]. Thus, it can be argued that Au-$O_x$ clusters were stabilized at the surface oxygen vacancies of ceria, and that these are the active sites for SRM. Another explanation may be through the water-reduced ceria interaction after the reduction pre-treatment. Kundakovic *et al.* [4] have reported that the interaction between water and ceria strongly depends on the presence of reduced cerium, $Ce^{3+}$, and Rh facilitates the adsorption of water on ceria. Water and hydrogen desorbed as products following water adsorption on the reduced ceria surface, while only weakly adsorbed water was found on the oxidized ceria [4]. It is worth to conduct a similar investigation on Au-$CeO_x$ surfaces.

### *4.1.2 $CO_2$ selectivity*

The $CO_2$ selectivity of 1%Au-Ceria(Rod) and Ceria (Rod) is compared in Figure 4.4. Gold-ceria has high $CO_2$ selectivity (> 93%) over the whole range of temperatures tested. Especially, in the temperature range 175-250 $^oC$, the $CO_2$ selectivity exceeded 97%. The same was also true for

the 1%Au-Ceria(Cube). The $CO_2$ selectivity measured was higher than the equilibrium $CO_2$ selectivity, which indicates that the water gas shift reaction is not involved in the pathway of steam reforming of methanol, as is the case for the PdZn alloy catalysts [5]. However, over the undoped ceria crystals, the $CO_2$ selectivity dropped with increasing methanol conversion. As discussed in Chapter 3, decomposition of methanol to CO + $H_2$ has been identified as the unique pathway for ceria. Thus, over pure ceria samples, all carbon dioxide derives from the water gas shift reaction whose equilibrium limits the selectivity.

*4.1.3 Stability tests*

In cyclic heating to 300 $^oC$/cooling to room temperature in the SRM reaction mixtures over the Au-ceria lasting a total of 15 h, no catalyst deactivation was observed. The stability of Au-Ceria (Rod) in shutdown/restart operation was further studied. As shown in Figure 4.5, after 2h on stream at 225$^oC$ under SRM conditions, shutdown to RT in the stream of mixture of methanol and water ( 2.0% $CH_3OH$/2.6% $H_2O$/He) for 2h was used twice, followed by reheating to 225$^oC$. The catalyst did not suffer any activity loss due to these treatments.

The morphologies of the used Au-Ceria nanorods and nanocubes after the SRM testing were also investigated by TEM. For the rod samples, it can be seen from Figures 4.6(a) and (b) that the reaction conditions had a minor effect on the morphologies of the $CeO_2$ crystals. Although the edge of the ceria nanorods became slightly rounded, gold particles were still absent as checked by TEM/HREM. This suggested that gold atoms and clusters (< 1 nm) were stable on the {110} surfaces even after 15 h on stream. Figures 4.6(c) and (d) show that the cube shape of ceria was maintained after reaction in the $CH_3OH/H_2O$ gas mixtures. The sizes of both $CeO_2$ nanocubes and Au nanoparticles did not change.

The state of gold after 15 h on-stream in the SRM reactions was also characterized by XPS. On the fresh gold samples, ionic gold ($Au^+$ and $Au^{3+}$) was found to be the main species in the rod sample, while metallic gold ($Au^0$) was found to be dominant on the ceria nanocubes. After pre-reduction of gold-ceria samples at 300 $^oC$ with 20% $H_2$/He and followed by 15 h on-stream in methanol steam reforming reaction condition , the dominant species was zerovalent gold species,

as shown in Figure 4.7. Furthermore, according to the TEM/HREM results (Figure 4.6), the zerovalent gold was still well dispersed on the SRM-used rod samples, since no gold particles bigger than 1 nm were found.

Temperature-programmed oxidation (TPO) tests were carried out on the fresh and used catalysts to investigate the catalyst stability in the SRM reaction. Only adventitious carbon from the atmospheric exposure was found on both the fresh and used samples. Decomposition of carbonates and desorption of water show peaks centered at ~ 120$^{o}$C, as shown in Figure 4.8. No higher temperature carbonate formation or carbon deposition took place. This corroborates the cyclic catalyst stability in heating-cooling tests discussed above and further shows that the SRM stability of the Au-Ceria system is good for practical application of this type of catalyst, *e.g.*, in fuel cell systems requiring frequent shutdowns during typical operation.

### *4.1.4 Proposed SRM pathway over Au-Ceria*

The mechanism of steam reforming of methanol is still being debated even for well-studied systems. For example, on the Pd-Zn alloy catalyst, the methyl formate route has been suggested [6]. Others also report the methyl formate route for copper catalysts [7, 8]. As mentioned in Chapter 3, formaldehyde will form after methanol is adsorbed on IB group metals (Cu, Ag and Au), because the intermediate methoxy ($CH_3O$) species is stabilized on those metal surfaces [9]. Compared with Pt and Pd, the Au (110), (111) surfaces catalyze the formation of methyl formate through methanol coupling reaction [10, 11]. While only physical methanol adsorption was found on clean gold surfaces, the formation of desorption products was identified on oxygen covered gold surfaces [10,11].

To explore the role of water in methanol decomposition, ($CH_3OH+H_2O$)-TPSR was carried out for the two Au-Ceria catalysts under investigation. In ($CH_3OH+H_2O$)-TPSR over 1%Au-Ceria(Rod), as shown in Figure 4.9, hydrogen and carbon dioxide were formed at temperatures as low as 175 $^{o}$C (Temp. I). This agrees with the activity test results that showed that hydrogen

and carbon dioxide was produced in this temperature region [12, 13]. Carbon monoxide was observed starting at ~ 250 $^{o}$C (Temp. II). In the temperature range from 275 $^{o}$C to 335$^{o}$ C, the formation of CO may be due to decomposition of methoxy on ceria [2]. Another possibility is that reverse water gas shift occurs. Either scheme would account for the corresponding drop in $CO_2$ selectivity. In the temperature range between III (335$^{o}$ C) and IV(395$^{o}$ C), the concentration of CO and water decreased sharply while $CO_2$ and $H_2$ increased. As methanol conversion is complete at 325$^{o}$ C, less methoxy is adsorbed; hence much more CO is able to absorb on the gold active site, and the water-gas shift reaction takes place. This suggests that the presence of methanol inhibits the water gas shift reaction. At temperatures above IV (395$^{o}$ C), the reverse water gas shift reaction dominates. Finally, the lack of methyl formate species and only trace amounts of methane in ($CH_3OH$+$H_2O$)-TPSR, suggests that methyl formate hydrolysis took place,

$$HCOOCH_3 + H_2O \rightarrow HCOOH + CH_3OH \quad .$$

Indeed, trace amounts of formic acid were detected in the effluent gas in this temperature region.

The rate and the activation energies were measured for the decomposition of methanol, and they were compared to those reported for the steam reforming of methanol over the Au-Ceria catalysts. Similar apparent reaction activation energies were found, and similar intermediate products were detected, suggesting that the rate limiting step in the two reactions is the same. Both reactions share the methyl formate route, and the SRM reaction pathway does not involve the water-gas shift reaction.

On the basis of these findings, the methyl formate pathway is proposed for the SRM reaction over Au-Ceria. Adsorbed water helps to hydrolyze methyl formate to formic acid, as in the set of reactions below:

$$2CH_3OH \rightarrow HCOOCH_3 + 2H_2 \quad \text{(I)}$$

$$HCOOCH_3 + H_2O \rightarrow HCOOH + CH_3OH \quad \text{(II)}$$

$$HCOOH \rightarrow CO_2 + H_2 \quad \text{(III)}$$

It should be pointed out that the 1% Au-Ceria(Rod) catalyst shows excellent activity for the water gas shift reaction, comparable to Au/ceria nanopowders, including Au on the Rhodia ceria which has a high surface area of 250 $m^2$/g. However, the Au-Ceria (Cube) is inactive [14]. The question then arises why the Au-Ceria (Rod) catalyst does not show any WGS activity at temperatures below 250 $^oC$. This may be explained by the competitive adsorption between CO and methanol [15, 16]; methanol likely absorbs more strongly than CO on the Au-$O_x$ species. Based on literature reports [17, 18], methanol has a higher heat of adsorption on Au (111) than carbon monoxide.

In order to further investigate the mechanism of steam reforming of methanol over Au-Ceria, carbon monoxide was added to the feed mixture of methanol and water. Two different concentrations of carbon monoxide (5% and 20% by volume) were introduced into the reaction gas mixture at 225 $^oC$. It was found that the production rates of hydrogen and the ratio of $H_2/CO_2$ did not change. When carbon monoxide was added into the mixture, the concentration of $H_2O$ did not change, and the conversion of methanol remained the same, as shown in Figure 4.10. This further suggests that the water-gas shift reaction is not involved in the SRM reaction pathway on gold catalysts.

In a separate experiment, the addition of methanol to the mixture of $CO_2$ and $H_2$ was carried out to investigate the methanol effect on the reverse water gas shift reaction. At 250 $^oC$, good conversion of methanol was noted accompanied by a reduced $CO_2$ conversion, as shown in Figure 4.11. This proves that the addition of methanol into a steady- state reverse water gas shift reaction condition changes the product gas distribution.

### *4.1.5 Active gold species*

The Au-$O_x$ species can stabilize HCHO through heterolytic activation of the C-H bond of the methoxy species adsorbed on the Au site by the oxygen bound to gold. The coupling of the formaldehyde with a nearby methoxy species produces methyl formate. The role of the ceria or another support can be viewed as a stabilizer of the active Au-$O_x$ species. It may be called a cooperative mechanism, but not in the narrow sense of the term, whereby the support participates

in the reaction. Since strongly bound gold species on ceria catalyze the methanol dehydrogenation, but the type of ceria surface ({110}, {100}, etc.) determines the number density of active Au-$O_x$ species, it is interesting to investigate whether these findings can be extended to other supports as well.

Au-ZnO was examined as a new catalyst for methanol reactions in our lab by Boucher *et al.* [19, 20]. Similar to the case for ceria, different shapes of ZnO support, namely polyhedral, short rods and long rods, were synthesized by controlled methods [21]. Gold was deposited on the ZnO nanoshapes by deposition-precipitation methods. For Au-ZnO there are two possibilities: Au may bind on Zn-vacancies and interact with neighboring under-coordinated lattice O atoms [22], or it may perturb the oxide defect equilibrium causing a dramatic rise in oxygen vacancies and consequently interact with adsorbed O at the periphery of the metallic particle [23]. The use of selected ZnO surfaces with different concentrations of defects can elucidate this issue.

It was observed that the rates were highest for the Au-ZnO polyhedra, followed by the short rods, then the long rods [19]. This could be explained by the fact that the higher the ratio of exposed {0001} surfaces to the bulk, the higher the activity expected. The {0001} surfaces of zinc oxide achieve better dispersion of gold than other surfaces, thus the ZnO polyhedra have a higher activity than other ZnO shapes. A comparison between the reaction rates over Au-ceria and Au-ZnO is shown in Figure 4.12. Au-Ceria (Rod) has the highest rate at 250 $^{o}$C compared with other gold catalysts.

Interestingly, the activation energy over all Au-ZnO samples is the same, i.e. it is independent of the ZnO shapes. It is also the same for the reaction on Au-$CeO_2$ samples. Thus, the same active site Au-$O_x$ appears to catalyze the low-temperature (175-225°C) SRM reaction on both supports. By TPSR it was found that the methyl formate intermediate pathway was followed on Au-ZnO [19, 20], similar to the Au-$CeO_2$ catalysts studied in this thesis. Overall, the shape effect of the oxide nanocrystals was found to be indirect; *i.e.*, the catalytic activity depends on the number of fully dispersed gold species on ceria or zinc oxide.

## 4.2 Steam reforming of methanol over platinum clusters

### *4.2.1 Steam reforming of methanol over Pt-Ceria*

As discussed in Chapter 3, methanol decomposition over Pt-Ceria takes place by decomposition of methoxy groups to produce hydrogen and carbon monoxide. In a ($CH_3OH$+ $H_2O$) -TPSR test, shown in Figure 4.13, carbon dioxide was formed along with carbon monoxide and hydrogen. Compared with $CH_3OH$-TPSR, where only carbon monoxide and hydrogen were generated, the formation of carbon dioxide with the addition of water confirms the occurrence of the water gas shift reaction. At the same time, methane and other carbon species were not observed. As is well known, Pt-$CeO_2$ is a very good low-temperature shift catalyst [24], while it is not a methanation catalyst [25]. As discussed previously, the choice of ceria improves the overall activity of Pt by keeping it dispersed and oxidized, but it does not change the reaction pathway and thus the selectivity to hydrogen which is dictated by the metal.

The population of active sites can also be characterized by $CO_2$-TPD. In Figure 4.14, in the range 80 – 200 $^oC$, a single and symmetrical peak was recorded over Pt-Ceria (Rod), and a very weak $CO_2$ desorption peak was observed over Pt-Ceria (Cube). The low temperature peak was assigned to the monodentate carbonate [26]. At higher temperatures, above 400 $^oC$, another set of $CO_2$ desorption peaks were observed over Pt-ceria samples. These were attributed to bidentate carbonate [26, 27]. Still larger amounts of $CO_2$ desorption were identified over the Pt-Ceria(Rod) compared with that of Pt-Ceria(Cube). $CO_2$-TPD is useful as it does not only identify the basic properties of the Pt-Ceria surface, but also measures the different amounts of active sites on the different ceria surfaces.

Steady-state activity tests were performed over Pt-Ceria. The light-off over Pt-Ceria(Rod) is at ~150 $^oC$, and full conversion of methanol was observed at 300 $^oC$, as shown in Figure 4.15. The same activation energy was calculated over all the platinum–ceria catalysts, suggesting that strongly bound Pt-$O_x$-Ce species are the active sites for methanol reactions; similar to the water-gas shift reactions [24, 28].

A small amount of sodium (3.0 wt%) was added to the Pt-Ceria(Rod), but not much enhancement in methanol conversion was seen by the addition of the alkali. Wachs and coworkers [29] have pointed out that the strength of the $PtO_x$-support interaction is determined by the reducibility of the support. A negative alkali effect on Pt-Ceria for the water gas shift and steam reforming of methanol was reported by Burtron Davis's group [30]. They suggested that addition of alkali may block the Pt surface sites and result in a reduction temperature shift to higher temperatures, thus inhibiting the low temperature activity for the water gas shift reaction. In any case, due to the strong Pt-$O_x$-Ce interaction, the alkali effect apprears to be less apparent on Pt-$CeO_2$ for methanol reactions. Instead, it would be interesting to investigate alkali addition on $PtO_x$ species weakly interacting with a support, such as silica.

### *4.2.2 Steam reforming of methanol over Pt-$SiO_2$*

To address the above issue, methanol activation was examined on Pt-$SiO_2$. This is not a low-temperature catalyst, as methanol begins to react at > 250 $^oC$. Figure 4.16 depicts this low-activity in $CH_3OH$-TPSR tests with carbon monoxide and hydrogen production as methanol began to decompose. We attribute this lack of reactivity to the lack of stabilized PtOx species on the surface of the silica support [31]. Methanol conversion did not change with the addition of water into the stream of methanol, and carbon monoxide and hydrogen were the main products. Figure 4.17 also shows a slight change of water concentration during reaction. Thus, water can not be activated on this surface and does not participate in the methanol reaction.

## 4.3 Promotion of Pt-$SiO_2$ by Na addition for the steam reforming of methanol

Our findings have demonstrated that dispersed and stabilized $PtO_x$ species catalyze the steam reforming of methanol. The decomposition of methanol, followed by the water gas shift reaction is proposed to comprise the main steps in the reaction network of methanol steam reforming.

Approaches which can improve either of these two basic reactions are expected to enhance the catalytic performance of platinum based catalysts for steam reforming of methanol. In this section, the enhanced water gas shift reaction through the addition of alkali is examined as one such approach to improve the catalytic performance of steam reforming of methanol. A sample with 3.0 wt% Na added on 1at%Pt-$SiO_2$, labeled as Na-Pt-$SiO_2$, was prepared and tested along with the Na-free sample.

$CH_3OH$-TPSR in Figure 4.18 shows that formation of carbon monoxide and hydrogen on the Na-Pt-$SiO_2$ sample begins at much lower temperature (~ 170 $^oC$) than on the Na-free catalyst shown in Figure 4.16. Thus, the addition of sodium enhanced the methanol conversion. Also, the formation of $CO_2$ along with consumption of methanol was observed. Recently, Zhai *et al.*[31] reported that alkali modified Pt-$SiO_2$ and Pt-$Al_2O_3$ surfaces have comparable activity with Pt-$CeO_2$ for the water-gas shift reaction. They also suggested that the same Pt-alkali-$O_x(OH)_y$ species is the active site for the low temperature Pt-catalyzed water gas shift reaction on all oxide support surfaces. Therefore, the concurrent appearance of $CO_2$ with CO and $H_2$ in Figure 4.18 is attributed to the enhancement of the WGS reaction on the Na-promoted catalyst. Also, Kucernak *et al.* [32] have shown that adsorbed hydroxyl species promoted the carbon monoxide oxidation on platinum: $CO + OH \rightarrow CO_2 + 1/2H_2$.

The addition of sodium also increased the amount of dimethylether (DME) produced in the lower temperature, which is shown in the inset in Figure 4.18. Previous work by Solymosi's group [33, 34] suggested the addition of potassium increased the strength of adsorption of methanol on Pt single crystal. This may also be used to explain the better stabilization and reactivity of methanol on the alkali- promoted Pt catalysts, as the one used here. The addition of sodium over Pt-$SiO_2$ could also improve the adsorption of methanol, thus facilitating the formation of DME.

Water response to the sodium addition was followed by $H_2O$-TPSR. ~3 vol% $H_2O$/He was passed through the samples with and without the addition of sodium. As shown in Figure 4.19, water was consumed over Na-Pt-$SiO_2$, while no change of water signal took place over Pt-$SiO_2$, suggesting that the addition of sodium promoted water adsorption and dissociation. This finding is worth investigating further.

($CH_3OH+H_2O$) –TPSR was conducted to follow the products on promoted Na-Pt-$SiO_2$. Figure 4.20 shows that carbon dioxide and hydrogen are the only products in the temperature range below 275 $^oC$, after which the formation of carbon monoxide was observed. The "lack" of CO at the lower temperature is due to a very fast consumption by the WGS reaction. However, CO would be observed in this range under different conditions at the concentration determined by equilibrium. Although Na-Pt-$SiO_2$ has similar SRM-TPSR profile as Au-ceria shown in Figure 4.9 , the reaction mechanism on gold and platinum catalysts is different.

## 4.4 Summary

In this chapter, the methanol reactivity on gold-based catalysts (gold-ceria as a main example) and platinum-based catalysts was investigated. Strong evidence was obtained that dispersed, oxidized gold or platinum clusters, Au-$O_x$ and Pt-$O_x$, respectively, are the active species catalyzing the steam reforming of methanol. Depending on the choice of support, these species were achieved through different strategies. Au-$O_x$ species were obtained by choosing ceria nanorods to increase the interaction between gold and the defects (oxygen vacancies) of ceria; stabilized and size-controlled Pt-$O_x$-(OH)-Na on $SiO_2$ were obtained by the addition of sodium.

Gold-ceria was demonstrated as a most efficient catalyst for steam reforming of methanol at low temperatures. The reaction pathway over gold- based catalysts was identified as the sequence of methyl formate to formic acid to $CO_2$ and $H_2$. First, the formation of methyl formate through methanol coupling (HCHO + $CH_3O$) reaction occurs, followed by the formation of formic acid through hydrolysis of methyl formate, and finally $CO_2$ is produced solely by dehydrogenation of formic acid. This explains why gold-ceria has high $CO_2$ selectivity, i.e. the water gas shift reaction is not involved in the reaction network. Strongly bonded $Au_n$-O-M species, independent of the choice of support ($CeO_2$, ZnO) and morphology of support, appear to be the common active sites for the methanol reactions. Furthermore, gold-ceria was stable under cyclic reaction conditions and shutdown/re-start conditions. In short, gold-ceria was identified as a new generation catalyst for the low temperature steam reforming of methanol with high activity, high hydrogen selectivity, and good stability.

The addition of alkali (sodium in this case) has minor effect on Pt-ceria in steam reforming of methanol due to the already present strong interaction between platinum and ceria support. However, significant activity enhancement of the Na-Pt-$SiO_2$ was observed. The temperature programmed reaction testing of the Na-promoted and Na-free catalysts showed that the beneficial effect of sodium was the combined improvement of the adsorption of methanol, thus boosting the decomposition rate of methanol, in addition to activating water and subsequent acceleration of the water- gas shift reaction. Thus, with the addition of alkali, Pt can catalyze the steam reforming of methanol on inert supports, such as silica, similar to the activity and selectivity observed in the same temperature range over ceria supports.

## 4.5 References


[1] C. J. Jiang, D. L. Trimm, M. S. Wainwright, N. W. Cant, *Appl. Catal. A* 97(1993) 145.

[2] R. M. Ferrizz, G. S. Wong, T. Egami, J. M. Vohs, *Langmuir* 17 (2001) 2464.

[3] Q. Fu, A. Weber, M. Flytzani-Stephanopoulos, *Catal. Letter.* 77 (2001) 87.

[4] L. Kundakovic, D. R. Mullins, S. H. Overbury, *Surf. Sci.* 457(2000) 51

[5] R. A. Dagle, A. Platon, D. R. Palo, A. K. Datye, J. M. Vohs, Y. Wang, *Appl. Catal. A* 342 (2008) 63.

[6] N. Iwasa, N. Takezawa, *Top. Catal.* 22 (2003) 215.

[7] K. M. Minachev, K. P. Kotyaev, G. I. Lin, A. Y. Rozovski, *Catal. Lett.* 3(1989) 299.

[8] K. Takahashi, N.Takezawa, H. Kobayashi, *Appl. Catal*. 2 (1982) 363.

[9] N. D. S. Canning, D. A. Outka, R. J. Madix, *Surf. Sci*. 141 (1984) 240.

[10] D. A. Outka, R. J. Madix, *J. Am. Chem. Soc*. 109(1987) 1708.

[11] B.J. Xu, X.Y. Liu, J. Haubrich, R. J. Madix, C. M. Friend, *Angew. Chem. Int. Ed*. 48 (2009) 4206.

[12] N. Yi, R. Si, H. Saltsburg, M. Flytzani-Stephanopoulos, *Appl. Catal. B* 95 (2010) 87.

[13] N. Yi, R. Si, H. Saltsburg, M. Flytzani-Stephanopoulos, *Energy Environ. Sci*. 3 (2010) 831.

[14] R. Si, M. Flytzani-Stehphanopoulos, *Angew. Chem. Int. Ed.* 47 (2008) 2884.

[15] C. J. Jiang, D. L. Trimm, M. S. Wainwright, N. W. Cant, *Appl. Catal. A* 93(1993) 245.

[16] J. P. Breen, F. C. Meunier, J. R. H. Ross, *Chem. Commun*. (1999) 2247.

[17] G. McElhiney, J. Pritchard, *Surf. Sci*. 60 (1976) 397.

[18] W. K. Chen, S. H. Liu, M. J. Cao, Q. G. Yan, C. H. Lu, *J. Mol. Struct. (Theochem)* 770 (2006) 87.

[19] M. B. Boucher, N. Yi, F. Gittleson, B. Zugic, H. Saltsburg, M. Flytzani-Stephanopoulos, *J. Phys. Chem. C* 115 (2011) 1261.

[20] M. B. Boucher, S. Goergen, N. Yi, M. Flytzani-Stephanopoulos, *Phys. Chem. Chem. Phys.* 13 (2011) 2517.

[21] B. Cheng, E. T. Samulski, *Chem. Commun*. (2004) 986.

[22] N. S. Phala, G. Klatt, E. Van Steen, S. A. French, A. A. Sokol, C. R. A. Catlow, *Phys. Chem. Chem. Phys*. 7 (2005) 2440.

[23] F. Boccuzzi, A. Chiorino, S. Tsubota, M. Haruta, *Sens. Actuators B* 24-25 (1995) 540.

[24] D. Pierre, W. Deng, M. Flytzani-Stephanopoulos, *Top. Catal*. 46 (2007) 363.

[25] J.R. Ladebeck, J. P. Wagner, "Catalyst development for water-gas shift" (Chapter 16), *Handbook of Fuel Cells- Fundamentals, Technology and Applications*, John Wiley & Sons. LTD, 2003.

[26] M. F. Luo, Y. J. Zhong, B. Zhu, X. X. Yuan, X. M. Zhang, *Appl. Surf. Sci.* 115 (1997) 185.

[27] F. Gaillard, *Catal. Lett.* 95 (2004) 23.

[28] Q. Fu, H. Saltsburg, M. Flytzani-Stephanopoulos, *Science* 301 (2003) 935.

[29] W. Lin, A. A. Herzing, C. J. Kiely, I. E. Wachs, *J. Phys. Chem. C* 112 (2008) 5942.

[30] H. N. Evin. G. Jacobs, J. Ruiz-Martinez, G. A. Thomas, B. H. Davis, *Catal. Lett.* 120 (2008) 166.

[31] Y. P. Zhai, D. Pierre, R. Si, W. L. Deng, P. Ferrin, A. U. Nilekar, G. Peng, J. A. Herron, D. C. Bell, H. Saltsburg, M. Mavrikakis, M. Flytzani-Stephanopoulos, *Science* 329 (2010)1633.

[32] A. R. Kucernak, G. J. Offer, *Phys. Chem. Chem. Phys.* 10 (2008) 3699.

[33] F. Solymosi, A. Berkó, T. I. Tarmóczi, *J.Chem. Phys.* 87 (1987) 6745.

[34] A. Koós, R. Bartho, F. Solymosi, *J. Phys. Chem. C* 112 (2008) 2607.

**Table 4.1 Physical properties and SRM activity of Ceria and Au-Ceria Nanoshapes**

| Sample | Au dispersion (%) [a] | $E_a$ ($kJ \cdot mol^{-1}$) [b] | *Rate* ($\mu mol \cdot g_{cat}^{-1} \cdot s^{-1}$) [c] |
|---|---|---|---|
| Ceria(nanorods) | / | 136 ± 2.7 | 4.3 |
| Ceria(nanocubes) | / | 168 ± 2.3 | 1.2 |
| 1%Au-Ceria(Rod) | 100[d] | 110 ± 0.9 | 12.3 |
| 1%Au-Ceria(Cube) | 30 | 110 ± 1.2 | 0.2 |

[a] The dispersion of gold was estimated from the particle size (avg. 100 particles) in the TEM images;

[b] Apparent activation energy of Steam Reforming of Methanol (SRM).

[c] Rate measured at 400 $^oC$ for ceria and at 250 $^oC$ for Au-Ceria; Gas composition: 2%$CH_3OH$/2.6%$H_2O$/95.4%.He;

[d] Dispersion of sub-nm particles (HRTEM- invisible) set at 100%.

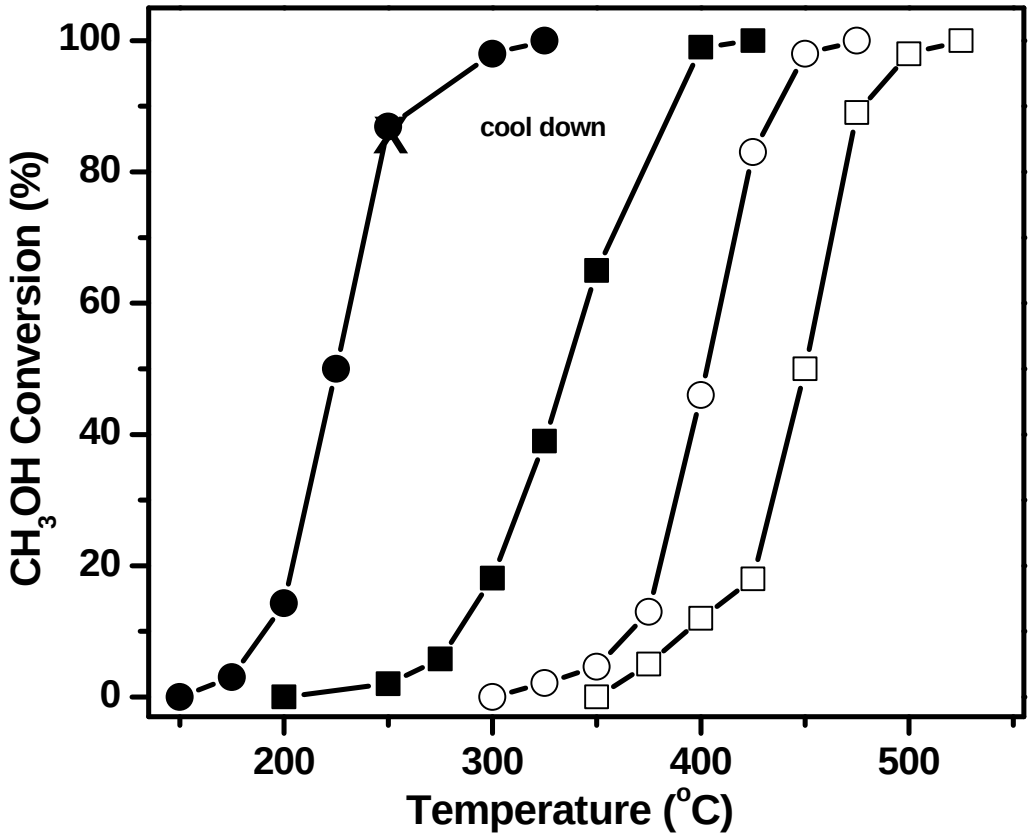


Figure 4.1 $CH_3OH$ conversion (%) in steady-state tests of steam reforming of methanol over nanoshapes of Ceria and Au-Ceria

1%Au-Ceria(Rod) (●); 1%Au-Ceria(Cube) (■);Ceria (Rod) (○); Ceria (Cube) (□) ; 1%Au-Ceria(Rod) after cooling down to 250 $^oC$ (χ); Gas composition: 2%$CH_3OH$/2.6%$H_2O$/bal. He; GSHV= 42,000 $h^{-1}$

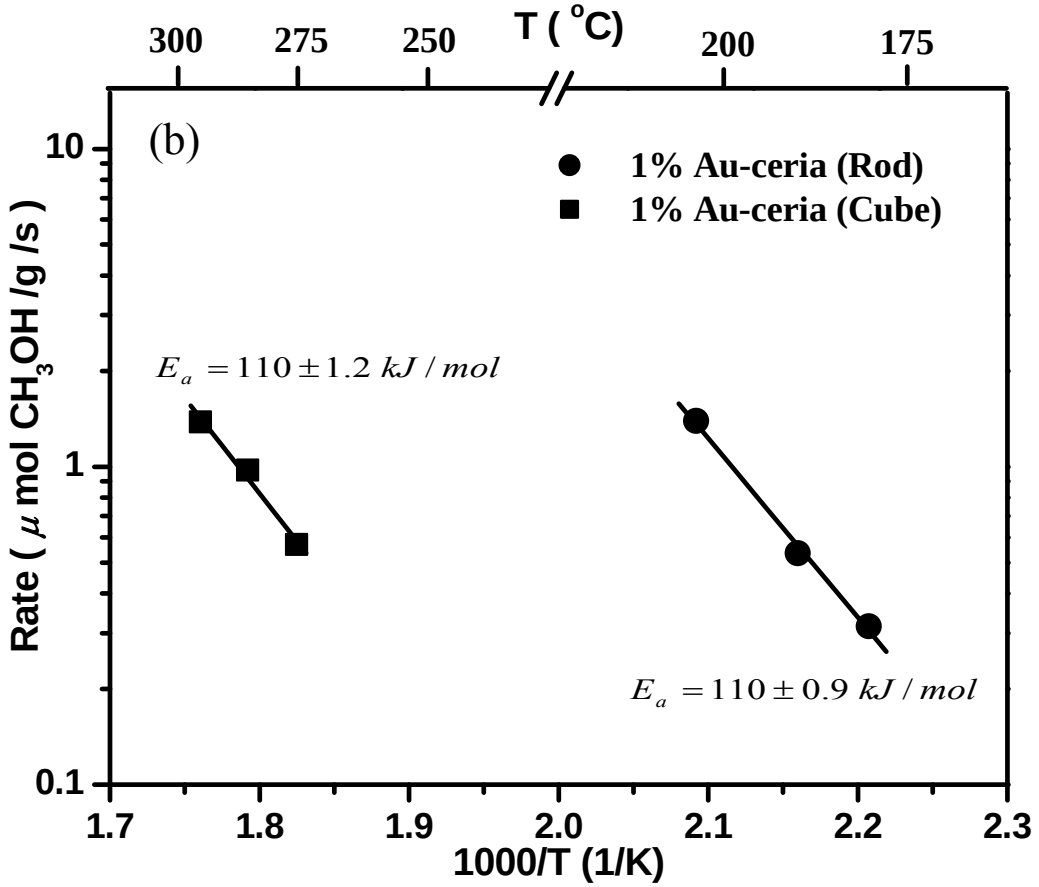


Figure 4.2 Steady-state reaction rates for steam reforming of methanol over gold-ceria

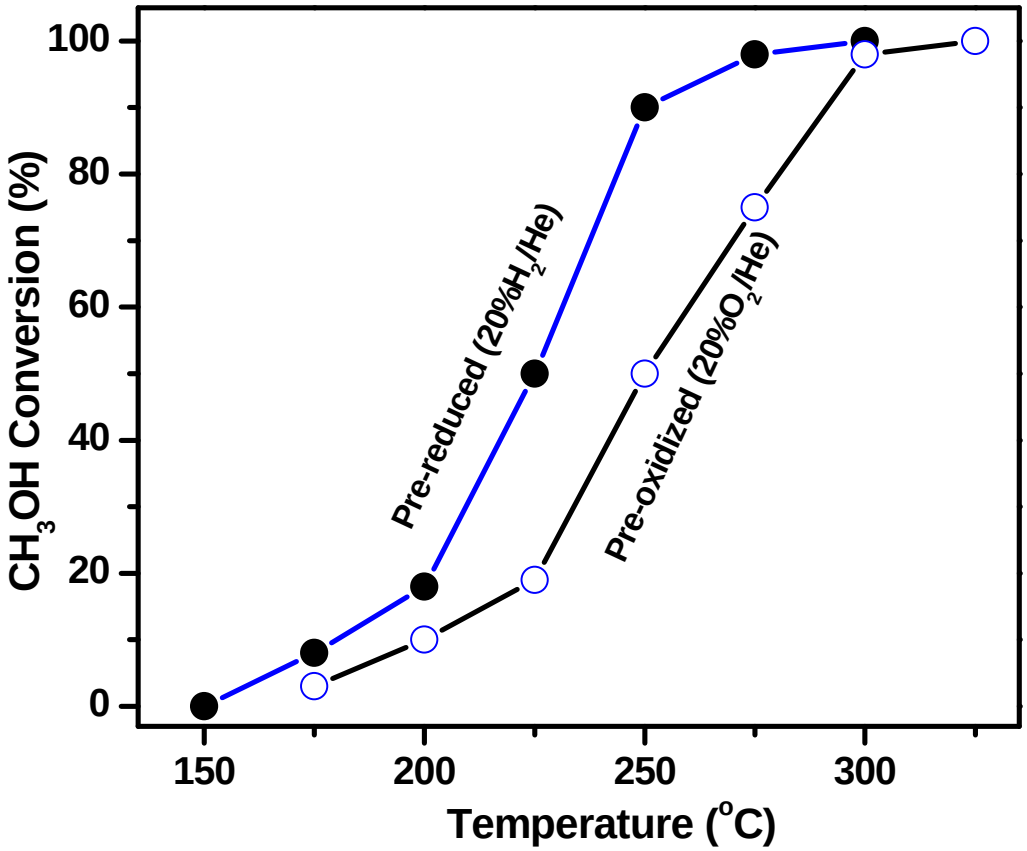


Figure 4.3 $CH_3OH$ conversion (%) in steady-state tests of steam reforming of methanol over 1 at% Au-Ceria(Rod) under different pretreatment conditions ( Pre-reduced and Pre-oxidized)

Gas composition: 2%$CH_3OH$/2.6%$H_2O$/bal. He; GSHV= 42,000 $h^{-1}$

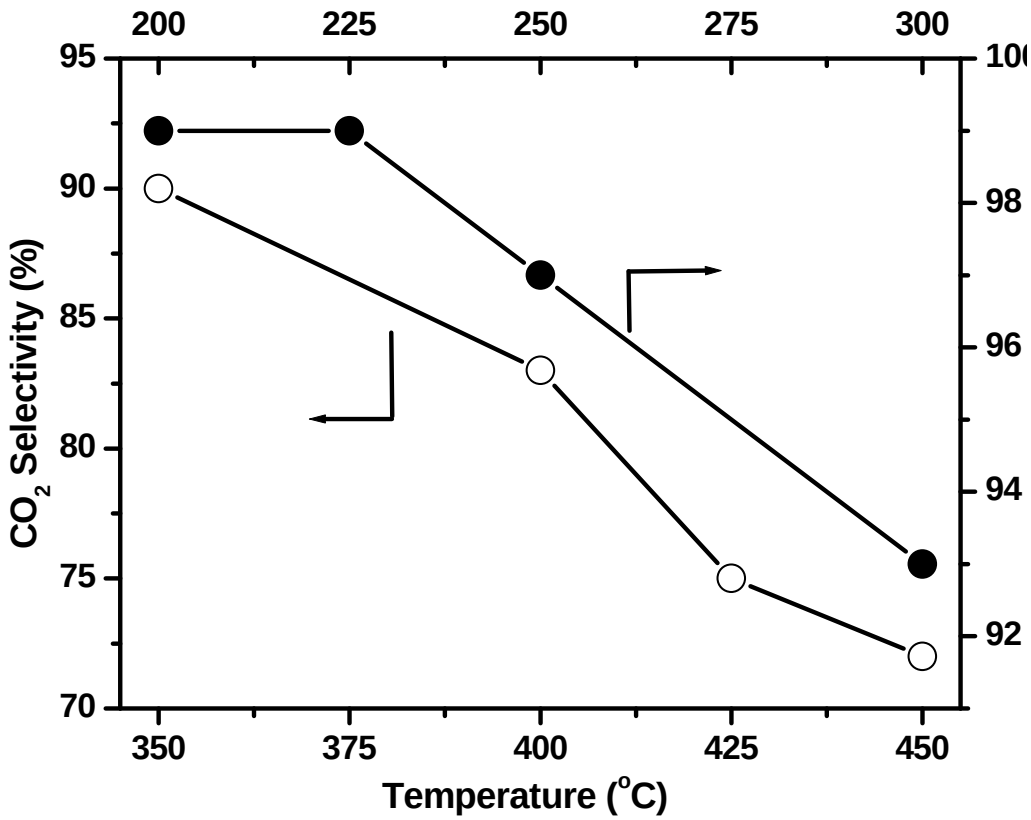


Figure 4.4 $CO_2$ selectivity (%) in steady-state light off tests of steam reforming of methanol over nanoshapes of Ceria (Rod) (○) and 1%Au-Ceria(Rod) (●)

Gas composition: 2%$CH_3OH$/2.6%$H_2O$/bal.He; GHSV= 42,000 $h^{-1}$

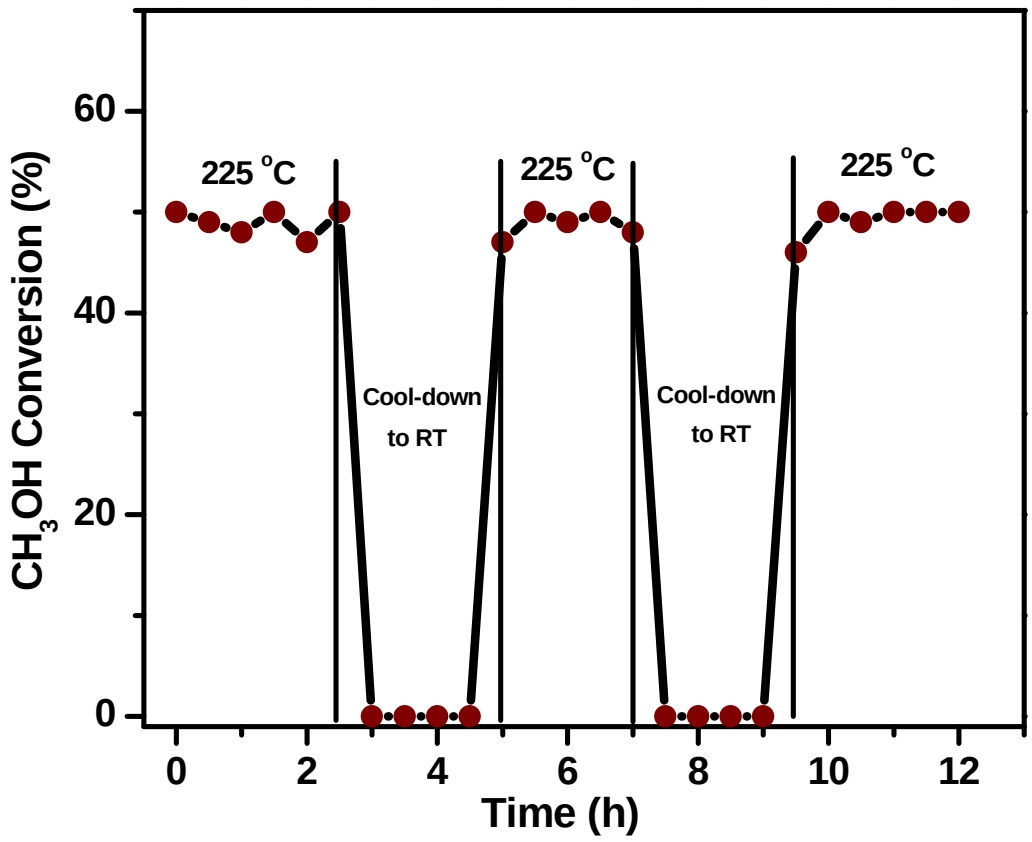


Figure 4.5 Stability of 1%Au-Ceria(Rod) in cyclic start up/ shutdown SRM tests

Gas composition: 2%$CH_3OH$/2.6%$H_2O$/bal.He; GHSV: 42,000 $h^{-1}$

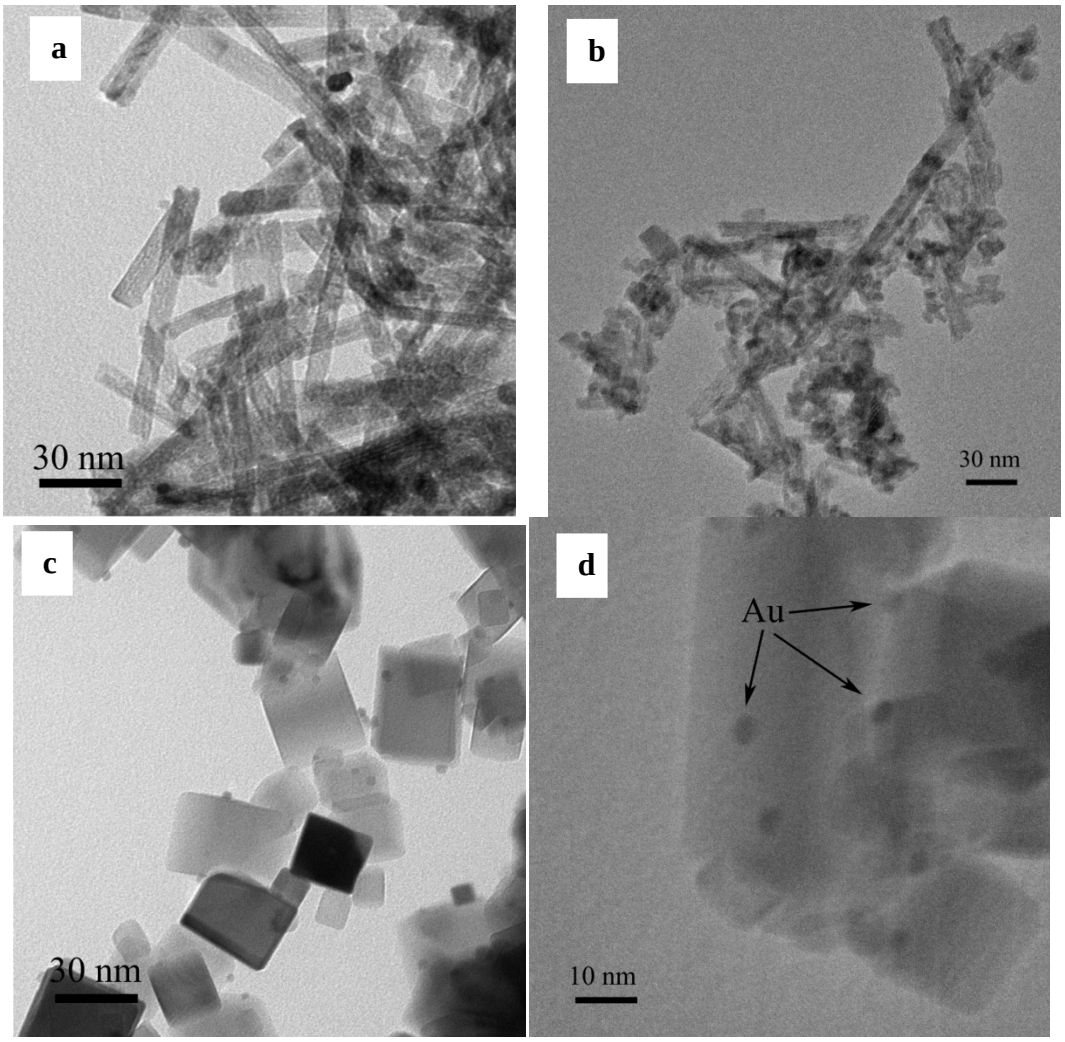


Figure 4.6 TEM images over Au-Ceria samples

(a) Fresh 1%Au-Ceria (Rod);
(b) after use in SRM (2%$CH_3OH$+2.6%$H_2O$/He;15 h-on-stream; T=300 $^oC$ );
(c) Fresh 1%Au-Ceria(Cube);
(d) 1%Au-Ceria(Cube) after use in SRM (2%$CH_3OH$+2.6%$H_2O$/He;15 h-on-stream; up to 300 $^oC$ ).

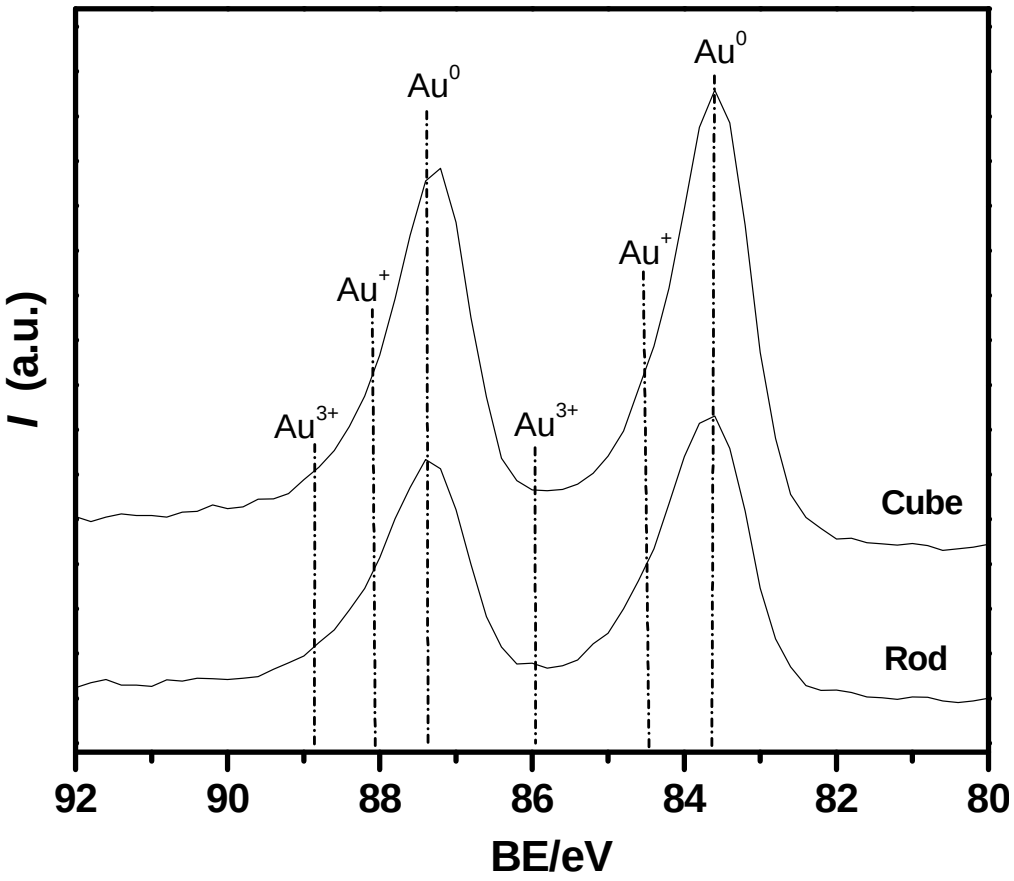


Figure 4.7 XP spectra of Au 4f over 1%Au-Ceria after used in SRM

Test conditions: 2%$CH_3OH$-2.6%$H_2O$/He, 15 h-on-stream, up to 300 $^oC$

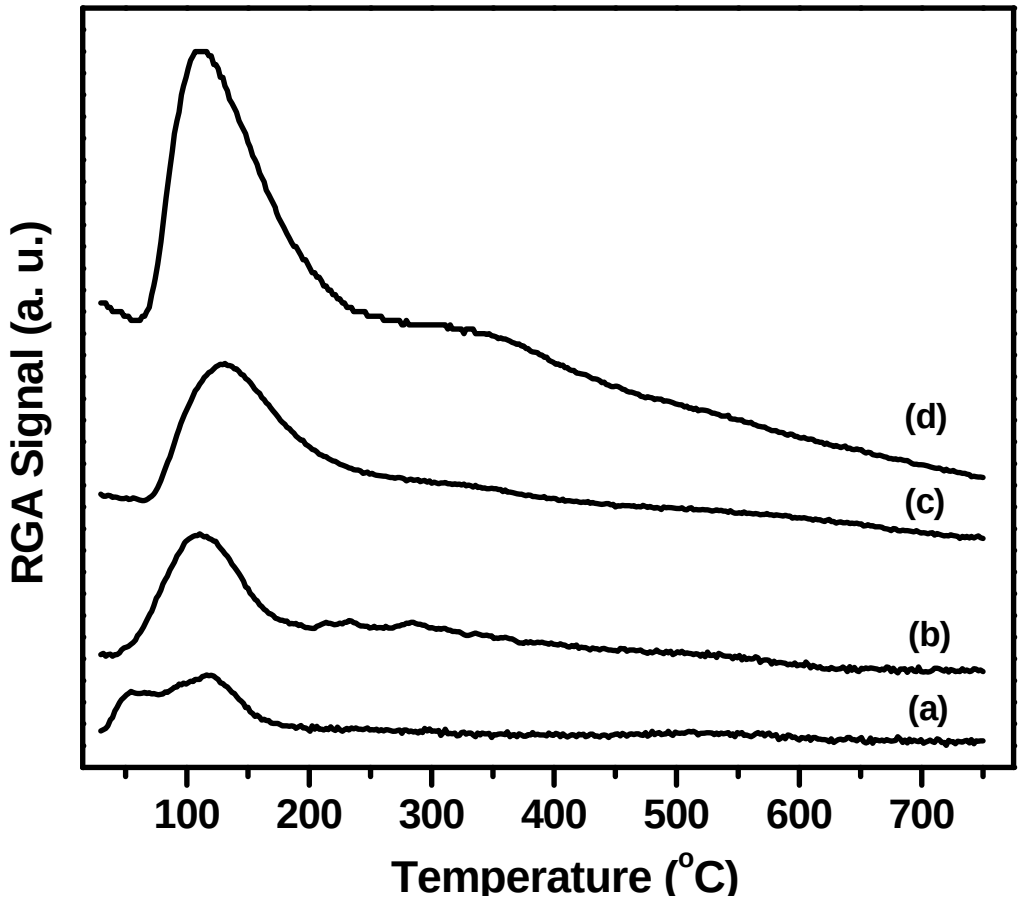


Figure 4.8 TPO Profiles over fresh and used (after SRM) 1%Au-Ceria(Rod)

Gas Condition: 2%$CH_3OH$/2.6%$H_2O$/bal.He, 15 h-on-stream, up to 300 $^oC$ . (a) $CO_2$ from fresh sample; (b) $CO_2$ from used sample; (c) $H_2O$ from fresh sample and (d) $H_2O$ from used sample.

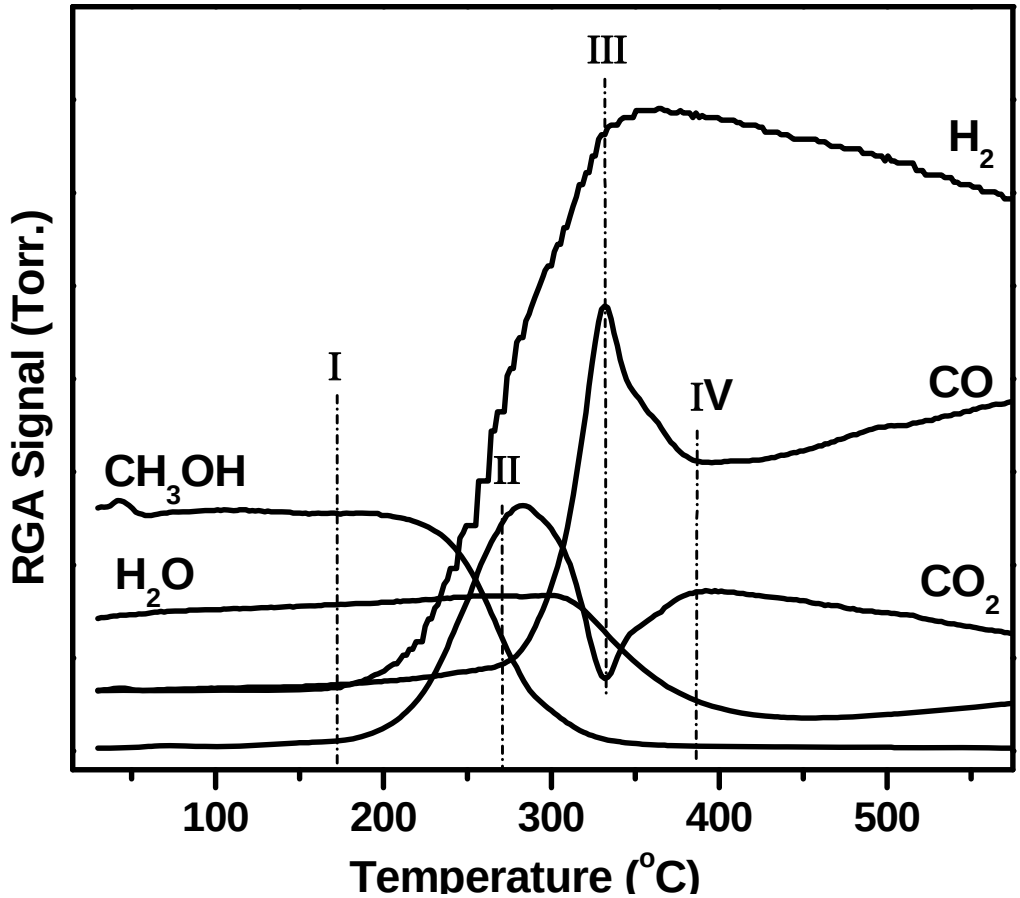


Figure 4.9 ($CH_3OH+H_2O$) –TPSR profile over 1%Au-Ceria(Rod)

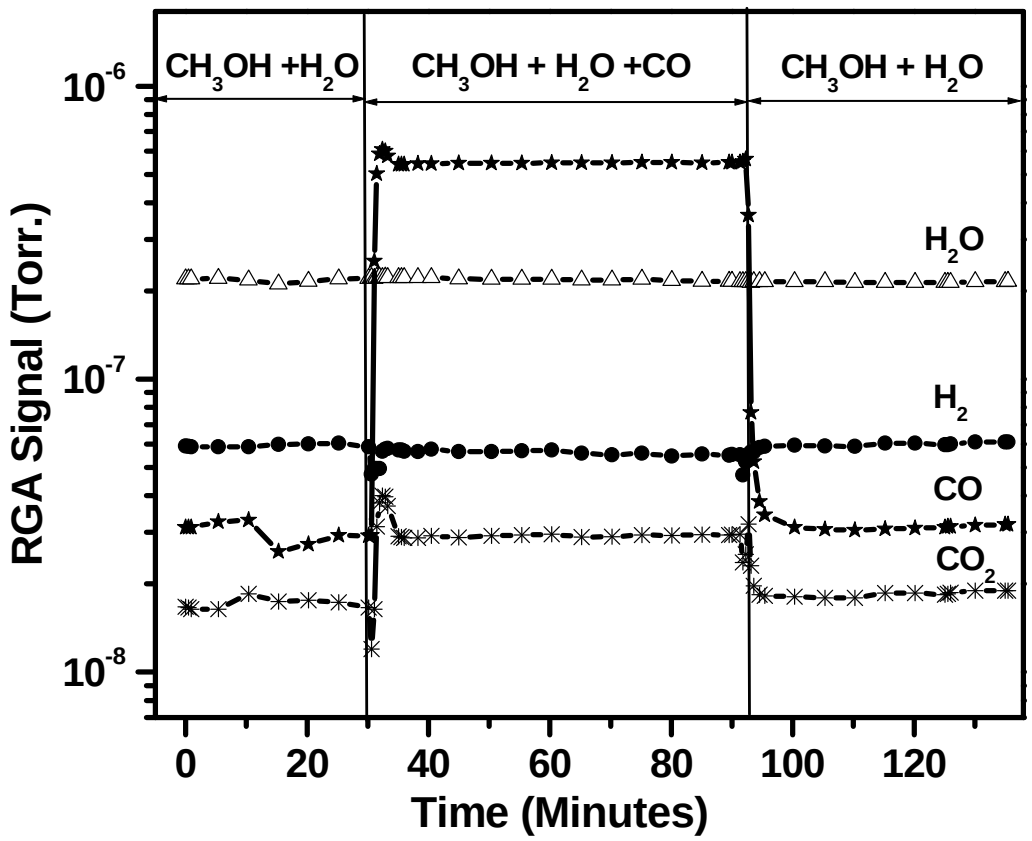


Figure 4.10 Effect of the addition/removal of carbon monoxide in the reaction gas mixture over 1%Au-Ceria (Rod)

operating at steady state SRM at 225 $^{o}$C; GHSV= 42,000 $h^{-1}$

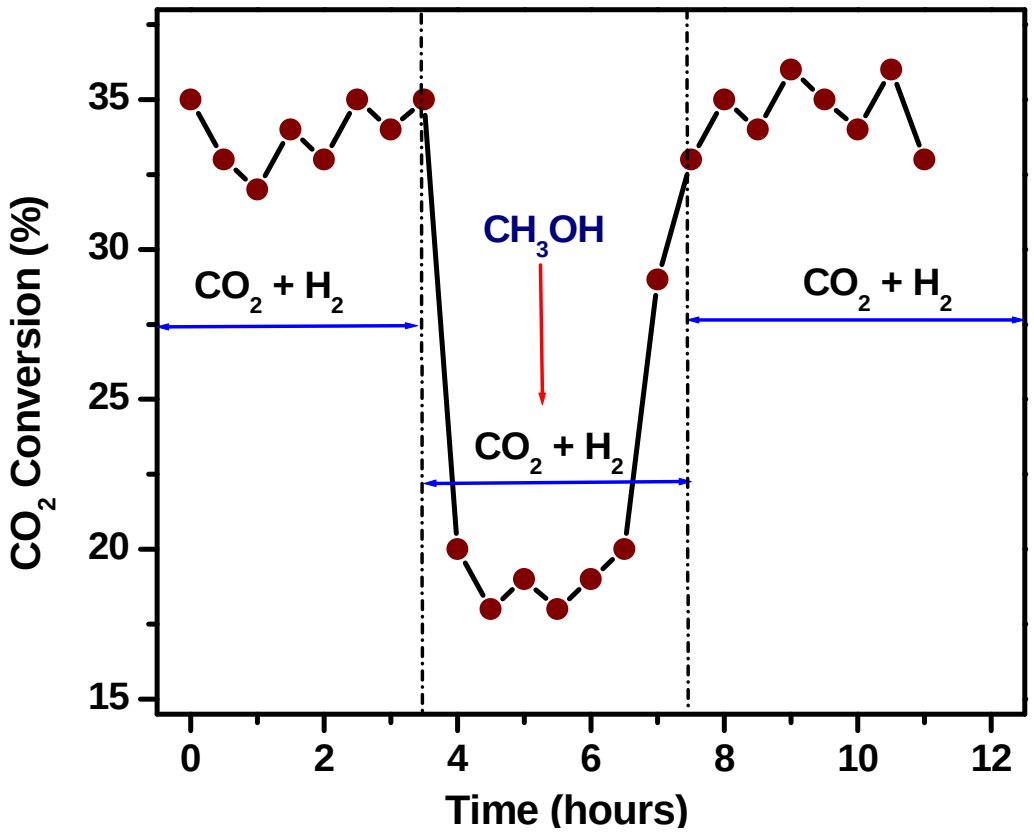


Figure 4.11 Effect of the addition/removal of methanol in the reverse water gas shift reaction over 1%Au-Ceria (Rod) at 225 $^{o}$C

Gas condition: 6.6% $CO_2$- 6.6%$H_2$-(16%$CH_3OH$)-balanced Helium GHSV= 25,000 $h^{-1}$

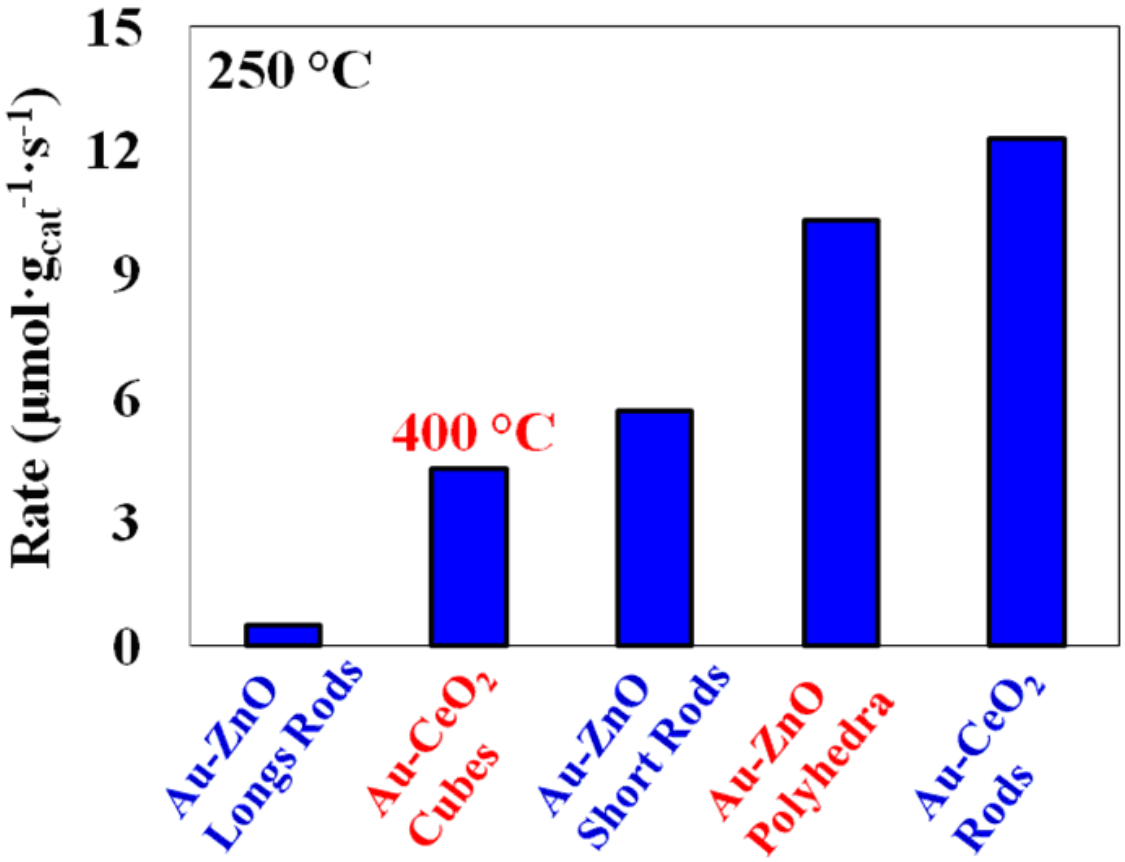


Figure 4.12 Comparison of steam reforming of methanol rates at 250°C over Au-ZnO and Au-$CeO_2$ nanoshapes

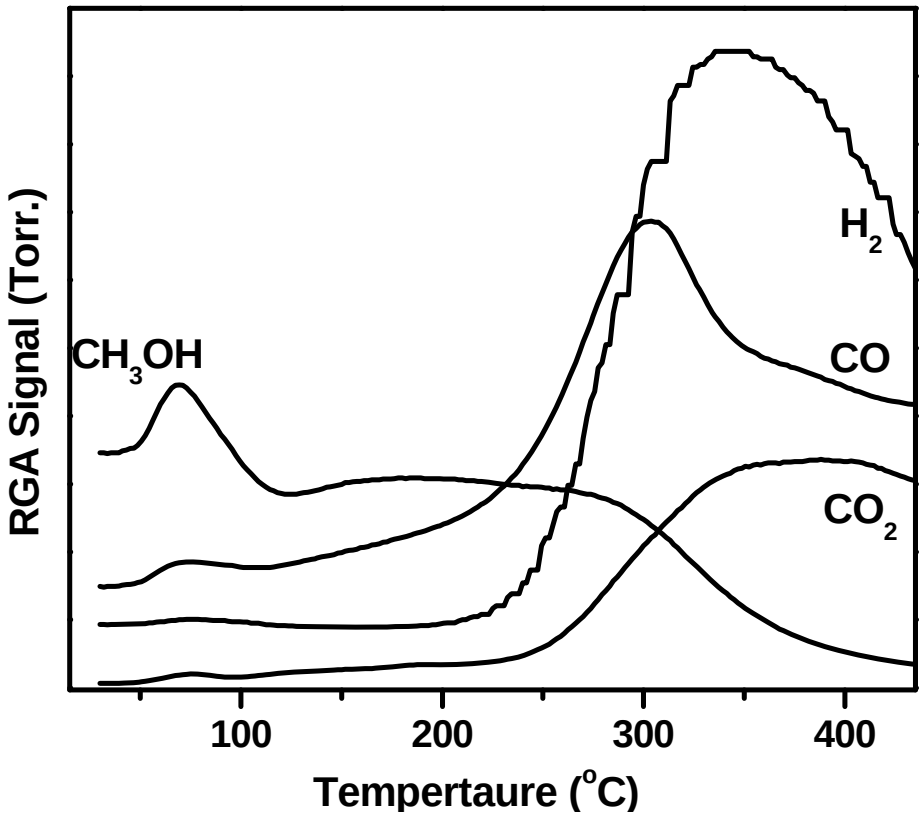


Figure 4.13 ($CH_3OH+H_2O$)-TPSR profile over 3%Pt-Ceria(Rod)

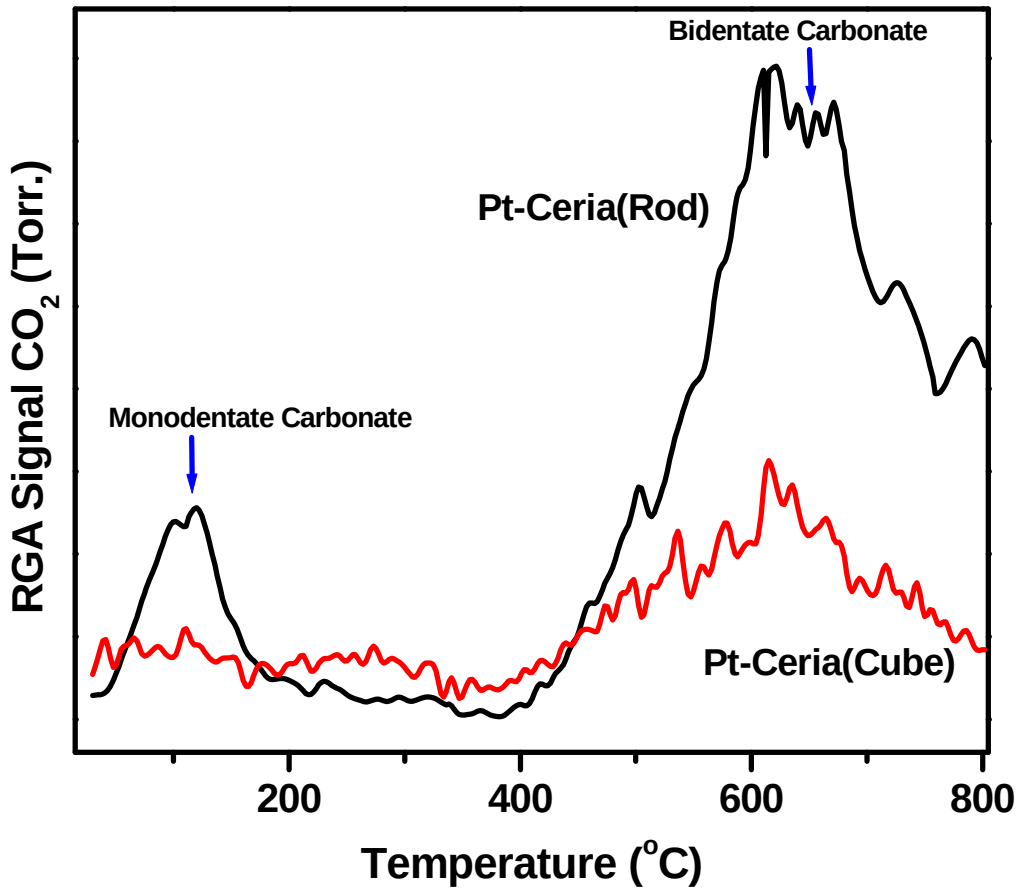


Figure 4.14 $CO_2$-TPD profiles over 3% Pt-Ceria

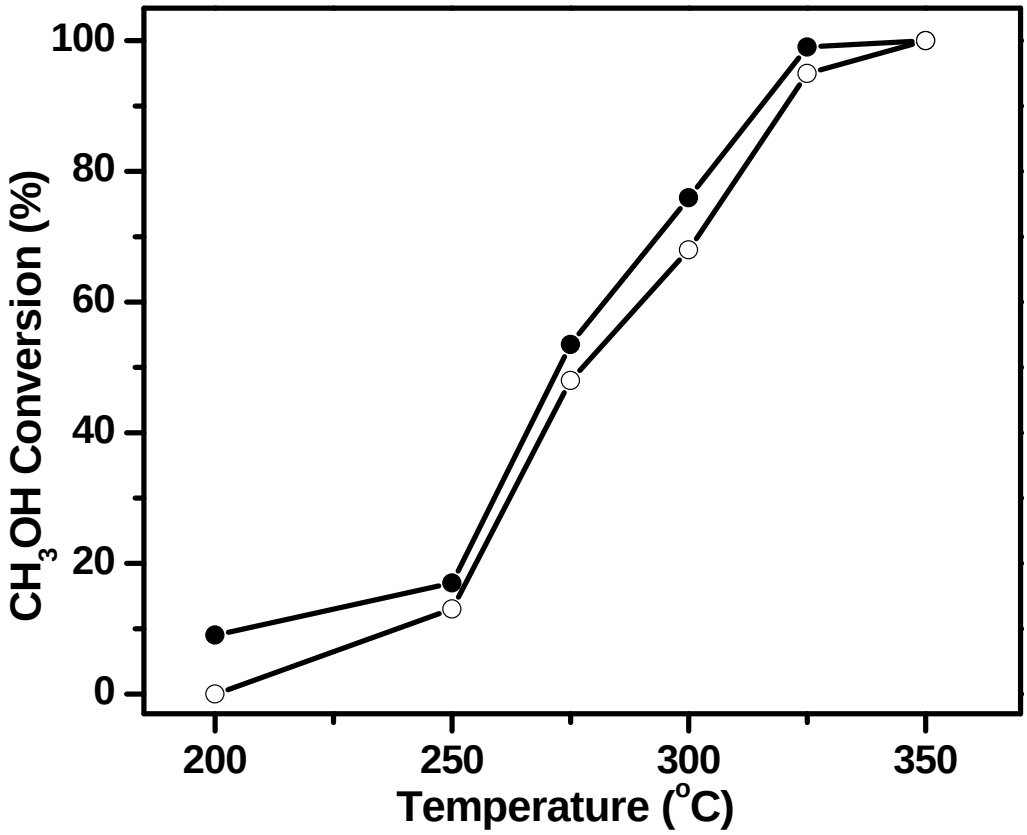


Figure 4.15 Methanol conversion (%) over 3% Pt-Ceria(Rod) (○) and Na modified 3%Pt-Ceri(Rod)(●)

Gas composition: 2%$CH_3OH$/2.6%$H_2O$/bal.He;. GHSV: 42,000 $h^{-1}$

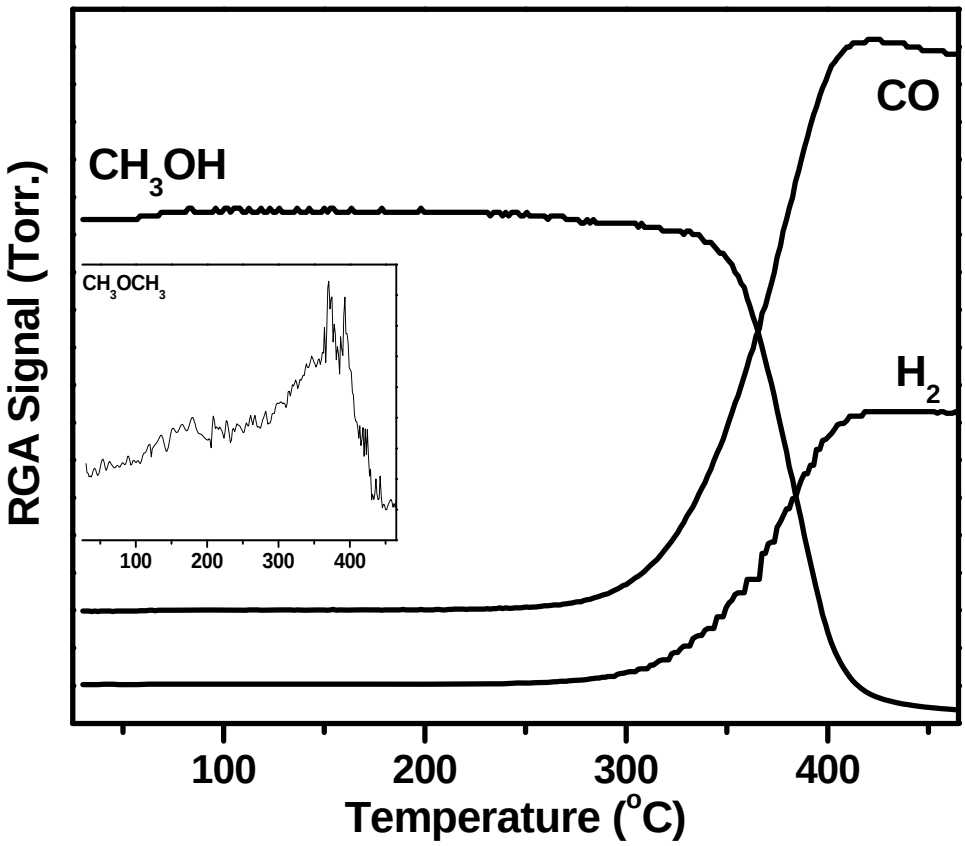


Figure 4.16 $CH_3OH$-TPSR profile over 1 at% Pt-$SiO_2$

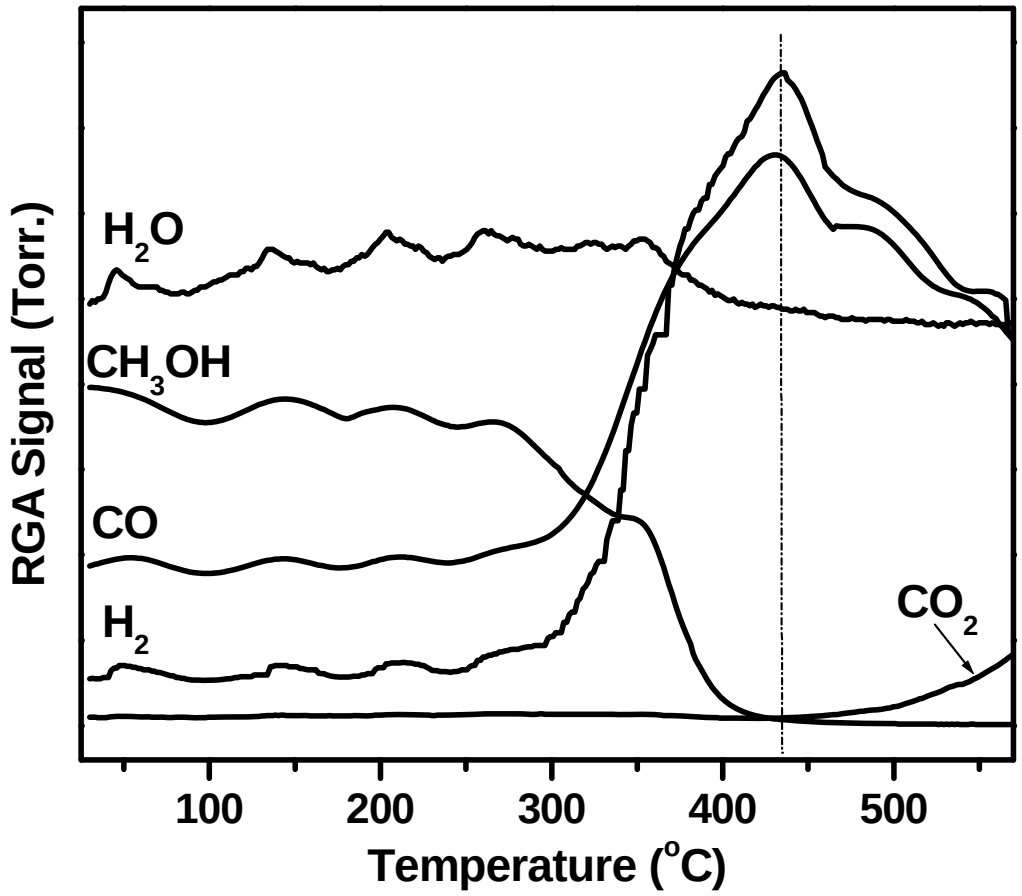


Figure 4.17 ($CH_3OH$+$H_2O$)-TPSR profile over 1 at%Pt-$SiO_2$

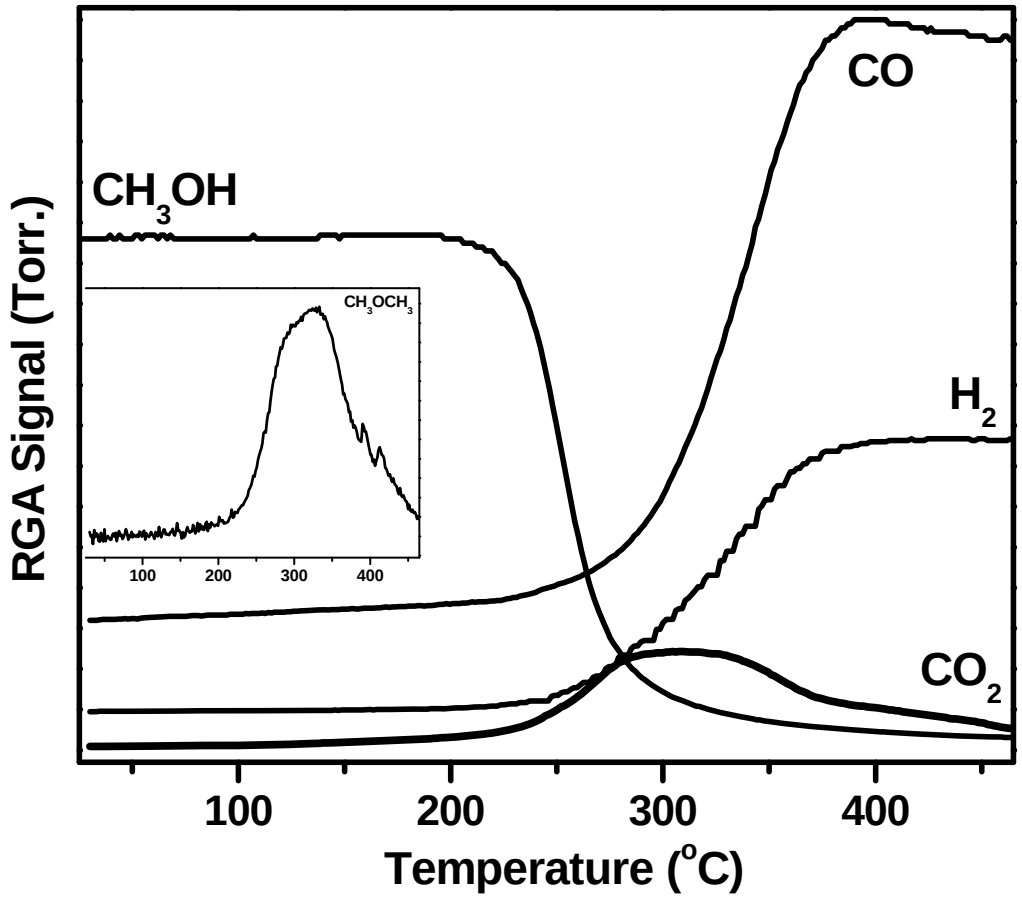


Figure 4.18 $CH_3OH$-TPSR profile over 3Na-1 at% Pt-$SiO_2$

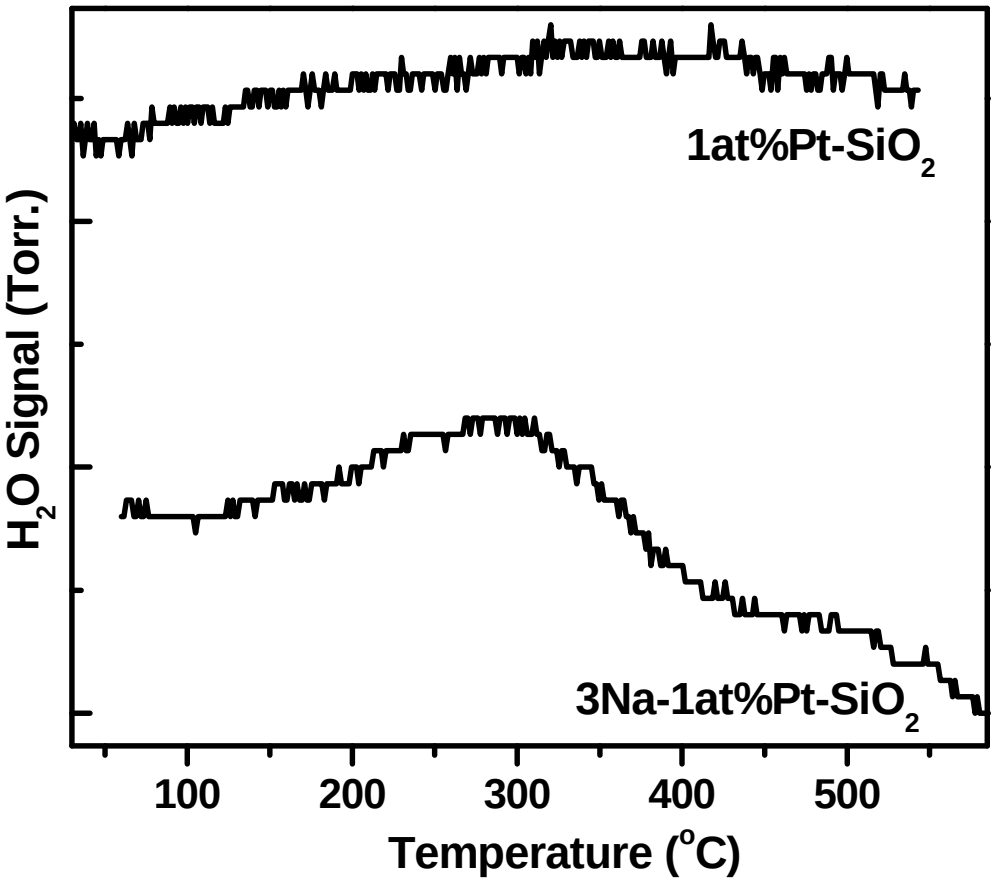


Figure 4.19 $H_2O$-TPSR profiles over 1at%Pt-$SiO_2$ and 3Na-1 at%Pt-$SiO_2$

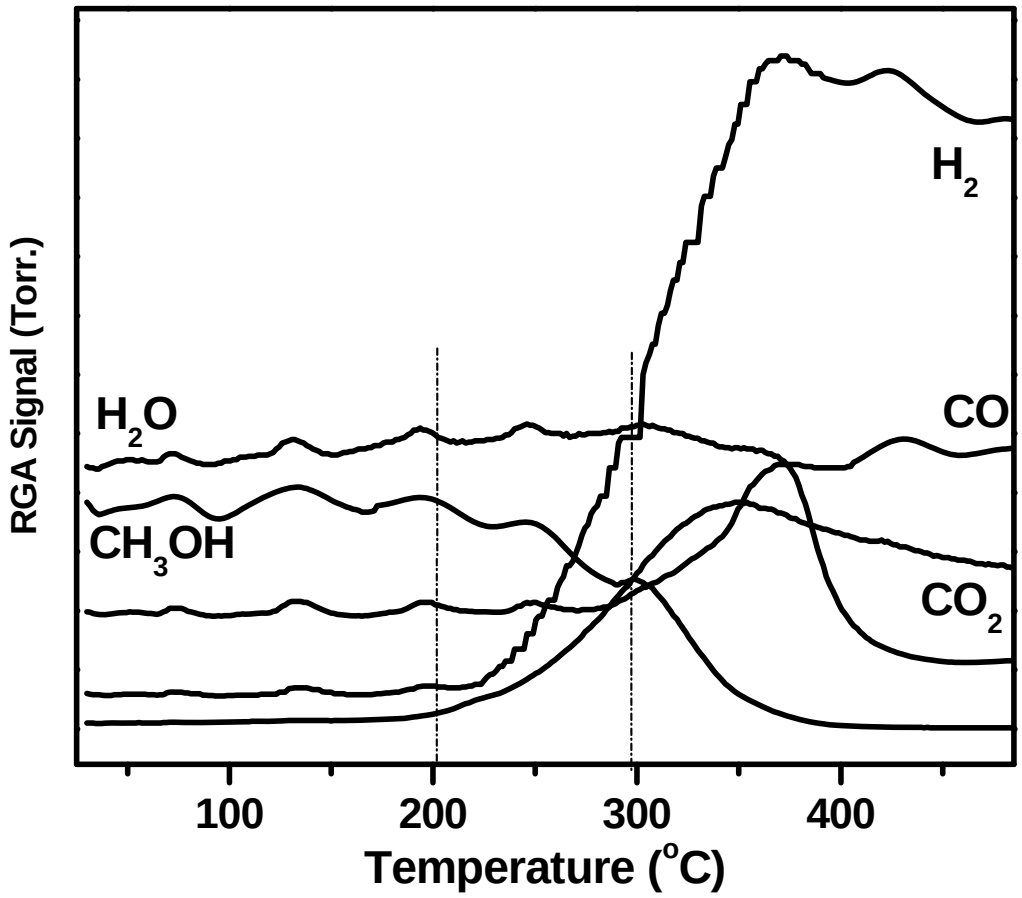


Figure 4.20 ($CH_3OH$+ $H_2O$) -TPSR profile over 3Na-1at% Pt-$SiO_2$

# Chapter 5: Decomposition of formic acid over dispersed gold and platinum clusters on oxides

Methanol is only one option among possible liquid fuel carriers for a hydrogen-based fuel cell [1]. As is the case with introducing any novel industrial application in competitive markets, other possible alternatives, such as formic acid, must be fully considered [2]. From the fundamental viewpoint, it is interesting to compare these two liquids in terms of the chemistry pathways involved and the selectivity of different catalysts to hydrogen. Formic acid was implicated in the pathway of methanol steam reforming reactions on gold catalysts as detailed in Chapter 3 and Chapter 4 of the thesis. The decomposition of formic acid into carbon dioxide and hydrogen was the last step in the reaction network. In this chapter, we present a comparison of gold- based and platinum-based catalysts and their potential application to low temperature decomposition of formic acid.

## 5.1 Dehydrogenation of formic acid over gold-ceria

Since methyl formate ($HCOOCH_3$) determines the $CO_2$ selectivity in methanol steam reforming over gold-ceria [3], and formic acid is derived by the hydrolysis of methyl formate, this naturally begs the question whether or not gold-ceria can be used for the direct decomposition of formic acid at low temperatures, potentially at ambient temperatures. Recently, it was reported that Au-$Al_2O_3$ was active for HCOOH dehydrogenation at close to ambient temperatures [4]. The activity was attributed to the presence of a minority species of sub-nm Au clusters (TEM-invisible) on the alumina surface. Here we examined dispersed gold species on ceria which is much more effective in dispersing gold and keeping it oxidized, Au-$O_x$, than alumina or other inert supports.

*5.1.1 Evaluation of dispersed Au-$O_x$ species as catalytic sites*

The interaction between catalyst species on the surface of each sample and formic acid was investigated with HCOOH-TPD. Before each test, all sample investigated here were reduced at 300 $^oC$ for one hour with 20% $H_2$/He. As shown in Figure 5.1(a), desorption of water and trace amounts of formic acid were observed under 200 $^oC$ over the ceria nanorods. By increasing the temperature, CO, $CO_2$, $H_2O$ and $H_2$ became the dominant desorbed species. This indicates that the dehydrogenation and dehydration pathways take place in parallel on the ceria surface [5]. However, it is more plausible that dehydration is the main mechanism, and $H_2$ and $CO_2$ are minor products from the WGS reaction on ceria rods which takes place also above 200 $^oC$. On the other hand, ceria nanocubes with {100} surfaces were inert to formic acid. As discussed before by using hydrogen and methanol as probe molecules [6, 7], the intensities of the desorption peaks were found to be much weaker on the ceria nanocubes after exposure to formic acid.

The Vohs group [8] concluded that the desorption of formic acid is similar on both the {111} and {100} $CeO_2$ surfaces, and $CO_2$, CO, $H_2O$, and trace amounts of formaldehyde were produced. Vacuum studies conducted by the Mullins group to investigate the pre-treatment effect on the single crystal $CeO_2$ (111) surfaces revealed that $H_2$ and $CO_2$, in addition to water, were formed at 350 K, while CO was predominantly produced above 400 K on an oxidized $CeO_2$ (111) surface. On reduced $CeO_2$ (111), on the other hand, only CO and $H_2$ were produced [9, 10], which indicates that the product distribution depends on the pretreatment conditions instead of the morphology of ceria. However, the contribution of the WGS reaction to the products was not evaluated.

With gold added onto the ceria nanoshapes, the interaction between formic acid and the catalyst surface changed dramatically. In HCOOH-TPD over 1% Au-Ceria(Rod), shown in Figure 5.2, hydrogen and carbon dioxide, as well as water, were formed below 200 $^oC$. This indicated that the addition of gold opened a new reaction pathway at temperatures < 200 $^oC$ [11]. Above 200 $^oC$, the product distribution was similar to pure ceria nanorods, hence the contribution from the ceria support remained unchanged at high temperatures.

In order to further elucidate the different pathways among ceria and gold-ceria, HCOOH-TPSR was used to capture the trend of the change in the products. In Figure 5.3, the formation of CO, $CO_2$ and $H_2$ with conversion of formic acid was followed over the ceria nanorods. As mentioned before, the hydrogen selectivity over ceria is low due to the parallel reactions (dehydrogenation and dehydration). However, as shown in Figure 5.4, only hydrogen and carbon dioxide were formed over gold-ceria beginning at ~ 75 $^{o}$C, i.e. the dehydrogenation pathway was opened on the catalyst at low temperatures. Furthermore, pure helium was replaced by 3%$H_2O$/Helium and HCOOH-TPD was carried out over the 1%Au-Ceria (Rod) again. No difference in the product distribution between the two different carrier gases took place, which confirmed that the direct dehydrogenation reaction $HCOOH \rightarrow H_2 + CO_2$ dominates over the gold-ceria samples.

We also conducted HCOOH-TPSR experiments with leached 1at%Au-Ceria (Cube) to investigate whether gold on these surfaces is efficient for formic acid reactions. It is not surprising to find the formation of identical products. The only difference from the parent gold-ceria was the onset temperatures for reaction, which can be explained by the available binding sites for dispersed gold species.

The conversion of formic acid vs. temperature for 1%Au-Ceria(Rod) is shown in Figure 5.5. The formation of $CO_2$ and $H_2$ as the only products began as low as 50 $^{o}$C, and total formic acid conversion was achieved at 175 $^{o}$C. The ratio between $CO_2$ and $H_2$ maintained a value of 1 during the entire reaction range. This further confirmed that only dehydrogenation occurred on the 1%Au-Ceria(Rod). Although the reaction rate was relatively low over 1%Au-Ceria(Cube), the apparent activation energy over both samples is similar, 55 ± 2 kJ/mol, as shown in Figure 5.6. Based on the assumption that 100% gold dispersion was achieved over the leached samples, the turnover frequency value over gold-ceria samples was calculated. The TOF value was found to be close to ~ 0.23 $s^{-1}$ at 130 $^{o}$C on the gold-ceria samples, independent of the type of ceria nanoshapes. Therefore, only residual, atomically dispersed gold clusters, Au-$O_x$, catalyze the formic acid decomposition, and dehydrogenation is the only reaction pathway on gold-ceria catalysts. This is similar to the results reported by Ojeda *et al.* [4] for Au-$Al_2O_3$ catalysts. We surmise that it holds true for all gold catalysts. The choice of support is important to disperse and stabilize these gold species, and in that respect ceria is superior to alumina.

*5.1.2 Effect of CO and $H_2O$ in the decomposition of formic acid*

It is possible that formic acid will be used in the presence of water vapor, and even in aqueous solutions for some applications. As an example, a significant amount of water is inevitably produced during catalytic biomass conversion processes. Practically, the catalysts used in the subsequent reactions should be water-resistant or at least maintain reasonable activity in the presence of water. For mechanistic studies, investigating the effect of water also helps us to determine whether the water-gas shift reaction is part of the formic acid decomposition pathway. In this work, this was examined by adding 3%$H_2O$ into the stream of 3.3%HCOOH/He and testing at 75 $^oC$ and 140 $^oC$ respectively. As shown in Figure 5.7, the addition of water neither changed the conversion of formic acid nor the $H_2$ selectivity over Au-Ceria. Recently, Bulushev *et al.* [12] reported the addition of water at 145 $^oC$ increased the hydrogen selectivity over Au-$TiO_2$ by catalyzing the water-gas shift reaction in parallel with the decomposition of formic acid. The different observation could be explained by the presence of big gold particles on Au-$TiO_2$ (3.5 nm) and Au-Carbon (10.5 nm) [12]. On such big gold nanoparticles the decomposition of formic acid will occur at a higher temperatures compared with that of dispersed, sub-nm gold species. Another possibility is that $TiO_2$ was reported to produce water and carbon monoxide as the only products [13]. In either case, the decomposition of formic acid will take place at a higher temperature range, in which the water gas shift reaction also takes place. That is, the close to ambient temperature pathway of formic acid dehydrogenation is found only on the atomically dispersed Au-$O_x$ species on various supports.

The effect of the addition of CO was also investigated in this thesis work. The same experimental conditions were used except ~3.0 % $H_2O$ was replaced by 5% CO. As shown in Figure 5.8, the formic acid conversion and hydrogen selectivity do not change as the gases are switched between HCOOH/He and CO/HCOOH/He. In Chapter 4, we also found that the addition of carbon monoxide to the mixture of methanol and water did not change the methanol conversion and hydrogen production rate. Gazsi *et al*. [14] reported a similar carbon monoxide effect in the formic acid reaction over gold based catalysts. Ojeda *et al.* [4] also reported that the water gas shift reaction was not involved in the pathway through isotope-exchange experiments

over their gold on alumina catalyst. Iglesia and Boudart studied formic acid decomposition on copper-based catalysts, and found that the turnover frequency was independent of the concentration of $H_2$ and CO [15]. Solymosi *et al.* [16] focused on the Rh catalysts, and they reported that the selectivity was related to the choice of support; for example, selectivity is close to 1 on $Rh/SiO_2$ but only 0.63-0.7 for Rh on $TiO_2$. However, for the case of gold catalysts, it appears that there is no support effect and the CO and $H_2O$ do not affect the HCOOH decomposition. Thus, formic acid must bind stronger on gold than carbon monoxide.

In summary, through the above two sets of experiments, by the addition of water and carbon monoxide into the stream of formic acid, we can exclude the occurrence of the water gas shift reaction from the reaction pathway at close-to-ambient temperatures.

### *5.1.3 Stability*

After heating to 175 $^{o}$C, then cooling to room temperature in formic acid over the 1%Au-Ceria (Rod), we carried out temperature programmed oxidation over the used sample. As shown in Figure 5.9, desorption of carbon dioxide with the consumption of oxygen was observed between 200 $^{o}$C and 250 $^{o}$C. Water desorption did not take place above 240 $^{o}$C. Because water and carbon dioxide were produced at different temperature ranges, it is suggested that the formation of carbon dioxide may come from the residual formic acid condensed on the surface at room temperature.

To further investigate the stability of 1%Au-Ceria (Rod) in formic acid reaction, the reaction was conducted at 135 $^{o}$C by alternating the GHSV between 21,000 $h^{-1}$ and 60, 000 $h^{-1}$. The cycle (3 h at the low flow rate, then 3 h at the higher flow rate) was repeated four times over the gold catalyst. 1%Au-Ceria (Rod) did not suffer any activity loss during this treatment, as shown in Figure 5.10.

After used samples were cooled down to room temperature under pure helium flow, the desorption products were monitored by linearly increasing temperature under helium. In Figure 5.11, it is interesting to find desorption of carbon dioxide and hydrogen as the only adsorbed

surface species below 200 $^{o}$C. Desorption of other carbon species ($CO_2$ and CO), water, and hydrogen was observed between 200 $^{o}$C and 350 $^{o}$C. The duplicated profiles over used samples strongly supported the assumption that large amounts of formic acid would be condensed on the surface after catalytic performance tests. Following the He-TPSR step, temperature programmed oxidation over the used samples was repeated again, and only trace amounts of carbon dioxide were observed without the formation of water.

Given all those treatments for the used catalysts, the decomposition of formic acid was carried out again, and the light-off curves were found to be similar to that of the fresh samples. This indicated that once the catalyst surfaces were cleaned of residual formic acid, the activity would be maintained. Thus gold-ceria is a promising new formic acid dehydrogenation catalyst for practical applications.

## 5.2 Alkali-enhanced dehydrogenation of formic acid over Pt-$SiO_2$

In this part of the work, we investigated the potential promotion of Pt on an inert surface like silica by alkali addition. Recently, Zhai *et al.* [17] reported a dramatic such promotion of Pt for the low-temperature WGS reaction. A major effect of the alkali is the stabilization of Pt-$O_x$ species on the inert catalyst surface. It was interesting to investigate the importance of such structures in the formic acid dehydrogenation reaction.

### *5.2.1 Ambient temperature activity through the addition of sodium*

The intermediate species and the reaction pathway for the formic acid decomposition were investigated by HCOOH-TPSR. Decomposition of formic acid did not take place over pure $SiO_2$ up to 350 $^{o}$C. On Na-$SiO_2$, dehydration of formic acid dominated, as shown in Figure 5.12. However, Pt-$SiO_2$ catalyzed the dehydrogenation reaction, as shown in Figure 5.13(a). Thus, HCOOH dehydrogenation takes place on platinum, as is well documented in the literature [18]. The addition of sodium on Pt-$SiO_2$ did not alter the product distribution but shifted the reaction

to near ambient temperatures as low as 50 $^{o}$C, as shown in Figure 5.13(b). As mentioned above, the stabilization of atomically dispersed Pt-$O_x$ species is significantly enhanced by the addition of sodium. Therefore, we conclude that these Pt-$O_x$ species catalyze the dehydrogenation of formic acid, while the sodium ions promote the activity of Pt-$SiO_2$ simply by increasing the concentration of and stabilizing these active Pt sites.

HCOOH-TPD was used to investigate the effect of sodium additives on the population and reactivity of the active sites on Pt-$SiO_2$. As shown in Figure 5.14, the desorption products over Pt-$SiO_2$ and Na-Pt/$SiO_2$ are the same, namely only $CO_2$ and $H_2$ were produced along with physical desorption of HCOOH. This corroborates the above finding that the dehydrogenation pathway occurs on the Pt sites. With the addition of sodium, the yield of the dehydrogenation products is much higher; *e.g.* the produced $CO_2$ is 10 fold that of the Na-free sample, but the onset temperature of the decomposition reaction is about the same on both samples. Such results indicate that sodium is a structural promoter, which facilitates and preserves the dispersion and oxidation state of Pt-$O_x$ species and hence creates more active sites for the reaction. To further prove that more sites were available on the investigated samples, $CO_2$ was chosen as another probe molecule to titrate the amount of active sites on the samples, as shown in Figure 5.15. Similar results were observed as when using HCOOH. The $CO_2$ desorbed from Na-Pt/$SiO_2$ is 313 μmol/$g_{cat.}$, compared with 88 μmol/$g_{cat}$ from Pt-$SiO_2$..

The promotion effect of alkali metals on formic acid decomposition has beed reported under UHV conditions. Pre-adsorbed potassium species was reported to enhance the adsorption of formic acid on the Pd (100) surface. The formation of HCOOK species changed the product distribution, and $CO_2$ was also produced [19]. A similar effect was reported over potassium modified Cu(110) surface [20]. The findings of the present work extend the promotion efect to Pt catalysts under ambient pressure.

It is worth mentioning that in steady-state light-off tests (shown in Figure 5.16) the addition of sodium greatly improved the low temperature catalyst activity. Without sodium, the reaction lightoff over Pt-$SiO_2$ was around 150 $^{o}$C. On the other hand, Na-Pt/$SiO_2$ can achieve full conversion of the formic acid at 130 $^{o}$C, under high space velocity, GHSV= 42,000 $h^{-1}$.This is in agreement with the temperature programmed reaction data. The $CO_2$

selectivity over both platinum catalysts is 100%, and the ratio of $H_2/CO_2$ is 1. In agreement with the literature [18], the dehydrogenation pathway is preferred over platinum catalysts.

Arrhenius-type plots of the reaction rates over Pt based catalysts are depicted in Figure 5.17. The apparent activation energy is almost the same for the $Pt/SiO_2$ samples with or without sodium (70 ± 2 kJ/mol). Recently, Ojeda *et al.* [4] reported a similar activation energy over platinum nanoparticles supported on $Al_2O_3$ for the formic acid decomposition. Based on these findings it is proposed that the same active sites, dispersed $Pt\text{-}O_x$ species, catalyze the dehydrogenation pathway, independent of the type of support and promoters. The addition of sodium on $Pt\text{-}SiO_2$ was shown by Zhai *et al*. [17] to stabilize the atomically dispersed oxidized $Pt\text{-}O_x$ sites, which are active for the WGS reaction, and as shown here, they are active also for the HCOOH decomposition.

Sodium modified $Pt\text{-}SiO_2$ had excellent stability under the reaction conditions used here. In cyclic steady-state tests, the conversion of formic acid was maintained over $Na\text{-}Pt/SiO_2$. Furthermore, during start-up and cool-down tests as well as in stability tests (15h at 150$^o$C), no deactivation was observed. In Figure 5.18, TEM images of the used $Na\text{-}Pt/SiO_2$ after the 15h-stability test showed that the Pt dispersion was almost the same as for the fresh sample. This is in agreement with the beneficial effect of Na on the Pt stabilization as atomically dispersed species on $SiO_2$ after the water-gas shift reaction. Also Chun *et al.* [21] have reported that $Pt_4$-cluster/$SiO_2$ showed higher activity compared with Pt-particles/$SiO_2$ in formic acid decomposition reaction.

### *5.2.2 The optimization of platinum amount*

Sodium-promoted platinum catalyzes the dehydrogenation of formic acid at ambient temperatures as was demonstrated in the previous section. The amount of platinum needed for this reaction was explored further. As reported by Zhai *et al.* [17], washing the samples with deionized water effectively removes all the weakly bound alkali species from the surface. However, some alkali, resistant to washing, remains. This amount was correlated with the

number of the active Pt-$O_x$ sites [17]. That is, stabilization of both the Pt-$O_x$ and Na species takes place on the active sites. The catalytic performance of washed, sodium-promoted 1wt%Pt-Na/$SiO_2$ silica catalysts and the corresponding parent samples (unwashed) was evaluated and is shown in Figure 5.19. All Na-Pt-$SiO_2$ showed enhanced ambient temperature activity compared with the sodium-free samples. The negligible difference between parent and washed Pt-$SiO_2$ samples is explained by the presence of the same number of strongly associated Pt-$O_x$-Na-$(OH)_x$ species on these samples. Zhai *et al.* suggested the ratio of surface $OH^-$ group and platinum atoms depends on the original platinum and sodium loading. More detailed work needs to be done to address different pre-treatment effects on the catalytic performance. However, the major result found here is that the Na-promoted Pt-$O_x$ clusters catalyze the dehydrogenation of formic acid at ambient temperatures.

### *5.2.3 CO effect on the sodium promoted Pt-$SiO_2$*

Instead of modifying Pt with other metals in order to maintain high activity, alkali addition is very effective. And the desired dehydrogenation pathway is followed over sodium-promoted Pt-$O_x$-$SiO_2$. The dehydrogenation pathway avoids downstream anode poisoning caused by trace amounts of CO in the hydrogen gas. Here, we examine whether the presence of carbon monoxide affects the decomposition of formic acid over the Na-promoted catalyst.

5%CO/He was used to replace pure helium as carrier gas at 120 $^oC$, keeping the total flow rate constant. It was found that formic acid conversion did not change with the replacement of carrier gases. Shown in Figure 5.20, cyclical change between 5%CO/Helium and pure helium was carried out, and the conversion of formic acid was kept constant. It has been reported that less CO adsorbs on a Pt/Pd alloy surface and that formic acid can displace CO from platinum during electroxidation at potentials below the CO oxidative stripping threshold [22]. Also different platinum surface planes have different affinities to CO. For example, the Pt(110) surface is poisoned more quickly than Pt (111) [23]. Addition of sodium on platinum could modify the electron density of the platinum surface [24], thus making catalysts more resistant to carbon monoxide. For the catalysts tested here, containing atomically dispersed Pt-$O_x$ species, it

was found by Zhai *et al.* [17] that the state of Pt in the cluster with the promoter, Pt-$O_x(OH)_y$-$Na_z$, remains oxidized even at highly reducing conditions. CO adsorbs weakly on the cluster [17]. Based on the above findings, CO must adsorb even more weakly than HCOOH on this site. Hence, it has no effect on the formic acid dehydrogenation reaction. These findings are worth exploring further for practical catalyst and electrocatalyst designs.

### 5.3 Summary

In this chapter, the viability of gold-ceria and sodium-promoted Pt-$SiO_2$ as robust catalysts for the decomposition of formic acid at ambient temperature was explored. The dehydrogenation pathway was identified as the exclusive pathway over both catalysts. The findings may guide the design of a new generation of catalysts for practical applications of formic acid decomposition.

Highly dispersed gold species, Au-$O_x$, catalyze the decomposition of formic acid at as low as 50 $^oC$ through the dehydrogenation pathway. Gold-ceria catalysts show good resistance to water and carbon monoxide. They also possess excellent stability as revealed by cyclic shut-down/start-up tests, and in long- term operation.

Sodium-promoted Pt-$SiO_2$ can use very low amounts of the precious metal and an Earth-abundant material as support. This has been demonstrated here to be a much more efficient approach to decrease the amount of platinum usage for formic acid decomposition compared with the traditional method of alloying platinum with other precious metals. A cost-effective catalyst can be developed. For this, the optimal Na/Pt ratio must be found and used. The unexpected carbon monoxide resistance is an additional attractive feature of the novel catalysts

## 5.4 References


[1] D. R. Palo, R. A. Dagle, J. D. Holladay, *Chem. Rev.* 107 (2007) 3992.

[2] X. Yu, P. G. Pickup, *J. Power Sources* 182 (2008) 124.

[3] N. Yi, R. Si, H. Saltsburg, M. Flytzani-Stephanopoulos, *Appl. Catal. B* 95 (2010) 87.

[4] M. Ojeda, E. Iglesia*, Angew. Chem. Int. Ed.* 48 (2009) 4800.

[5] D. E. Fein, I. E. Wachs, *J. Catal.* 210 (2002) 242.

[6] N. Yi, R. Si, H. Saltsburg, M. Flytzani-Stephanopoulos, *Energy Environ. Sci*. 3 (2010) 831.

[7] R. Si, M. Flytzani-Stehphanopoulos, *Angew. Chem. Int. Ed.* 47 (2008) 2884.

[8] J. Stubenrauch, E. Brosha, J. M. Vohs, *Catal. Today* 28 (1996) 431.

[9] S. D. Senanayake, D. R. Mullins, *J. Phys. Chem. C* 112(2008) 9744.

[10] W. O. Gordon, Y. Xu, D. R. Mullins, S. H. Overbury, *Phys. Chem. Chem. Phys.* 11 (2009) 11171.

[11] D. A. Outka, R. J. Madix, *J. Am. Soc. Chem*. 109 (1987) 1708.

[12] D. A. Bulushev, S. Beloshapkin, J. R. H. Ross, *Catal. Today* 154 (2010) 7.

[13] K. S. Kim, M. A. Barteau, *Langmuir* 6 (1990) 1485.

[14] A. Gazsi, T. Bansagi, F. Solymosi, *J. Phys. Chem. C* 115 (2011) 15459.

[15] E. Iglesia, M. Boudart, *J. Catal*. 81 (1993) 224.

[16] F. Solymosi, A. Erdohelyi*, J. Catal*. 91 (1985) 327.

[17] Y. P. Zhai, D. Pierre, R. Si, W. L. Deng, P. Ferrin, A. U. Nilekar, G. Peng, J. A. Herron, D. C. Bell, H. Saltsburg, M. Mavrikakis, M. Flytzani-Stephanopoulos, *Science* 329 (2010) 1633.

[18] M. R. Columbia, P. A. Thiel, *Surf. Sci*. 235(1990) 53.

[19] F. Solymosi, I. Kovács, *Surf. Sci*. 259(1991) 95.

[20] P. M. Moller, P.J. Godowski, J. Onsgaard, *Vacuum* 54(1999)31.

[21] W. J. Chun, K. Tomishige, M. Hamakado ,Y. Iwasawa, *J. Chem. Soc. Faraday Trans.* 91(1995) 4161.

[22] T. Iwasita, X. H. Xia, E. Herrero, H. D. Liess, *Langmuir* 12 (1996) 4260.

[23] F. S. Thomas, R. I. Masel, *Surf. Sci*. 573 (2004) 169.

[24] H. Yoshitake, Y. Iwasawa, *J. Phys. Chem*. 95 (1991) 7368.

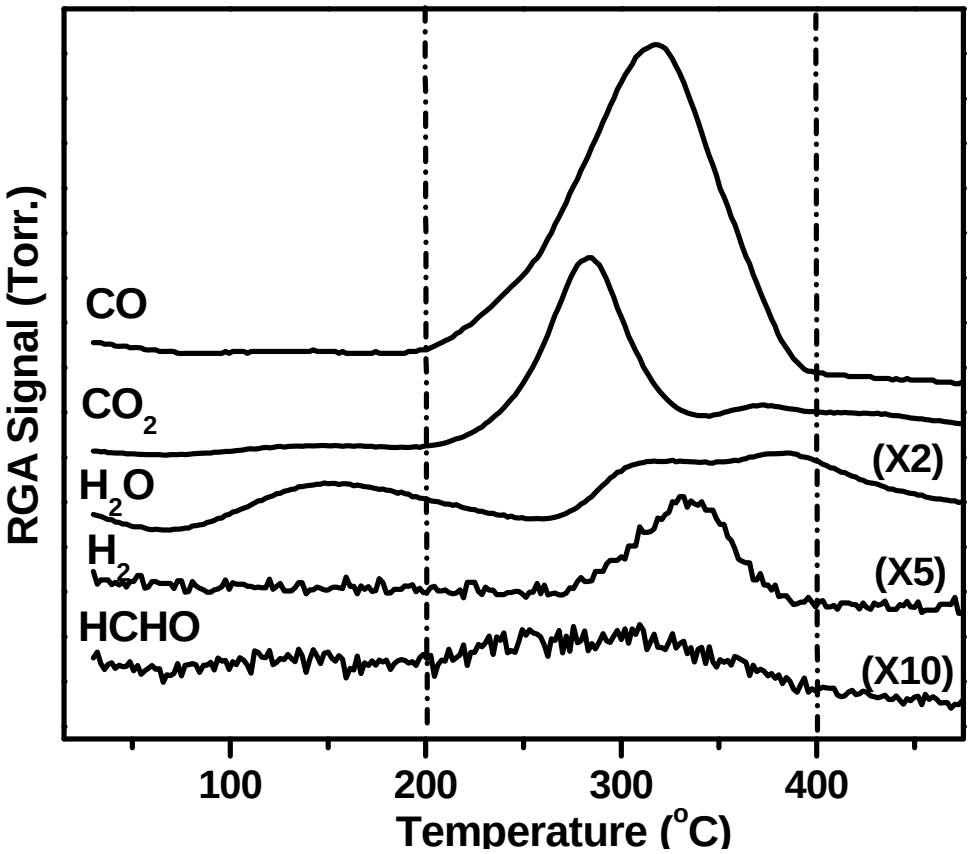


Figure 5.1 HCOOH-TPD profile over Ceria(Rod)

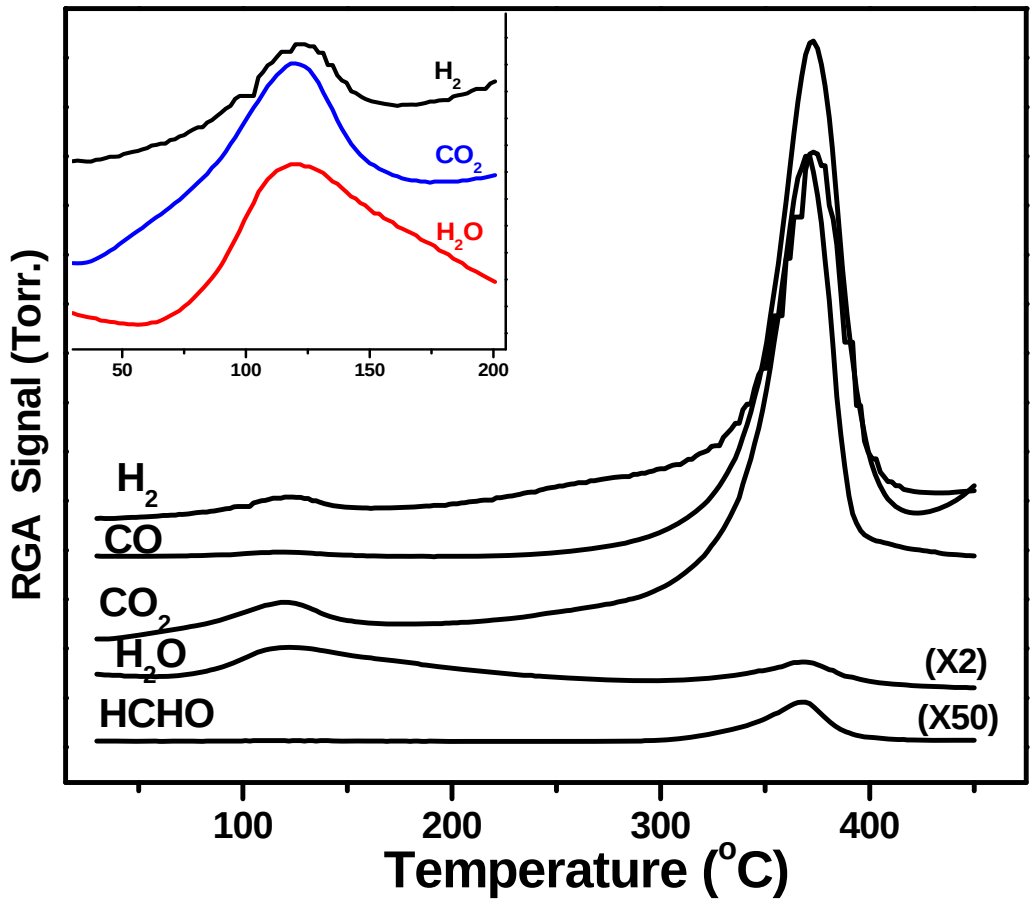


Figure 5.2 HCOOH-TPD profiles over 1%Au-Ceria(Rod)

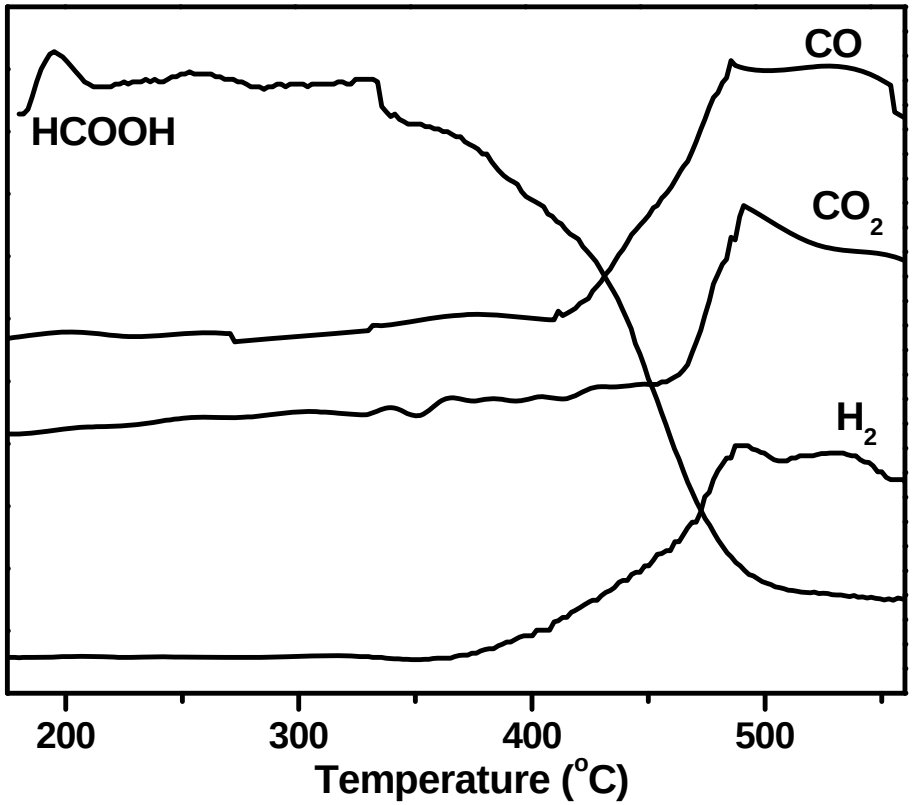


Figure 5.3 HCOOH-TPSR profile over Ceria (Rod)

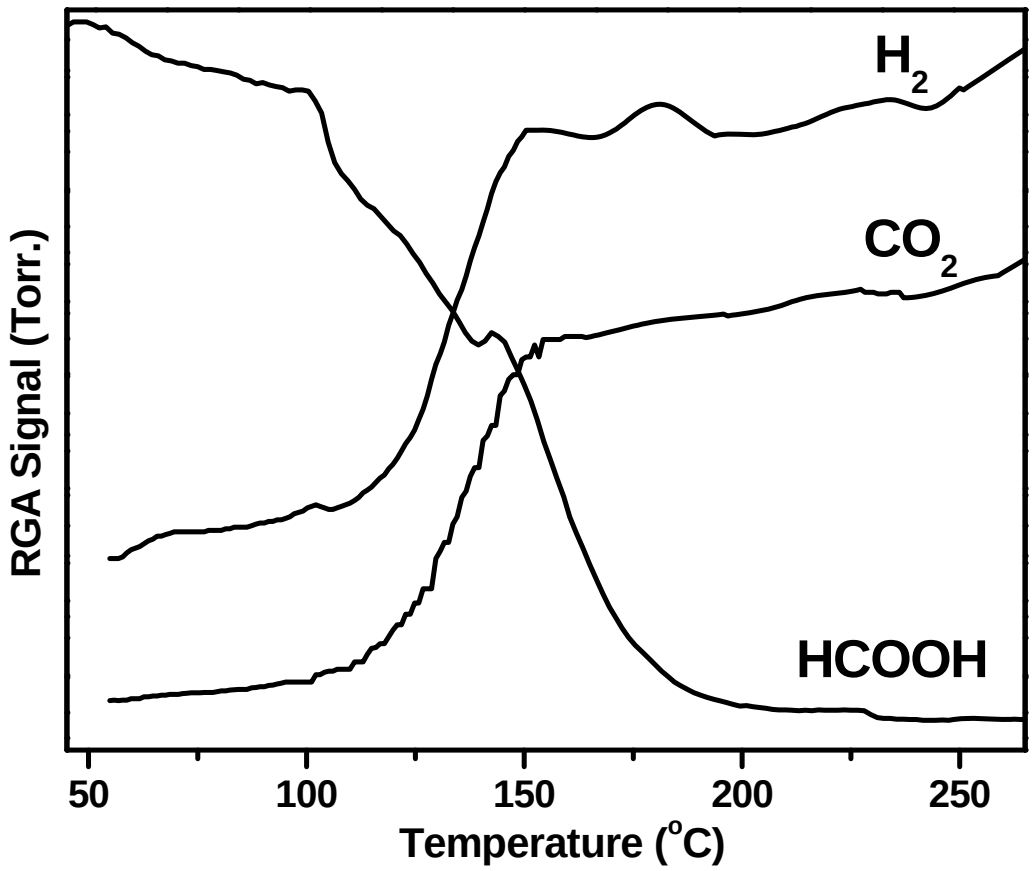


Figure 5.4 HCOOH-TPSR profile over 1%Au-Ceria(Rod)

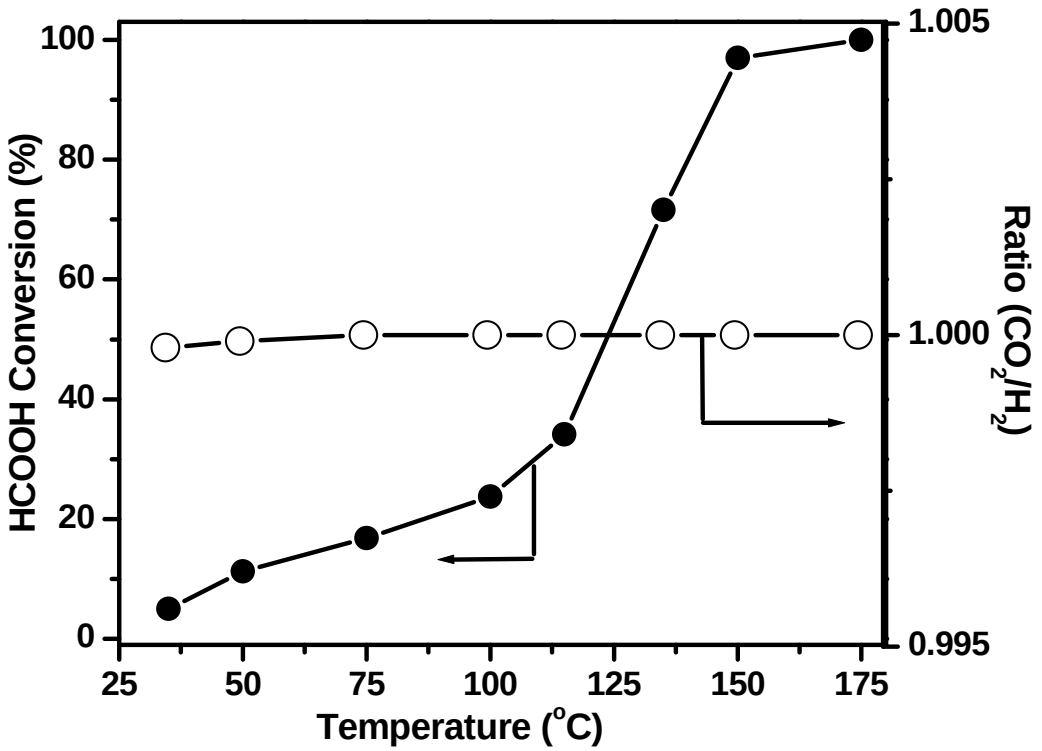


Figure 5.5 Formic acid conversion (%) and the ratio of products ($CO_2/H_2$) over 1%Au-Ceria(Rod)

Gas composition: 3.3%HCOOH/bal.He; GHSV: 42,000 $h^{-1}$

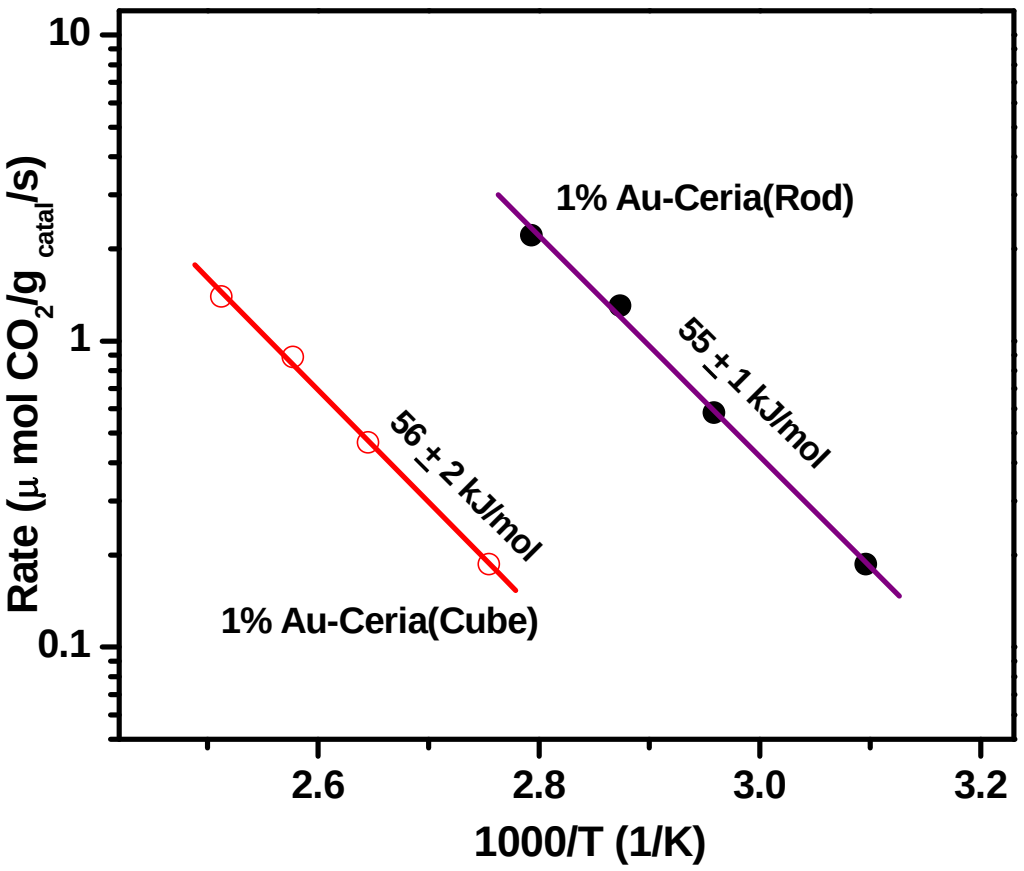


Figure 5.6 Steady-state reaction rates for the decomposition of formic acid over 1%Au-Ceria

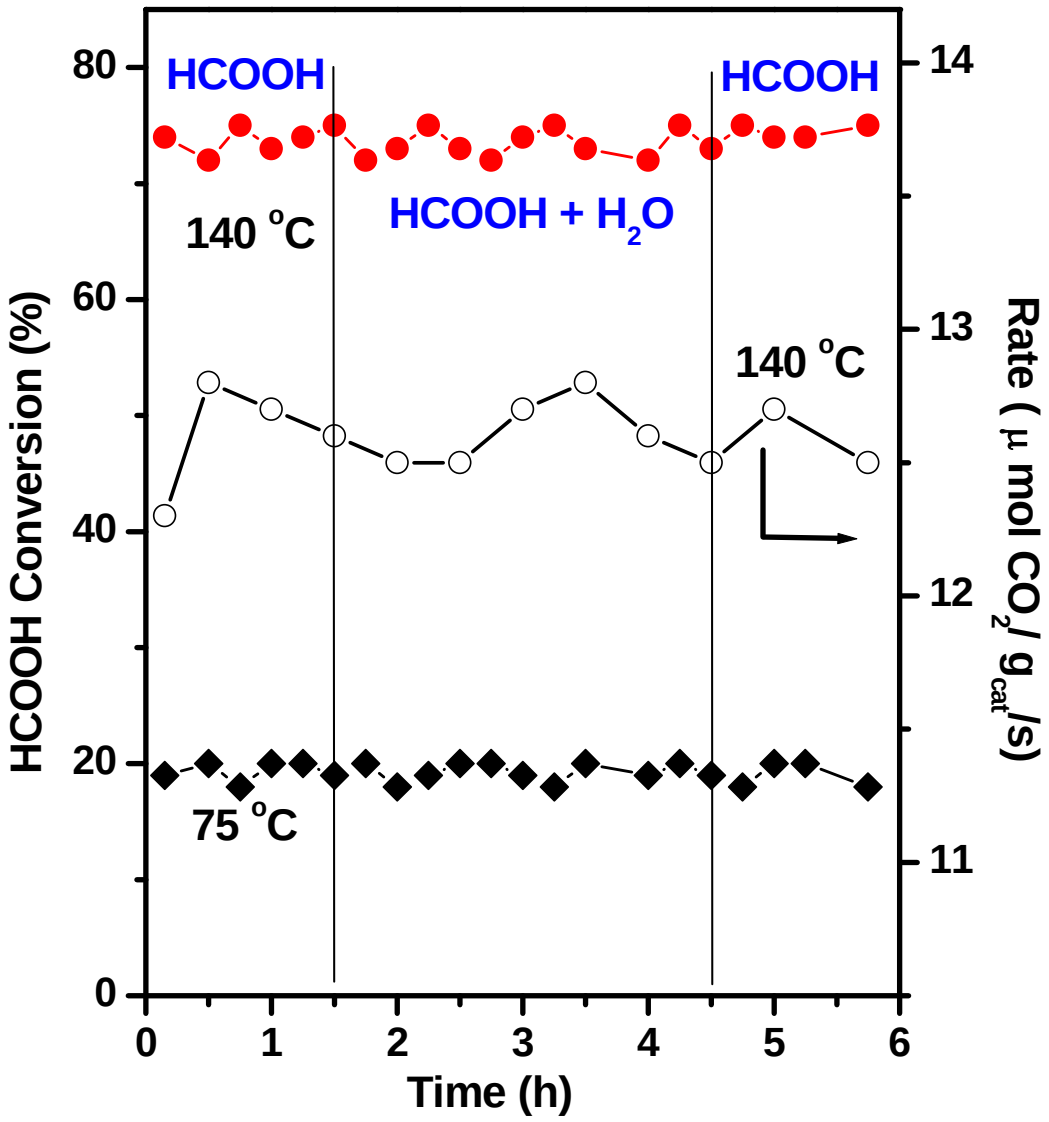


Figure 5.7 Effect of the addition/removal of water in the reaction gas mixture over 1%Au-Ceria (Rod) operating at steady state of decomposition of formic acid

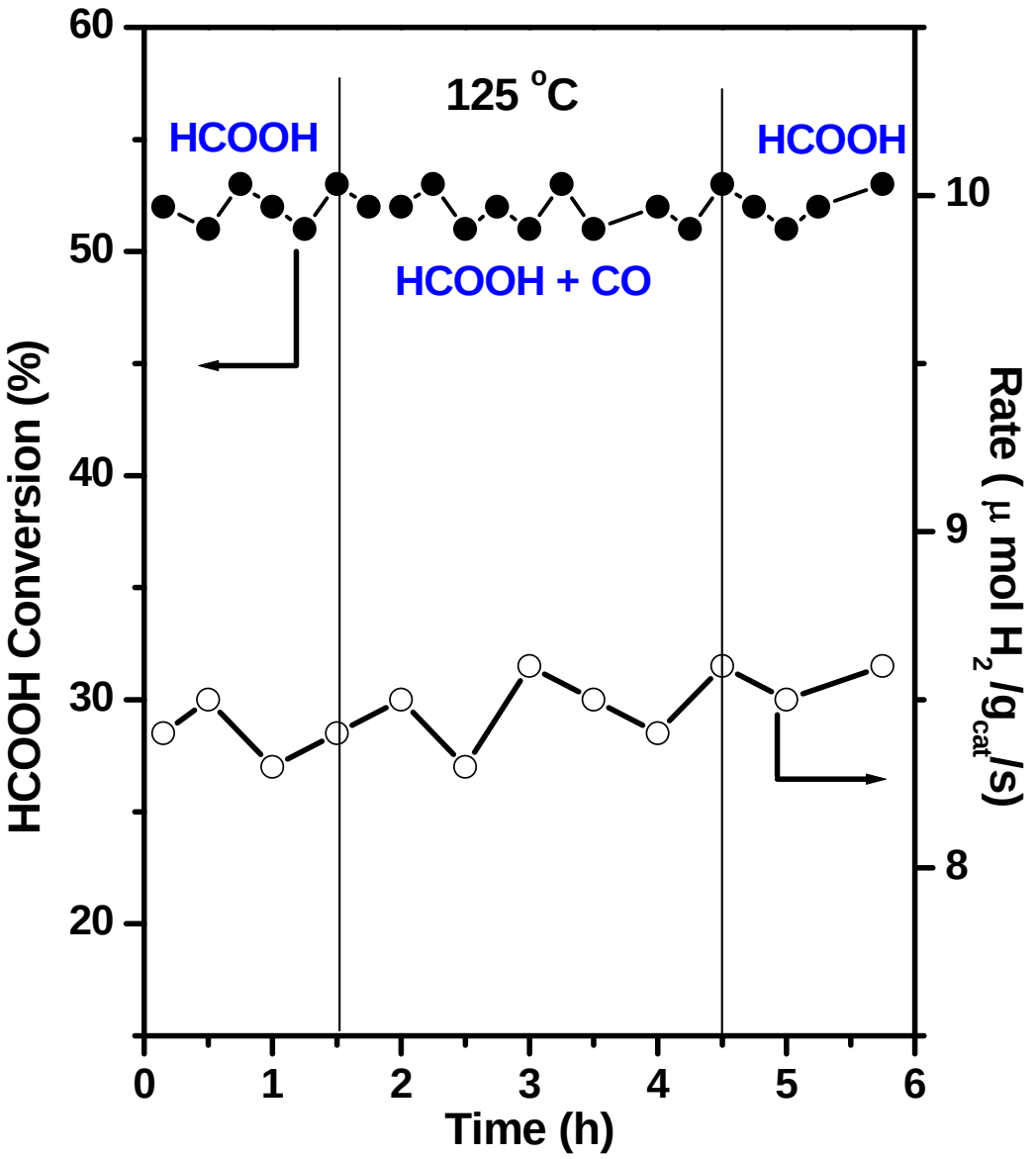


Figure 5.8 Effect of the addition/removal of carbon monoxide in the reaction gas mixture over 1%Au-Ceria (Rod) operating at steady state of decomposition of formic acid

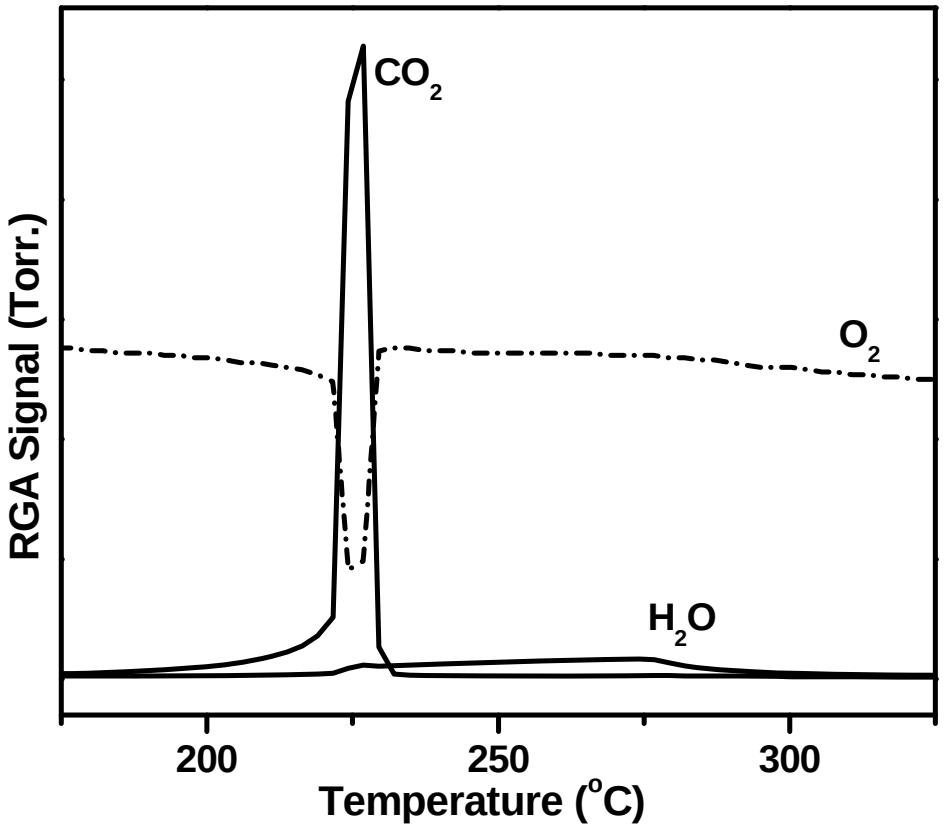


Figure 5.9 TPO profile over used 1%Au-Ceria(Rod) after decomposition of formic acid reaction

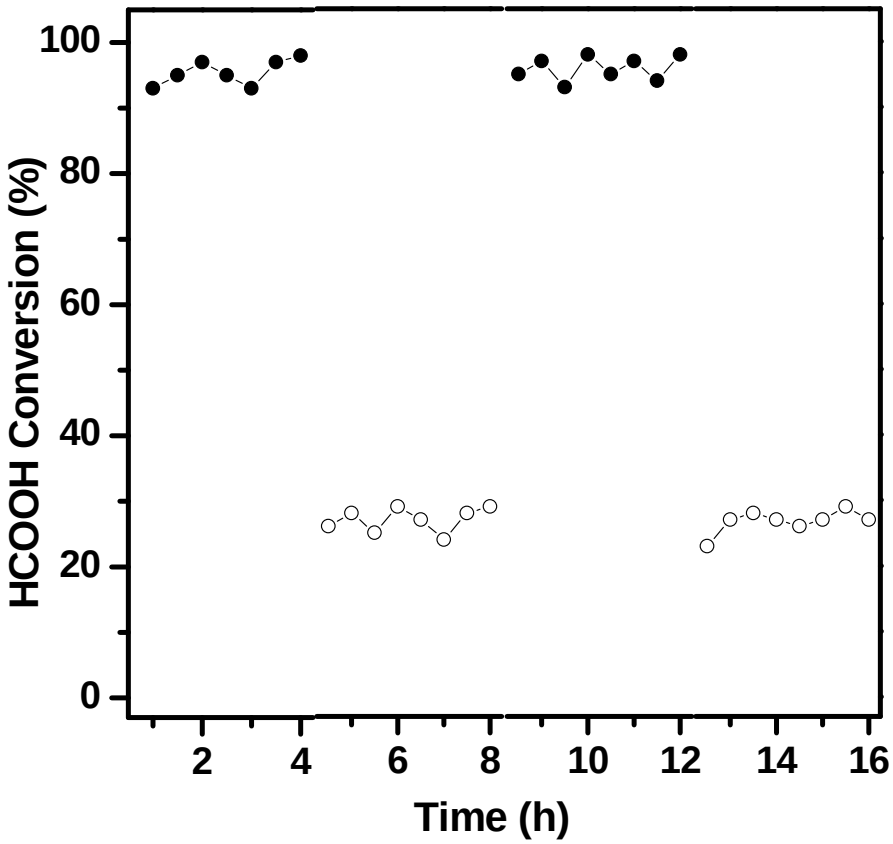


Figure 5.10 HCOOH conversion (%) over 1%Au-Ceria(Rod) under different space velocities GHSV = 21,000 $h^{-1}$(●) and GHSV= 60,000 $h^{-1}$(○)

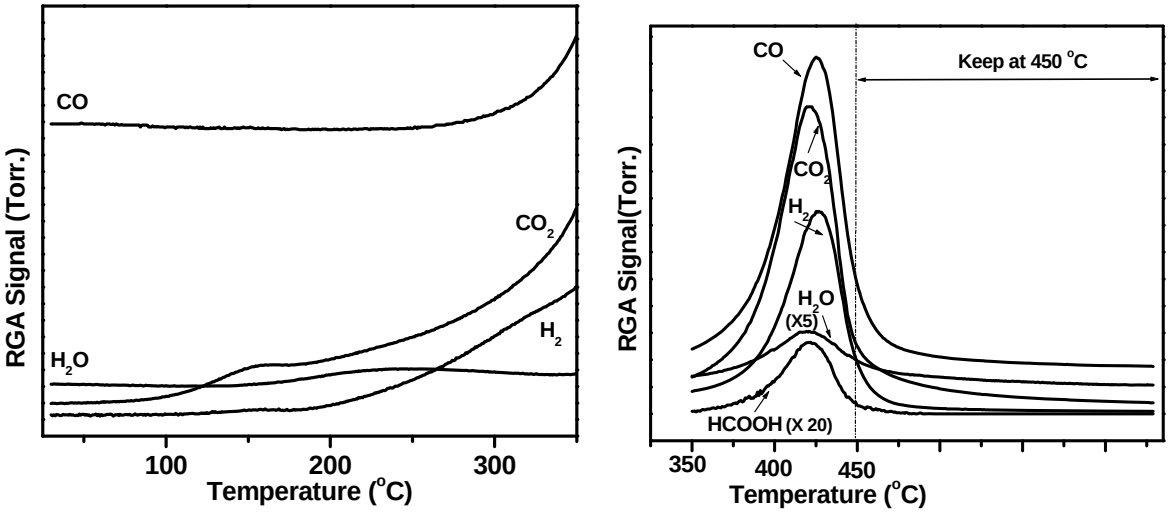


Figure 5.11 He-TPSR profiles over used 1%Au-Ceria(Rod)

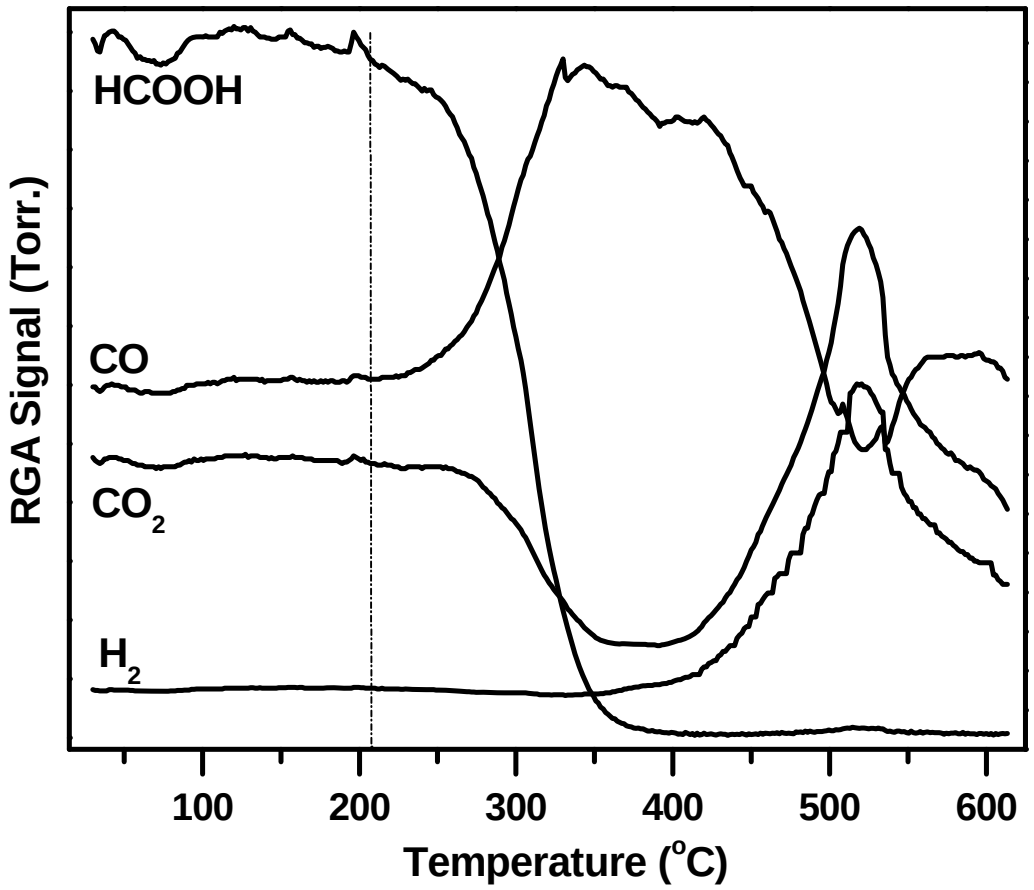


Figure 5.12 HCOOH-TPSR profile over 3Na-$SiO_2$

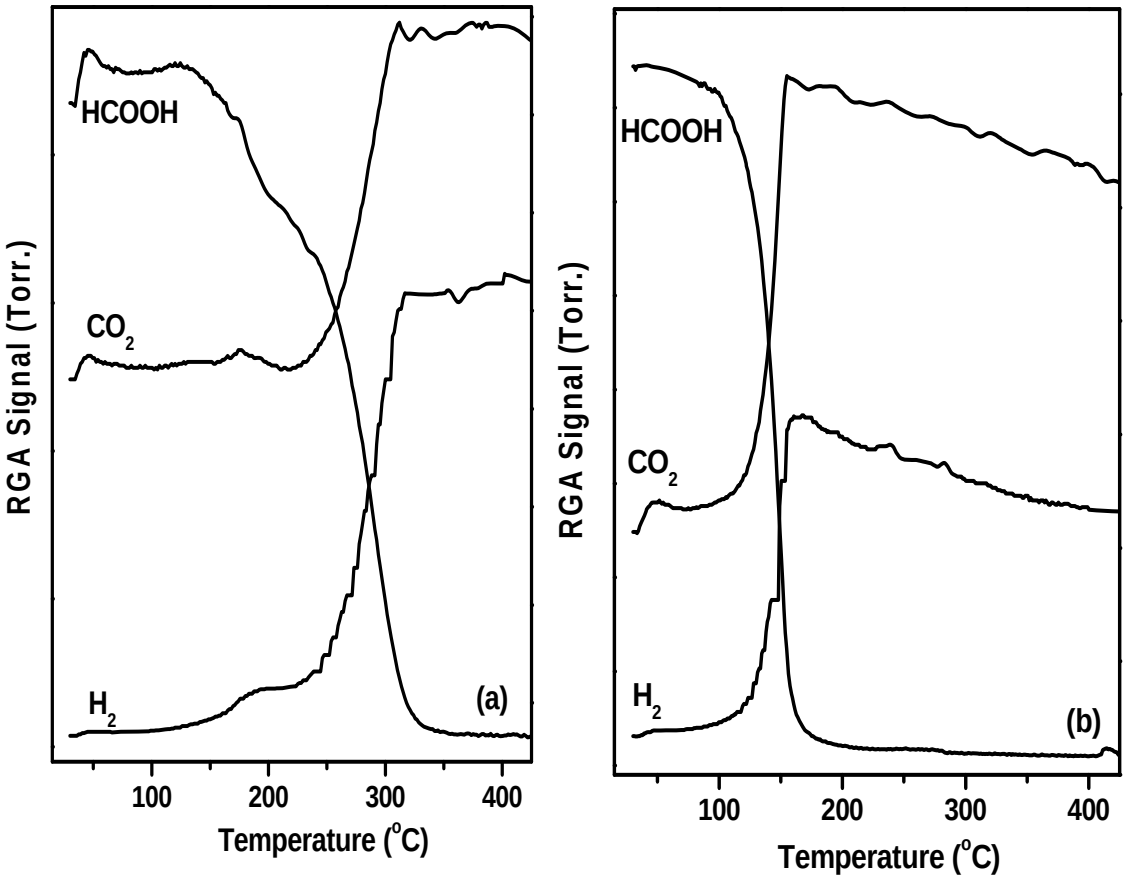


Figure 5.13 HCOOH-TPSR profiles over (a) 1at%Pt-$SiO_2$ and (b) Na-1at%Pt-$SiO_2$

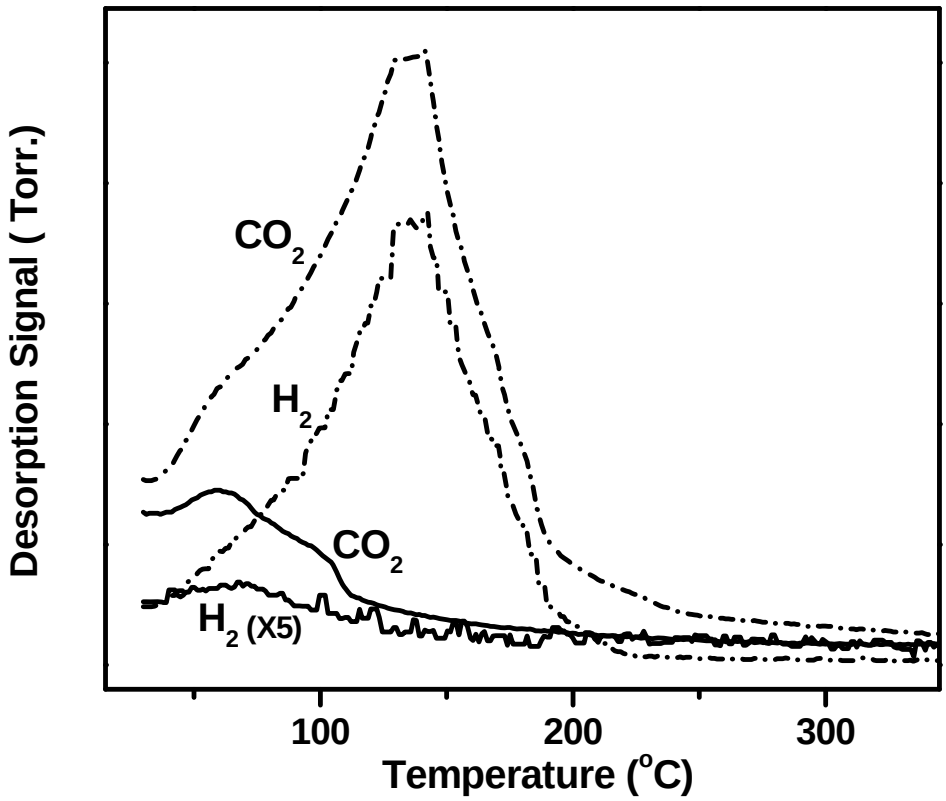


Figure 5.14 HCOOH-TPD profiles over 1at%Pt-$SiO_2$ ( solid lines) and Na-1at%Pt-$SiO_2$ (dotted lines)

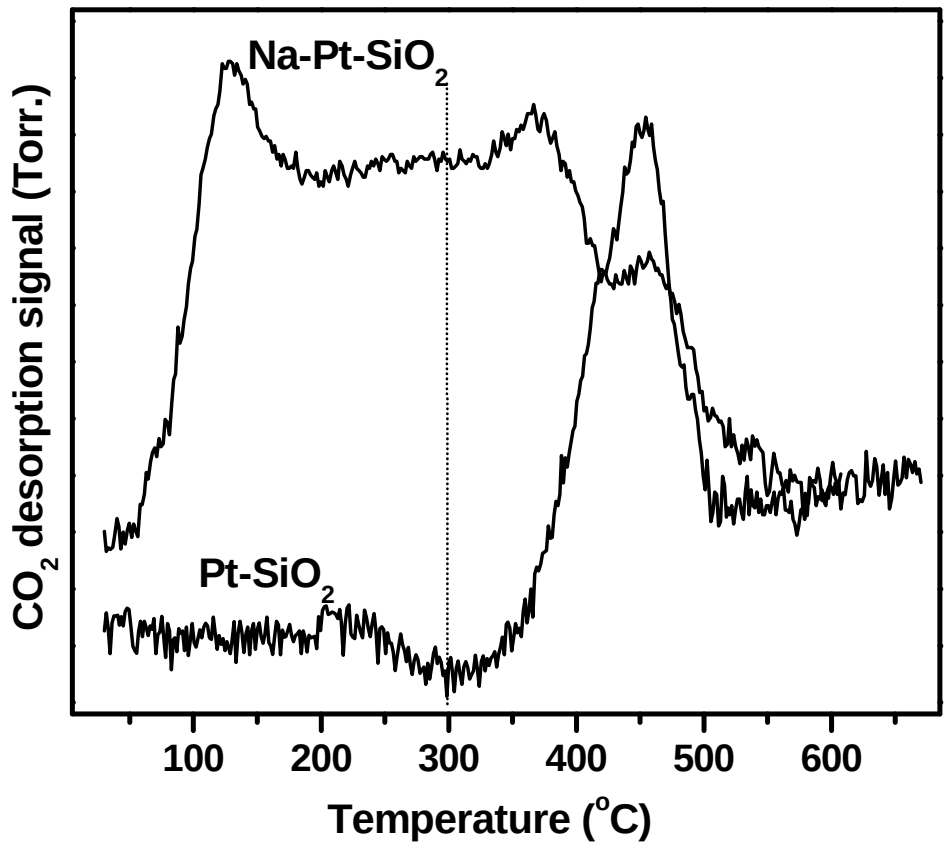


Figure 5.15 $CO_2$-TPD profile over 1at%Pt-$SiO_2$ and Na-1at%Pt-$SiO_2$

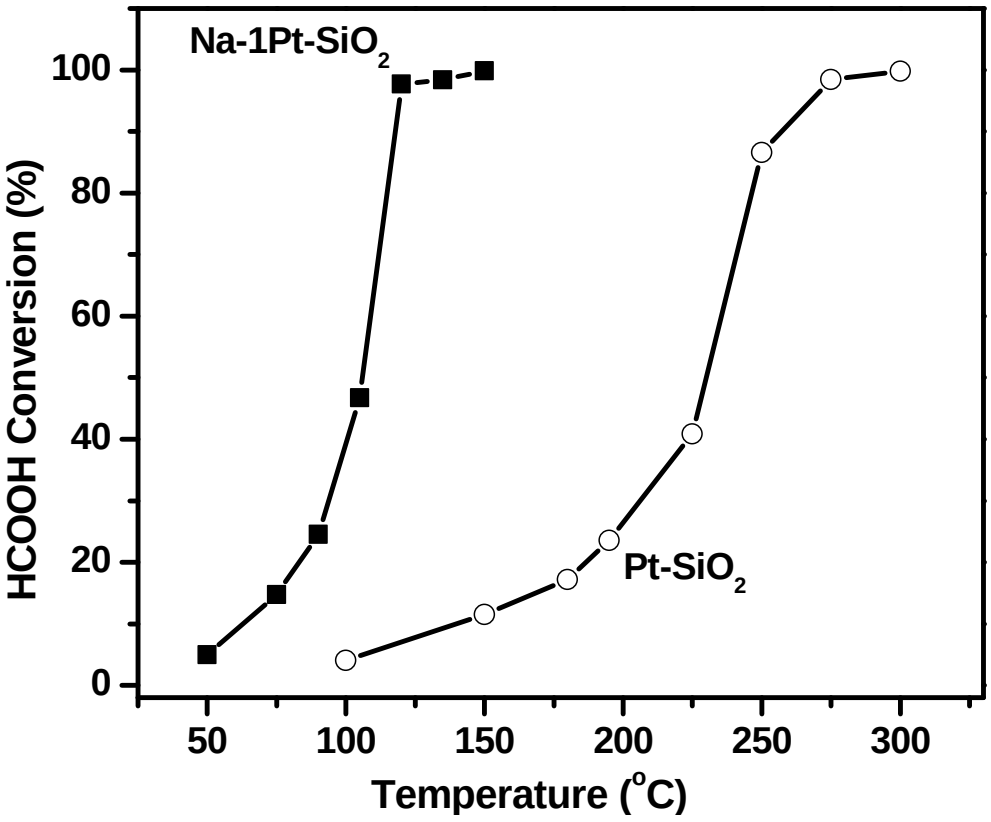


Figure 5.16 HCOOH conversion over 1at%Pt-$SiO_2$ and Na-1at%Pt-$SiO_2$

Gas composition: 3.3%HCOOH/bal.He; GHSV: 42,000 $h^{-1}$

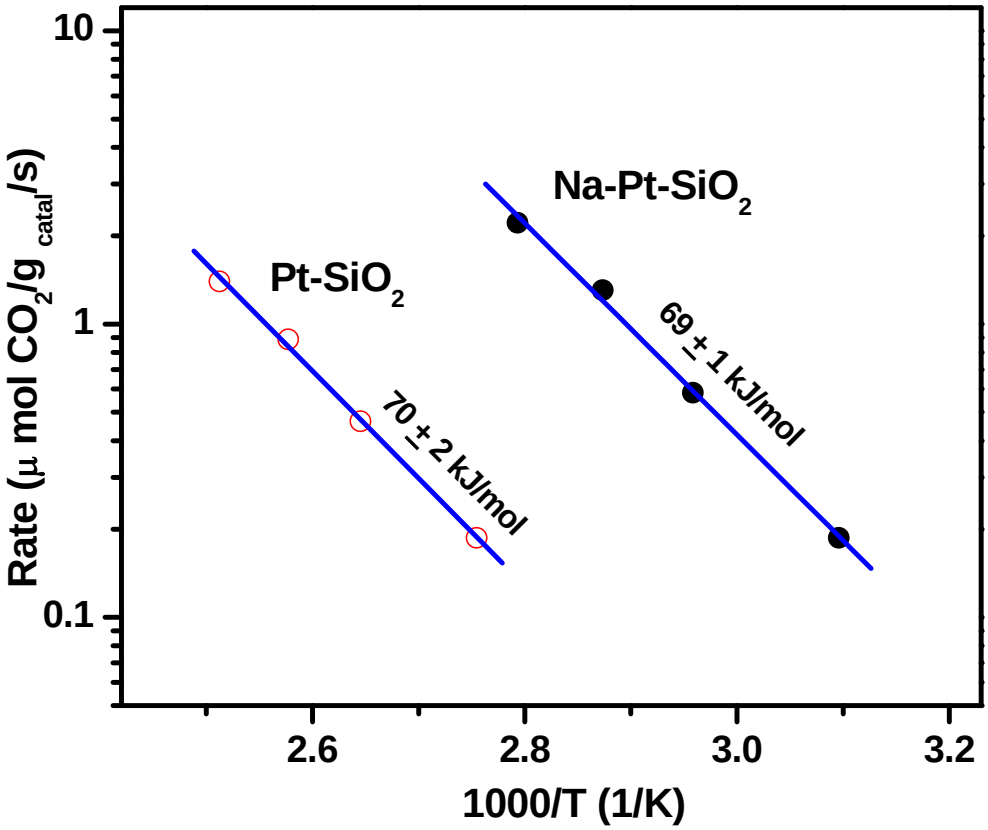


Figure 5.17 Steady-state reaction rates for the decomposition of formic acid over 1at%Pt-$SiO_2$ and Na-1at%Pt-$SiO_2$

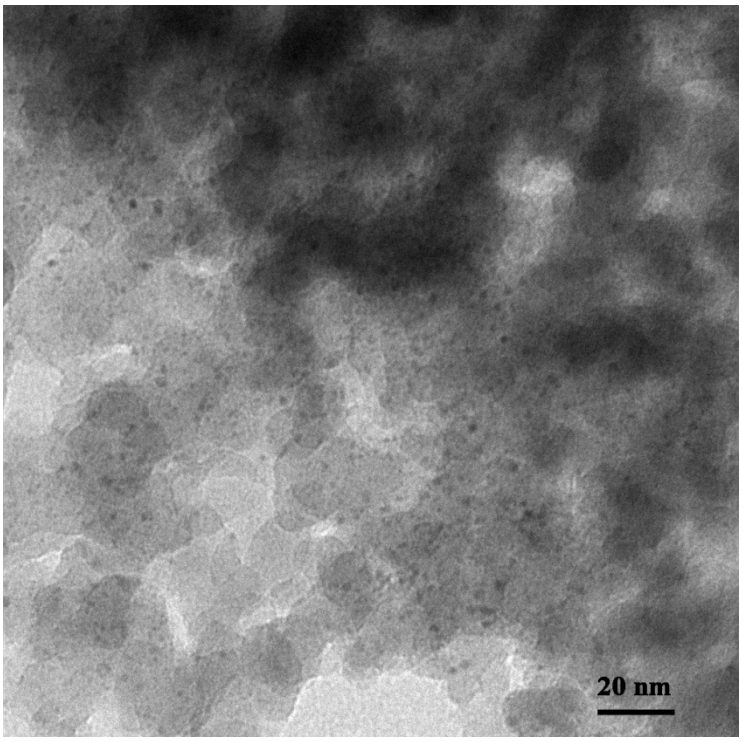


Figure 5.18 TEM image of used Na-1at%Pt-$SiO_2$

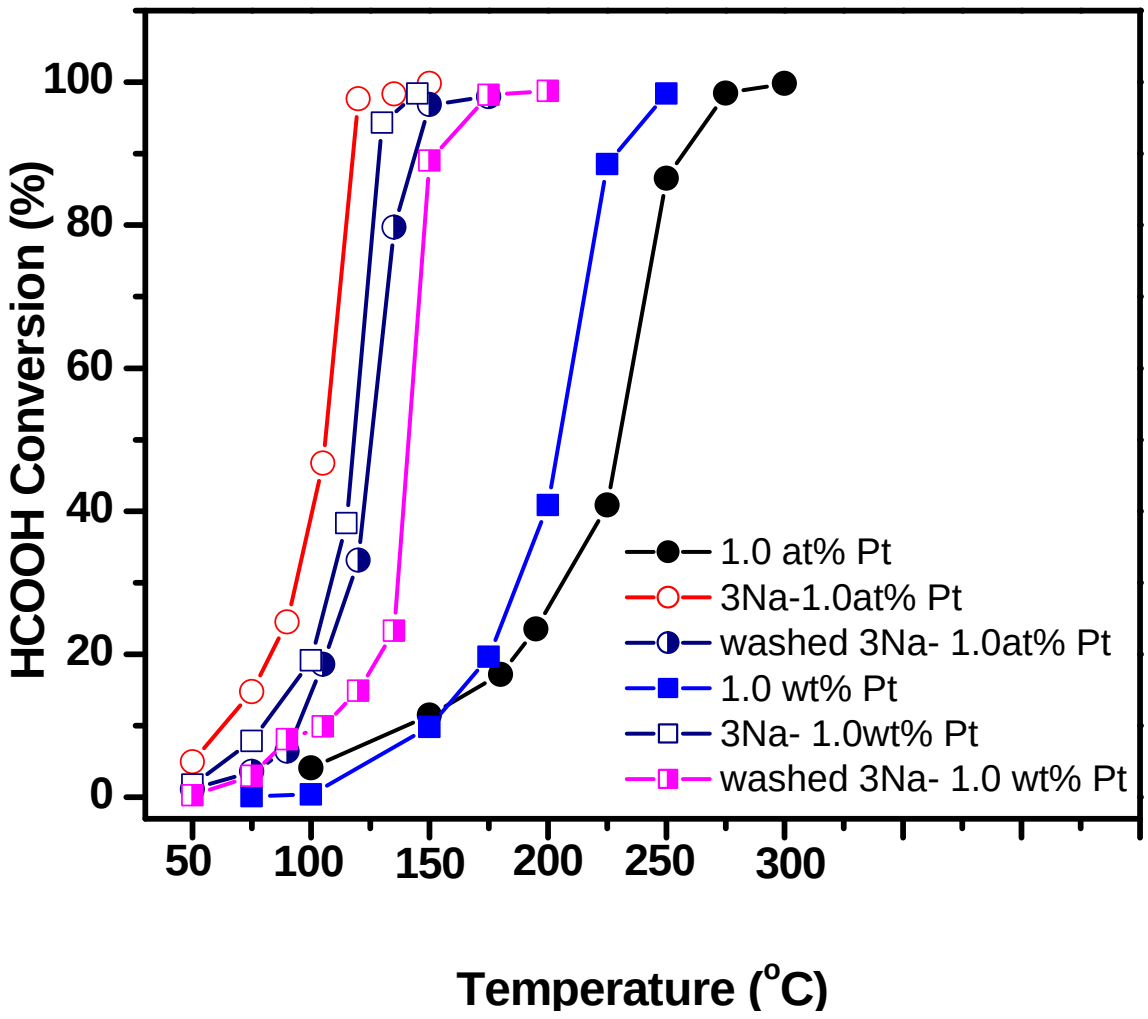


Figure 5.19 Steady-state formic acid conversion (%) over various Pt-$SiO_2$ catalysts

Gas composition: 3.3%HCOOH/bal.He; GHSV: 42,000 $h^{-1}$

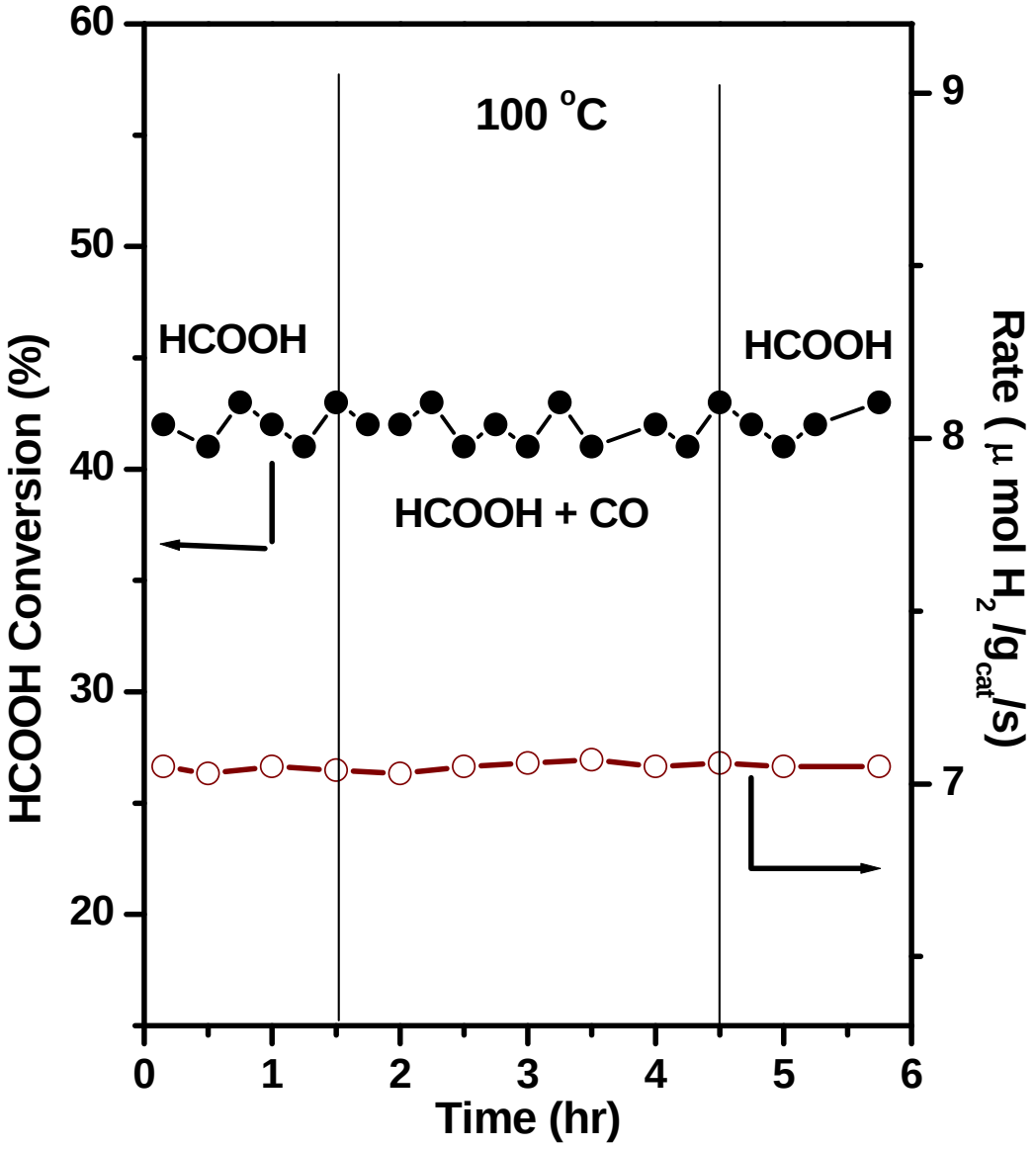


Figure 5.20 Effect of the addition/removal of carbon monoxide in the reaction gas mixture over Na-1at%Pt-$SiO_2$ operating at steady state of decomposition of formic acid

# Chapter 6: Conclusions and Recommendations

## 6.1 Conclusions

The activity, selectivity, and stability of atomically dispersed gold, copper, platinum and palladium supported on nanoscale cerium oxide, as a new generation catalysts to activate methanol and formic acid were investigated in this dissertation. Particularly new was the gold-ceria system at the beginning of this work. The key finding from the thesis is that atomically dispersed M-$O_x$ species catalyze the low-temperature methanol and formic acid decomposition reactions with selectivity depending on the metal. The highest selectivity to hydrogen was achieved over gold and copper, while the selectivity of the platinum and palladium species is limited by the equilibrium of the water-gas shift reaction. The potential for application to fuel processing for fuel cells is thus better for the Group IB metals. In order to improve the activity and selectivity of platinum, alkali promoters may be used as demonstrated in this thesis.

### *6.1.1 Metal clusters dispersed on ceria nanoshapes*

Different ceria nanoshapes were synthesized by hydrothermal methods. Ceria nanorods, which are bound by {110} and {100} planes, facilitated the M-$O_x$ adsorption and dispersion on the {110} surfaces, while ceria nanocubes which only have {100} planes had little interaction with gold after the heat treatment in air at 400 $^{o}$C. Gold is assumed to bind on an oxygen vacancy site. Thus, certain shapes of ceria with larger concentration of surface oxygen vacancies will better bind and stabilize the gold species. The same holds true for other metals on ceria, *e.g.* copper, platinum, and palladium. These bound M-$O_x$ species were found to catalyze the low-temperature water-gas shift (WGS) reaction in previous work at Tufts [1]. Here we have demonstrated that the M-$O_x$ species catalyze the methanol and formic acid reactions. The support is important as a ligand, and other supports, *e.g.* ZnO, can be used to prepare them in active form. Therefore, increasing the abundance of Au-$O_x$ sites would increase the catalyst activity.

Metal nanoparticles, if present on the surface, do not participate in these reactions—they are spectator species.

Au-ceria significantly enhances the rate of hydrogen production and totally inhibits the formation of CO at low temperatures (< 250 $^{o}$C) in steam reforming of methanol. Additionally, it has excellent stability, as shown by measurements of constant activity even after several start-up and shut-down tests. Different reaction pathways between Group IB metals (Au and Cu) and Group VIII metals (Pd and Pt) on ceria for steam reforming of methanol were established. The methanol decomposition-WGS sequence was identified for Group VIII metals (Pt, Pd), while the methyl formate pathway is unique to Group IB metals (Au). This particular finding is significant because it provides the necessary insight into how to rank order and select the precious metals for practical application to PEM fuel cells.

Furthermore, gold-ceria was demonstrated to be a most efficient catalyst for ambient temperature decomposition of formic acid. As in the case of the steam reforming of methanol, an indirect shape effect was identified over gold-ceria nanoshapes in formic acid decomposition. The reaction rate depended on the number of active Au-$O_x$-Ce sites, while the apparent activation energy was the same over all gold-ceria nanoshapes. Hence, the same reaction mechanism, namely: the dehydrogenation pathway ($HCOOH \rightarrow CO_2 + H_2$) was the preferred formic acid decomposition pathway over all gold-based catalysts. Ceria played no role in this pathway. Also gold-ceria maintained a stable catalytic performance in the presence of added water or carbon monoxide.

*6.1.2 Sodium modified platinum-silica*

The addition of alkali (sodium) had a minor positive effect on the activity of Pt-$CeO_2$ for steam reforming of methanol due to the already strong interaction between platinum and ceria. However, significant promotion of the activity of Pt-$SiO_2$ was observed upon addition of small amounts of sodium. Temperature programmed reactions along with the catalytic activity tests enabled us to explore the role of sodium, which has the combined effect of first improving the

adsorption of methanol on the catalyst, thus facilitating the reaction rate of the decomposition of methanol, and second boosting the water gas shift reaction.

Sodium-promotion of Pt-$SiO_2$ is a cheaper and a much more efficient way to decrease the amount of platinum used for formic acid decomposition compared with the traditional method of alloying platinum with other precious metals. The ratio between sodium and platinum plays an important role in obtaining the optimized strongly bonded Pt-O-Na-$(OH)_x$ species. Although the dehydrogenation pathway did not change with the addition of sodium, sodium-promoted Pt-$SiO_2$ showed enhanced formic acid adsorption at ambient temperature, which increased the subsequent formic acid decomposition reaction rate. Also an unexpected tolerance to carbon monoxide addition was found and attributed to the specific nature of the active site containing oxidized platinum that weakly adsorbs carbon monoxide.

## 6.2 Recommendations

### *6.2.1 The chemistry behind the methanol interaction with metals*

It was demonstrated here that methyl formate was formed by the coupling reaction between methoxy group and formaldehyde. Its subsequent hydrolysis to formic acid in the presence of water became the pathway of steam reforming of methanol network over group IB metals.

The selective oxidation of methanol produces methyl formate on $ReO_x$-$CeO_2$ [2] and over Au-ZnO [3]. Also, esters are produced by oxidation of methanol and higher alcohols through coupling reactions on unsupported nanoporous gold [4]. The latter, produced by leaching of AgAu alloys, contains a small amount of residual silver, hence it is easy to envision Au-$O_x$ site formation at the interface of the two metals. Among other metal oxides, vanadium oxides have been demonstrated to be very good catalysts for the production of formaldehyde by the selective oxidation of methanol [5]. Good insights to the various oxide catalyst activity and selectivity are found in the extensive work by Israel Wachs and his group [6, 7]. It would be extremely

instructive and useful to understand how these very different oxides catalyze the selective oxidation of methanol, and whether a hemolytic or heterolytic abstraction of hydrogen is present.

In regard to the findings of this thesis for the active Au-$O_x$ species, any oxide support would be suitable at low-temperatures as long as it is a stabilizer of the gold. For example, the {110} surfaces of $CeO_2$ and the {0001} polar surfaces of ZnO are suitable. On the other hand, for those oxide surfaces that have minimal interaction with gold, such as silica, it may be possible to promote them with alkali, similar to what has been found here for the Pt-$SiO_2$ system. In future work, alkali additives are recommended to examine the validity of this argument on gold supported on non reducible inert oxides, such as silica, and even on non oxide supports, such as various carbons. Mechanistically, it would be exciting to examine the selective oxidation mechanism (hemolytic vs. heterolytic) as a function of the size of the Au-$O_x$ cluster.

### *6.2.2 Kinetic implication of the reaction pathway*

When one designs methanol reformers, the kinetics of the reforming reactions are important in sizing the reactor. Both power-law and Langmuir-Hinshelwood rate expressions have been proposed in the literature [8]. There is little agreement among the expressions, even across the same kinds of catalysts and across the components affecting the reaction rate. Therefore, detailed kinetic studies are recommended in future work. These should include the investigation of kinetic isotope effects as a tool to discriminate between different oxygen species on the catalyst surfaces.

### *6.2.3 In-situ monitoring structure transformation*

As mentioned in Chapter 5, an unexpected carbon monoxide resistance of Na-Pt-$O_x$(OH)-$SiO_2$ was observed. The Pt site remains oxidized even at highly reducing conditions [9]. As one experimental approach to study this, Quick-XAFS could be applied to follow the reaction-relevant Pt structure changes with different promoters under reaction conditions. The same

should be explored for gold catalysts. DFT work should also complement these studies to assist in rational catalyst designs.

## 6.3 References


[1] Q. Fu, H. Saltsburg, M. Flytzani-Stephanopoulos, *Science* 301 (2003) 935.

[2] J. Liu, E. Zhan, W. Cai, J. Li, W. Shen, *Catal. Lett.* 120 (2008) 274.

[3] M. B. Boucher, N. Yi, F. Gittleson, B. Zugic, H. Saltsburg, M. Flytzani-Stephanopoulos, *J. Phys. Chem. C* 115 (2011) 1261.

[4] A. Wittstock, V. Zielasek, J. Biener, C. M. Friend, M. Bäumer, *Science* 327 (2010) 319.

[5] F. Roozeboom, P. D. Cordingley, P. J. Gellings, *J. Catal*. 68 (1981) 464.

[6] X. Wang, I. E. Wachs, *Catal. Today* 96 (2004) 211.

[7] K. Routray, W. Zhou, C. J. Kiely, I. E. Wachs, *ACS Catal*. 1 (2011) 54.

[8] B. Frank, F. C. Jentoft, H. Soerijanto, J. Kröhnert, R. Schlögl, R. Schomäcker, *J. Catal.* 246 (2007) 177.

[9] Y. P. Zhai, D. Pierre, R. Si, W. L. Deng, P. Ferrin, A. U. Nilekar, G. Peng, J. A. Herron, D. C. Bell, H. Saltsburg, M. Mavrikakis, M. Flytzani-Stephanopoulos, *Science* 329 (2010) 1633.